Interacting global invariant sets in a planar map model of wild chaos

Stefanie Hittmeyer, Bernd Krauskopf, Hinke M. Osinga
Department of Mathematics, The University of Auckland
Private Bag 92019, Auckland 1142, New Zealand

December 2012

Abstract

Wild chaos is a new type of chaotic dynamics that can arise in a continuous-time dynamical system of dimension at least four. We are interested in the possible bifurcations or sequence of bifurcations that generate this type of chaos in dynamical systems. We focus our investigation on a planar noninvertible map that has been introduced by Bamón, Kiwi and Rivera-Letelier to prove the existence of wild chaos in a five-dimensional Lorenz-like system. The map opens up the origin (the critical point) to a disk and wraps the plane twice around it; points inside the disk have no preimage. The bounding critical circle and its images, together with the critical point and its preimages form the so-called critical set. This set interacts with the stable and unstable sets of a saddle fixed point. Advanced numerical techniques enable us to study how the stable and unstable sets change as a parameter is varied along a path towards the wild chaotic regime. We find four types of bifurcations: The stable and unstable sets interact with each other in homoclinic tangencies (which also occur in invertible maps) and they interact with the critical set in three types of bifurcations specific to noninvertible maps, which cause changes (such as self-intersections) of the topology of these global invariant sets. Overall, a consistent sequence of all four types of bifurcations emerges, which we present as a first attempt towards explaining the geometric nature of wild chaos. Using two-parameter bifurcation diagrams we show that essentially the same sequences of bifurcations occur along different paths towards the wild chaotic regime, which we utilize to obtain an indication of the size of the parameter region where wild chaos exists.

1 Introduction

Vector fields and diffeomorphisms with chaotic attractors arise in numerous fields of applications, including neuroscience [20], chemical reactions [21] and laser systems [39]. One of the first and best known examples of a chaotic three-dimensional vector field is the *Lorenz system* [38]. It was introduced in 1963 by meteorologist Edward Lorenz as a simplified model of convection dynamics in the earth's atmosphere. At the classical parameter values, its chaotic attractor – the *Lorenz attractor* – has the shape of the wings of a butterfly. The dynamics on this attractor has been studied in great detail; see, for example, [2, 3, 27, 53, 54]. More recently, the focus has shifted to what this means for the global behavior on the entire phase space [16, 17].

The approach taken for studying the Lorenz system at the classical parameter values is of a geometric nature. We discuss it briefly, because a similar approach is used to derive a map that exhibits so-called *wild chaos*. The Lorenz system has three equilibria: the origin, which is a saddle, and two secondary equilibria, which are saddle-foci. The origin and its one-dimensional unstable manifold are part of the Lorenz attractor. The two-dimensional stable manifold of the origin is not part of the attractor but fills the phase space densely. This manifold organizes the sensitivity to initial conditions that characterizes the chaotic dynamics in the Lorenz system. In 1979, Guckenheimer and Williams introduced the concept of the *geometric Lorenz attractor* as a geometric model of the Lorenz attractor [27]. It is formulated in an abstract way such that it displays all the features of the Lorenz attractor that were known at the time. The dynamics on the geometric Lorenz

attractor can be reduced to a one-dimensional noninvertible map – the *Lorenz map* – as follows. Consider a two-dimensional Poincaré section through the two secondary equilibria and perpendicular to the z-axis. The Poincaré return map is defined as a two-dimensional local diffeomorphism on the open subset of this section on which the flow points in the direction of negative z. One can identify a strong stable foliation on the Poincaré section (i.e. an invariant foliation that is uniformly contracted by the Poincaré return map). The quotient map, defined on the quotient space of the Poincaré section induced by this foliation, is the one-dimensional noninvertible Lorenz map. Note that the intersection curves of the two-dimensional stable manifold of the origin and the Poincaré section are dense in the leaves of the strong stable foliation. They consist of points that eventually do not come back to the Poincaré section under the flow of the system. One of these leaves consists of points that do not return to the Poincaré section at all. Therefore, the two-dimensional Poincaré map is not defined on this leaf and the one-dimensional Lorenz map has a corresponding point of discontinuity, called the *critical point*. This point represents the boundary of the domain of the Lorenz map and splits the domain into a left and a right subdomain, which correspond to orbits following the left or the right wing of the Lorenz attractor, respectively. By construction, interactions with the critical point in the one-dimensional Lorenz map correspond to interactions with the stable manifold of the origin and, therefore, to homoclinic or heteroclinic bifurcations in the three-dimensional Lorenz system.

In 1999, Tucker proved that the Lorenz system satisfies the conditions of the geometric Lorenz attractor and, therefore, is chaotic [54]. Already in 1976, Henón constructed a chaotic planar diffeomorphism as a phenomenological model of the two-dimensional Poincaré return map of the Lorenz system, which is now referred to as the Henón map [29]. The Lorenz system and the Henón map are the classical examples for the type of chaos that arises in three-dimensional vector fields and two-dimensional diffeomorphisms, respectively; see, for example, the textbooks [26] and [49]. This type of chaos is characterized by homoclinic tangencies at certain parameter values between the stable and unstable manifolds of saddle fixed points of the Poincaré return map of the Lorenz system or the Henón map, respectively. These tangencies are well known to generate nearby homoclinic tangencies and *homoclinic tangles*, which are transverse intersections of the stable and unstable manifolds and associated with horseshoes and chaotic attractors [52]. The Lorenz attractor is a *robust singular attractor*, which means that this attractor contains an equilibrium as well as regular orbits of the vector field and every sufficiently C^1-close vector field has such an attractor nearby. In [43] it was proven that every robust singular attractor of a three-dimensional vector field is a geometric Lorenz attractor. Hence, the geometric Lorenz attractor is a typical kind of chaos that can appear in three-dimensional vector fields.

In applications, one generally expects more than three variables to play a role and, therefore, higher-dimensional vector fields or diffeomorphisms arise. In higher-dimensional dynamical systems, one can encounter chaotic behavior created by the same mechanisms as in the Lorenz system and the Henón map, but possibly also more complicated types of chaos. Therefore, a natural question to ask is whether one can find robust singular attractors with richer dynamical behavior in higher-dimensional vector fields.

In this paper, we study a robust singular attractor of an n-dimensional vector field, with $n \geq 5$, that was constructed by Bamón, Kiwi and Rivera-Letelier in [9]. This attractor is called *Lorenz-like*, because it is a "geometric Lorenz-attractor" in higher dimensions. Analogous to the construction by Guckenheimer and Williams discussed above, the authors of [9] reduce the n-dimensional vector field to the dynamics of an $(n-1)$-dimensional invertible Poincaré return map to a suitable section. This section has an $(n-3)$-dimensional strong stable foliation and the resulting quotient map is a two-dimensional noninvertible map. This map has a critical point that corresponds to the stable manifold of an equilibrium of the vector field, in a similar fashion as the critical point of the Lorenz map corresponds to the stable manifold of the origin in the Lorenz system. As a consequence, interactions with the critical point of the two-dimensional map correspond to homoclinic or heteroclinic bifurcations in the n-dimensional vector field. We discuss the Lorenz-like construction of the vector field, the reduction to the two-dimensional map and the correspondences between bifurcations of the map and the vector field in more detail in section 6.

Even though the construction of this attractor in at least five dimensions is similar to the construction of the geometric Lorenz attractor in three dimensions, it exhibits a much more complicated type of chaotic dynamics, called *wild chaos*. In order to discuss what this means, let us first introduce some notation. From now on, we will confine ourselves to the case of diffeomorphisms, because, in general, vector fields can be reduced (locally) to diffeomorphisms by means of Poincaré return maps and, conversely, any diffeomorphism can be suspended

as the time-1 map of a vector field.

A *hyperbolic set* of a diffeomorphism is a set that admits a continuous decomposition of its tangent bundle under the diffeomorphism into stable and unstable subspaces and, thereby, admits stable and unstable manifolds. The simplest examples of hyperbolic sets are saddle fixed points and saddle periodic points. A *homoclinic tangency* of a hyperbolic set is a nontransversal intersection of the stable and unstable manifolds of this hyperbolic set. A *nonwandering point* is a point such that each of its neighborhoods contains a point that comes back to this neighborhood after a finite number of iterations of the diffeomorphism. Examples are fixed points, periodic points, homoclinic points and limit points. A diffeomorphism is *uniformly hyperbolic* if the set of nonwandering points is hyperbolic and the set of periodic points is dense in it. The occurrence of a homoclinic tangency implies that a diffeomorphism is not uniformly hyperbolic or simply *nonhyperbolic*: A point of homoclinic tangency is nonwandering, but at this point the tangent bundle of the set of nonwandering points cannot be decomposed into stable and unstable subspaces.

The theory of uniformly hyperbolic diffeomorphisms [31, 50, 51] and the theory of nonhyperbolic diffeomorphisms on the boundary of uniform hyperbolicity [13, 45] are well developed. We are interested in the question whether nonhyperbolic diffeomorphisms can also appear in a robust fashion far away from uniformly hyperbolic ones. A diffeomorphism is *robust nonhyperbolic* if it has a C^1-neighborhood of nonhyperbolic diffeomorphisms. One way to study robust nonhyperbolicity is to look for robust homoclinic tangencies. A homoclinic tangency is *C^r-robust* for some $r \geq 1$, if the diffeomorphism has a C^r-neighborhood consisting of diffeomorphisms with homoclinic tangencies. For $r = 1$ we simply speak of a *robust* homoclinic tangency. A hyperbolic set is called *wild* if it has robust homoclinic tangencies [47], and we refer to the existence of a wild hyperbolic set as *wild chaos*.

In the space of two-dimensional diffeomorphism, each diffeomorphism with a homoclinic tangency is accumulated by infinitely many diffeomorphisms with nearby homoclinic tangencies. Therefore, the set of diffeomorphisms with homoclinic tangencies is a union of Cantor sets. In [46], Newhouse constructed the first example of C^2-robust homoclinic tangencies in two-dimensional diffeomorphisms, but these are not C^1-robust [55]. In fact, in [44] it is argued that (C^1-)robust homoclinic tangencies and, therefore, wild chaos can only exist in diffeomorphisms of dimension at least three.

Another way to show robust nonhyperbolicity of a diffeomorphism is via the concept of heterodimensional cycles [12]. A *heterodimensional cycle* is a cycle that is formed by the intersections of the stable and unstable manifolds of two hyperbolic sets with different unstable dimensions; this phenomenon is also known as a heteroclinic cycle with *unstable dimension variability* [33]. The easiest example is a cycle that connects two saddle points with unstable dimensions one and two in a three-dimensional diffeomorphism; see the example studied in [5]. Reference [56] gives the first known example of a four-dimensional vector field model (of intracellular calcium dynamics) that admits a heterodimensional cycle. The authors also provide a numerical method of how to find heterodimensional cycles between two saddle periodic orbits in four-dimensional vector fields and how to continue them in system parameters. By definition, heterodimensional cycles can only exist in diffeomorphisms of dimension at least three, so again, it appears that robust nonhyperbolicity is a higher-dimensional phenomenon.

Many aspects of robust nonhyperbolic systems are still unknown. For example, one expects robust homoclinic tangencies to play a role in the generation of heterodimensional cycles, but the nature of their interrelation is unknown [11]. One of the difficulties is that, thus far, there are not many concrete examples. A three-dimensional diffeomorphism with wild chaos is constructed in [6, 7]; see also [23, 24] for a three-dimensional Henón-like diffeomorphism with a wild hyperbolic set contained in a Lorenz-like attractor.

Although two-dimensional diffeomorphisms are free of robust nonhyperbolicity, two-dimensional noninvertible maps can be robustly nonhyperbolic. For noninvertible maps, uniform hyperbolicity, (robust) homoclinic tangencies and heterodimensional cycles can be defined in the same way as for diffeomorphisms with the difference that their stable and unstable sets, in general, are not immersed manifolds. An example of a two-dimensional noninvertible map with unstable dimension variability is studied in [33]. In this paper, we study a

different example, namely, the two-dimensional noninvertible map

$$\begin{aligned} f : \mathbb{C}\backslash\{0\} &\to \mathbb{C} \\ z &\mapsto (1-\lambda+\lambda|z|^a)\left(\frac{z}{|z|}\right)^2 + c, \end{aligned} \tag{1}$$

with $c \in \mathbb{C}$ and $a, \lambda \in \mathbb{R}$. This map was constructed in [9] as the reduction of a Lorenz-like attractor in an n-dimensional vector field for $n \geq 5$. For $\lambda, a \in (0,1)$ sufficiently close to 1 and $c = 1$, the authors of [9] showed that this map exhibits wild chaos. The regime of existence constructed in the proof is a very small neighborhood of the point $(a, \lambda) = (1, 1)$ for fixed $c = 1$, but the wild chaos is expected to extend to a larger parameter regime. In order to understand the dynamics inside this regime and estimate its size, we study the transition from uniform hyperbolicity to wild chaos in map (1). In particular, we start far away from the point $(a, \lambda, c) = (1, 1, 0)$ and vary the parameters towards $(1, 1, 0)$. On the way, we encounter bifurcations between the stable and unstable sets with the critical set.

Map (1) has two symmetries: It is symmetric under rotation by π for all $c \in \mathbb{C}$ (i.e., $f(z) = f(-z)$ for all $z \in \mathbb{C}\backslash\{0\}$) and symmetric under complex conjugation for all $c \in \mathbb{R}$ (i.e., $f(\overline{z}) = \overline{f(z)}$ for all $z \in \mathbb{C}\backslash\{0\}$). Its domain is $\mathbb{C}\backslash\{0\}$ and we call the set

$$J_0 := \{0\}$$

the *critical point* of the map. The map (1) acts on the punctured complex plane by opening up J_0 to a circle of radius $1-\lambda$, wrapping the plane twice around it and translating it by c. In particular, the plane is mapped outside the disk $\overline{\mathbb{D}}_{1-\lambda}(c)$ in a 2-to-1 fashion, where $\overline{\mathbb{D}}_r(z)$ denotes the closed disk with radius $r > 0$ centered at $z \in \mathbb{C}$. The boundary of the range of the map (1) is given by the circle

$$J_1 := \partial\overline{\mathbb{D}}_{1-\lambda}(c),$$

which we call the *critical circle*. It builds the boundary between areas with different numbers of preimages: points inside J_1 have no preimage, points outside J_1 have two preimages. The two branches of inverses of the map (1) are symmetric under rotation by π and can be computed explicitly.

As in the Lorenz map, the critical point J_0 of the map (1) corresponds to the last intersection of the stable manifold of an equilibrium of the vector field with the Poincaré section before it does not return under the flow. Analogously, the critical circle J_1 corresponds to the last intersection of the unstable manifold of this equilibrium with the Poincaré section before it does not return under the backward flow.

The backward iterates of J_0 and the forward iterates of J_1 correspond to all intersections of these stable and unstable manifolds with the Poincaré section and they play a special role in the organization of the dynamics of (1) on the punctured complex plane. The preimages $J_{-k} := f^{-k}(J_0),\ k \geq 0$, of J_0 under the two inverses of the map consist of up to 2^k isolated points and we will refer to their union as the *backward critical set*

$$\mathcal{J}^- := \bigcup_{k\geq 0} J_{-k}. \tag{2}$$

The images $J_k := f^{k-1}(J_1),\ k \geq 1$, of J_1 are topological circles and we will refer to them as the circles in the *forward critical set*

$$\mathcal{J}^+ := \bigcup_{k\geq 1} J_k. \tag{3}$$

We will also simply refer to the union of the forward and backward critical sets as the *critical set* $\mathcal{J} := \mathcal{J}^+ \cup \mathcal{J}^-$.

In the parameter regime we consider, the map (1) has three fixed points denoted p, q^+ and q^-. The point p is a saddle and the points $q^\pm$ are sinks in the upper and lower half plane, respectively. The points $q^\pm$ become sources in Neimarck-Sacker bifurcations when the parameters are moved towards the chaotic regime. If c is real, the map is symmetric under complex conjugation, p lies on the positive real axis and $q^\pm$ are complex conjugates.

In addition to the critical set and the fixed points, the overall dynamics of the map (1) is organized by the stable and unstable sets of p: For a given neighborhood V of p, the *local stable manifold* $W^s_{loc}(p)$ is defined as

$$W^s_{\mathrm{loc}}(p) := \{z \in \mathbb{C} : f^k(z) \in V \text{ for all } k \geq 0\}.$$

The local stable manifold is tangent to the stable eigenspace at p. The *stable set* $W^s(p)$ is defined as all preimages of the local stable manifold $W^s_{loc}(p)$ [49]; i.e.,

$$W^s(p) := \bigcup_{k\geq 0} f^{-k}(W^s_{\rm loc}(p)). \tag{4}$$

In the study of diffeomorphisms, the stable set $W^s(p)$ is an immersed manifold. However, the noninvertible map (1) has multiple preimages and the stable set $W^s(p)$ consists of infinitely many branches; therefore, it is not an immersed manifold [42]. The infinitely many branches of $W^s(p)$ have the points in the backward critical set $\mathcal{J}^-$ as branch points. In fact, the intersection of $W^s(p)$ and $\mathcal{J}^-$ is empty, but the closure of the stable set is

$$\overline{W^s(p)} = W^s(p) \cup \mathcal{J}^+.$$

Similarly, for a given neighborhood V of p, the *local unstable manifold* $W^u_{\rm loc}(p)$ is defined as the local stable set with respect to the local inverse $f^{-1}_{\rm loc}$ of f that satisfies $f^{-1}_{\rm loc}(p) = p$. In other words,

$$W^u_{\rm loc}(p) := \{z \in \mathbb{C} : (f^{-1}_{\rm loc})^k(z) \in V \text{ for all } k \geq 0\},$$

and it is tangent to the unstable eigenspace at p. The *unstable set* $W^u(p)$ is defined as all images of the local unstable set $W^u_{\rm loc}(p)$ [49]; i.e.,

$$W^u(p) := \bigcup_{k\geq 0} f^{k}(W^u_{\rm loc}(p)). \tag{5}$$

For a diffeomorphism, the set $W^u(p)$ is an immersed manifold, but for a noninvertible map, the images of $W^u_{\rm loc}(p)$ form a single continuous curve that may have self-intersections. Due to the rotational symmetry of map (1), $W^u(p)$ intersects itself at a point $f(z)$, with $z \in \mathbb{C}^*$, if the two preimages z and $-z$ are both contained in $W^u(p)$.

In this paper, we consider the two-dimensional noninvertible map (1) and study the bifurcations of the forward critical, backward critical, stable and unstable sets that are involved in the transition between the nonchaotic parameter regime and the regime of existence of the wild Lorenz-like attractor. These bifurcations are:

1. the *homoclinic tangency*, where the stable set $W^s(p)$ and the unstable set $W^u(p)$ become tangent; see section 3.1;

2. the *forward critical tangency*, where the stable set $W^s(p)$ becomes tangent to the circles in the forward critical set $\mathcal{J}^+$; see section 3.2;

3. the *backward critical tangency*, where a sequence of points in the backward critical set $\mathcal{J}^-$ lies on the unstable set $W^u(p)$; see section 4.1;

4. the *forward-backward critical tangency*, where a sequence of points in the backward critical set $\mathcal{J}^-$ lies on the circles in the forward critical set $\mathcal{J}^+$; see section 4.2.

Homoclinic tangencies are bifurcations that are also encountered in diffeomorphisms, but the other three bifurcations are new and specific to this type of noninvertible map. Note that the two sides of the unstable set $W^u(p)$ can become tangent in an *unstable tangency*; see section 3.1. Unlike the other four bifurcations, the unstable tangency only occurs due to the projection from the four-dimensional Poincaré return map to the two-dimensional map (1) and does not correspond to a bifurcation in the underlying vector field. Thus, it does not contribute to the generation of wild chaos. However, the first unstable tangency is used in [9] to define a region bounded by segments of the unstable set.

Our results indicate that these five types of tangency bifurcations appear consecutively in infinite sequences that accumulate on each other: As we move the parameters towards the wild chaotic regime, we first encounter a homoclinic tangency. This homoclinic tangency is the first of an infinite sequence of homoclinic tangencies accumulating on each homoclinic tangency. At or after the first homoclinic tangency, a first unstable tangency

occurs. Similar to the homoclinic tangency, an infinite sequence of unstable tangencies accumulates on each unstable tangency. After the first homoclinic tangency, the stable set $W^s(p)$ interacts with the curves in the forward critical set $\mathcal{J}^+$ in forward critical tangencies. There is no first forward critical tangency, but an infinite sequence of forward critical tangencies accumulates on each homoclinic tangency, because $\mathcal{J}^+$ accumulates on $W^u(p)$. When the parameters are moved further towards the wild chaotic regime, in addition to the three initial bifurcations, the unstable and the backward critical sets interact in a first backward critical tangency. This first backward critical tangency is followed by an infinite sequence of backward critical tangencies that accumulate on each backward critical tangency, because $W^u(p)$ accumulates on itself. After the first backward critical tangency, the forward critical set $\mathcal{J}^+$ and the backward critical set $\mathcal{J}^-$ interact in forward-backward critical tangencies. Since $\mathcal{J}^+$ accumulates on $W^u(p)$, an infinite sequence of forward-backward critical tangencies accumulates on each backward critical tangency.

Two-dimensional noninvertible maps have been studied for some time now; see, for example, the textbooks [1, 28, 42]. Famous examples include the coupled logistic map and polynomial maps. The classical examples of maps with two preimages fold the plane along a curve J_0 and map it onto one side of the image curve J_1 of J_0 in a 2-to-1 fashion. Often, J_0 is defined as the set of points where the Jacobian of the map is singular. The curves J_0 and J_1 are called *critical curves* or *"lignes critiques"* in the literature [40, 48]. In the case of fold maps, bifurcations of the critical curves with the boundaries of basins of attractions have been investigated in [4, 14, 32, 37, 41]. The approach taken in [19, 30, 36] reveals that the myriad of exotic transformations of basin boundaries for fold maps are different global manifestations of local tangencies of a stable or unstable set with the critical curves. The bifurcations we find for system (1) share some overall mechanisms with the results presented in [19, 30, 36], such as changes in the connectivity of the stable set and loop forming of the unstable set. However, the map (1) maps the plane onto itself in a 2-to-1 fashion that is different from that of fold maps. It doubles the angles in a way that is reminiscent of the complex quadratic map $z \mapsto z^2 + c$; in fact, for $a = 2$ and $\lambda = 1$, map (1) reduces to the complex quadratic map. Due to the different nature of the double-cover of the plane and the organization of the stable set, the bifurcations we find for map (1) are new and specific to this different class of noninvertible maps.

This paper is organized as follows. In section 2 we discuss the basic properties of map (1) and the roles of the forward and backward critical sets and the stable and unstable sets. In section 3 we explain the local behavior and the global consequences of the three initial tangency bifurcations that appear when the parameter c is decreased along the real line with $a = 0.8$ and $\lambda = 0.8$ fixed; these are the homoclinic, forward critical and unstable tangencies. In section 4 we introduce the two subsequent tangency bifurcations that occur when c is decreased further; these are the backward and forward-backward critical tangencies. In section 5 we present bifurcation diagrams in two parameters to show that one encounters the same sequences of bifurcations when the other parameters a and λ are varied, or when c has a small complex part. In section 6 we explain the Lorenz-like construction of the five-dimensional vector field and its reduction to map (1) and present the implications of the tangency bifurcations of (1) for this vector field. We end with conclusions in section 7.

In the appendix to this paper, we explain how we use the algorithm proposed in [34] and implemented in the DsTool environment [8, 18, 35] to compute the stable and unstable sets of (1). Furthermore, we describe how we modify the boundary value problem proposed in [10] for the continuation of homoclinic tangencies in order to continue the other tangency bifurcations encountered in (1). We then changed the associated algorithm in Cl_MatContM [15, 22, 25] to follow all bifurcation curves in two parameters.

2 Background and Notation

In this section we discuss the basic properties of map (1) and the role of the critical, stable and unstable sets in the dynamics on the complex plane.

2.1 Basic Properties of the Map

Figure 1 shows the action of the map (1) for the parameter values $a = 0.8$, $\lambda = 0.8$ and $c = 1$ in three steps. Panel (a) shows the punctured disk $\overline{\mathbb{D}}_2(0)\backslash J_0$ with a yellow-to-red color gradient. The critical point $J_0 = \{0\}$

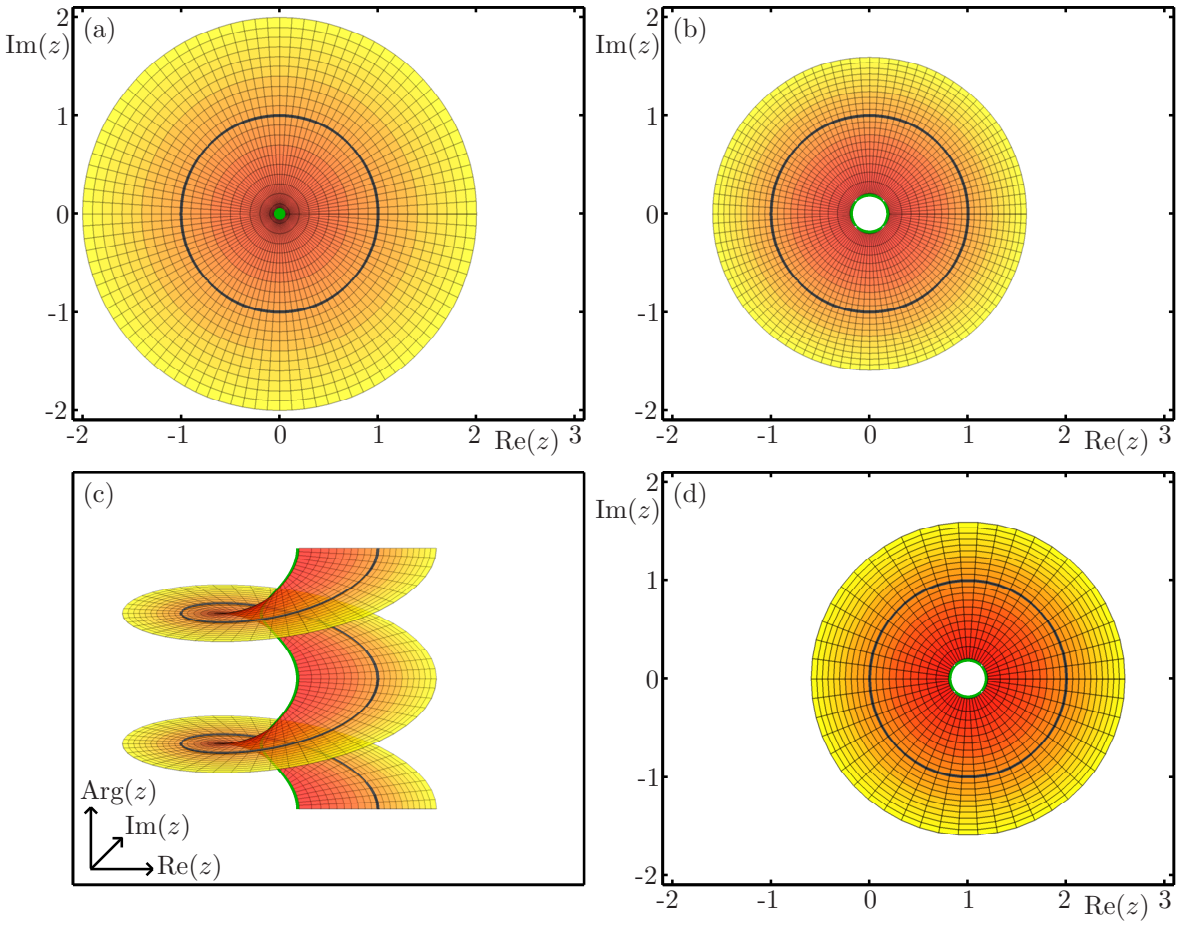

Figure 1: The action of the map (1) on the punctured disk $\overline{\mathbb{D}}_2(0)\backslash J_0$ (yellow-orange), the unit circle (black circle) and the critical point J_0 (green dot) for the parameter values $a = 0.8$, $\lambda = 0.8$ and $c = 1$. Panel (a) shows the punctured disk $\overline{\mathbb{D}}_2(0)\backslash J_0$; panel (b) illustrates the transformation via $|z| \mapsto 1 - \lambda + \lambda|z|^a$ to the annulus $\{z : 1 - \lambda < |z| \leq 1 - \lambda + \lambda 2^a\}$. Then the angles are doubled via $z/|z| \mapsto (z/|z|)^2$ as illustrated in $(\mathrm{Re}(z), \mathrm{Im}(z), \mathrm{Arg}(z))$-space in panel (c), and finally the now double-covered annulus is translated by c to $\{z + c : 1 - \lambda < |z| \leq 1 - \lambda + \lambda 2^a\}$ as shown in panel (d).

is denoted by a green dot and the unit circle is highlighted in black. In the first step, the map (1) transforms $|z|$ to $1 - \lambda + \lambda|z|^a$, so $\overline{\mathbb{D}}_2(0)\backslash J_0$ is opened up to the annulus $\{z : 1 - \lambda < |z| \leq 1 - \lambda + \lambda 2^a\}$ as shown in Figure 1(b). In the second step, the angle doubling $z/|z| \mapsto (z/|z|)^2$ wraps this annulus twice around itself as illustrated in $(\mathrm{Re}(z), \mathrm{Im}(z), \mathrm{Arg}(z))$-space in Figure 1(c). Finally, in the third step, this double-covered annulus is translated by c as shown Figure 1(d) in the z-plane. Hence, the images of $\overline{\mathbb{D}}_2(0)\backslash J_0$ under the map (1) is $\{z + c : 1 - \lambda < |z| \leq 1 - \lambda + \lambda 2^a\}$ and its inner bound (the green circle in panel (d)) is the critical circle $J_1 = \partial\overline{\mathbb{D}}_{1-\lambda}(c)$.

Points in $\mathbb{C}\backslash\overline{\mathbb{D}}_{1-\lambda}(c)$ have two preimages under map (1), which are symmetric under rotation by π. We call the branch of preimages in the upper half plane and the positive real line the *first preimage*, denoted f_0^{-1}, and the branch in the lower half plane and the negative real line the *second preimage*, denoted f_1^{-1}. For $a, \lambda \in (0, 1)$,

$c \in \mathbb{C}$ and each point $z \in \mathbb{C}\backslash\overline{\mathbb{D}}_{1-\lambda}(c)$, they are given by

$$\begin{aligned} f_0^{-1}(z) &= +\left(\frac{|z-c|-1+\lambda}{\lambda}\right)^{1/a}\sqrt{\frac{z-c}{|z-c|}} \\ \text{and} \qquad f_1^{-1}(z) &= -\left(\frac{|z-c|-1+\lambda}{\lambda}\right)^{1/a}\sqrt{\frac{z-c}{|z-c|}}. \end{aligned} \tag{6}$$

Where it is defined, the k-th preimage $f^{-k}(z)$ of z consists of 2^k points; each of these points is given as a sequence of preimages

$$f_{s_k\cdots s_1}^{-k}(z) := f_{s_k}^{-1} \circ \cdots \circ f_{s_1}^{-1}(z),$$

where $(s_l)_{1\le l\le k} \in \{0,1\}^k$.

Though map (1) is not defined at the critical point J_0, we could think of the critical circle J_1 as the multivalued image of J_0 by looking at the limit

$$\left\{\lim_{r\to 0} f(re^{i\varphi}) \mid \varphi \in [0,2\pi)\right\} = \left\{(1-\lambda)e^{i2\varphi}+c \mid \varphi\in[0,2\pi)\right\} = J_1.$$

In particular, angles at J_0 correspond to points on J_1: For each $\varphi \in [0,2\pi)$ the "image" of the angles $\varphi/2$ and $\varphi/2+\pi$ at J_0 is the point $(1-\lambda)e^{i2\varphi}+c$ on J_1.

For $|c| > 1-\lambda$, map (1) maps the disk $\overline{\mathbb{D}}_R(0)$ inside itself, where $R := 2|c|/(1-\lambda)$. Since $J_1 \subset \overline{\mathbb{D}}_R(0)$, the entire forward critical set $\mathcal{J}^+$ is bounded inside $\overline{\mathbb{D}}_R(0)$. Furthermore, the circles in $\mathcal{J}^+$ are elongated closed curves that contain segments with very high curvature. On the other hand, the backward critical set $\mathcal{J}^-$ is unbounded.

Figure 2(a) illustrates the critical set $\mathcal{J}$ for the parameter values $a = 0.8$, $\lambda = 0.8$ and $c = 1.3$. Here, we plot the circles $J_1, \ldots, J_{17} \subset \mathcal{J}^+$ and the points J_0, J_{-1}^0, J_{-1}^1, J_{-2}^{00}, J_{-2}^{01}, J_{-2}^{10}, J_{-2}^{11}, J_{-3}^{000}, J_{-3}^{111}, J_{-4}^{0000}, $J_{-4}^{1111} \in \mathcal{J}^-$. For $k = -1,-2,-3,-4$, these points in J_{-k} are labeled according to a sequence of preimages of J_0, written as $J_{-k}^{s_k\cdots s_1} := f_{s_k\cdots s_1}^{-k}(J_0)$ with $(s_l)_{1\le l\le k} \in \{0,1\}^k$. The critical point J_0 and its first and second preimages J_{-1}^0 and J_{-1}^1 lie on the imaginary axis. All four points in the set J_{-2} are shown, where the points J_{-2}^{00} and J_{-2}^{10} are the first and second preimages of J_{-1}^0 and the points J_{-2}^{01} and J_{-2}^{11} are the first and second preimages of J_{-1}^1. Of the higher-order preimages, only the next two first preimages J_{-3}^{000} and J_{-4}^{0000} of the point J_{-2}^{00} and the next two second preimages J_{-3}^{111} and J_{-4}^{1111} of the point J_{-2}^{11} are shown. At these parameter values, all other points in $\mathcal{J}^-$ lie outside the region shown in Figure 2.

2.2 The Stable and Unstable Sets

The unstable set $W^u(p)$ of the saddle point p of map (1) was defined in eq. (5). We denote the sides of $W^u(p)$ that start in p and go towards the upper or lower half plane with $W_+^u(p)$ and $W_-^u(p)$, respectively. Analogously to $\mathcal{J}^+$, $W^u(p)$ stays bounded in the disk $\overline{\mathbb{D}}_R(0)$ if $|c| > 1-\lambda$.

Figure 2(b) shows the critical set $\mathcal{J}$ (green), the saddle point p (black cross), the two sources q^+ and q^- (red squares) and the unstable set $W^u(p)$ (red) of the map (1) at the same parameter values as in Figure 2(a). The saddle point p is located at approximately 3.85 on the real axis, the sources $q^\pm$ lie at approximately $0.85 \pm 1.22i$. The two sides $W_+^u(p)$ and $W_-^u(p)$ of $W^u(p)$ are shown up to arclength 45 each. Since $c = 1.3 \in \mathbb{R}$, $W_\pm^u(p)$ and $q^\pm$ are symmetric under complex conjugation, respectively. At these parameter values, $W^u(p)$ is an immersed manifold, because it does not intersect itself.

The stable set $W^s(p)$ of p was defined in eq. (4). There is a unique branch of $W^s(p)$ that contains the fixed point p, which we call the *primary manifold* $W_0^s(p)$. Note that the local stable manifold $W_{\text{loc}}^s(p)$ is contained in $W_0^s(p)$. Since $W^s(p)$ is formed by all preimages of $W_{\text{loc}}^s(p)$ or $W_0^s(p)$ and the map (1) has two preimages, $W^s(p)$ consists of infinitely many branches. Furthermore, it is unbounded and an infinite number of its branches go to infinity. If $a, \lambda \in (0,1)$ are sufficiently close to 1 and $\text{Im}(c)$ is sufficiently small, the primary manifold $W_0^s(p)$ intersects the critical circle J_1. Then, $W_0^s(p)$ goes from J_0 through p to infinity and the critical point J_0 lies in the closure of $W_0^s(p)$. Therefore, $\mathcal{J}^-$ lies in the closure of $W^s(p)$ and, more specifically, the points in $\mathcal{J}^-$ act as branch points of $W^s(p)$: at each point in $\mathcal{J}^-$ at least four branches of $W^s(p)$ connect. If the primary

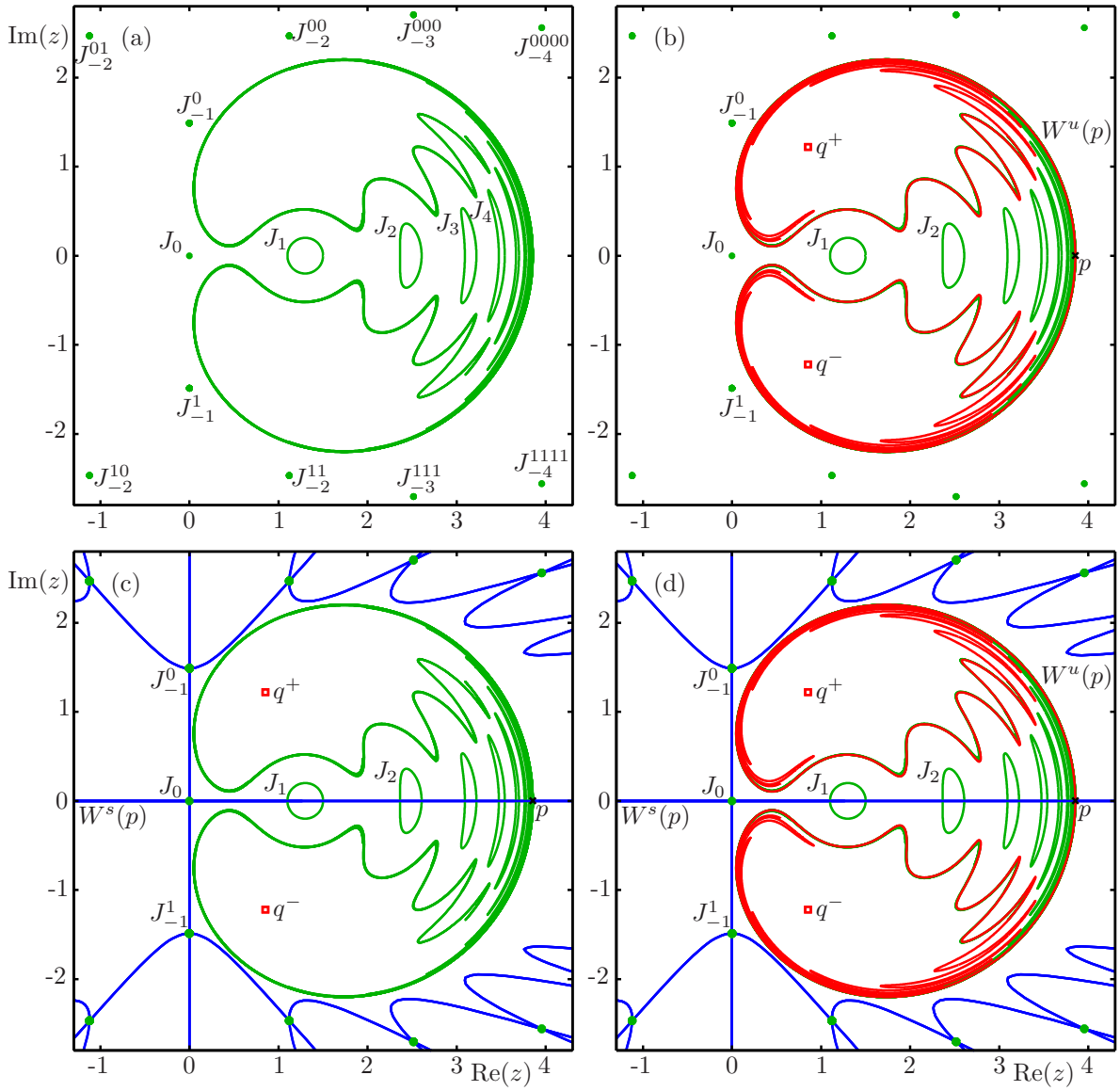

Figure 2: Organization of the phase plane in the nonchaotic parameter regime for $a = 0.8$, $\lambda = 0.8$ and $c = 1.3$. Panel (a) shows the forward critical set $\mathcal{J}^+$ (green curves) and the backward critical set $\mathcal{J}^-$ (green dots); panel (b) shows the critical set $\mathcal{J} = \mathcal{J}^+ \cup \mathcal{J}^-$, the saddle fixed point p (black cross), the sources q^+ and q^- (red squares) and the unstable set $W^u(p)$; panel (c) shows $\mathcal{J}$, the fixed points p, q^+ and q^- and the stable set $W^s(p)$ (blue curves); panel (d) shows the fixed points p, q^+ and q^- and the sets $\mathcal{J}$, $W^s(p)$ and $W^u(p)$ together.

manifold $W_0^s(p)$ does not intersect J_1, it goes from one of the sources q^+ or q^- through p to infinity or from infinity through p to infinity. We will discuss this case in more detail in Section 5.4.

Figure 2(c) shows the critical set $\mathcal{J}$ (green), the saddle point p, the sources $q^\pm$ and the stable set $W^s(p)$ (blue) at the same parameter values as in Figures 2(a) and (b). Since $c = 1.3 \in \mathbb{R}$, the primary manifold $W_0^s(p)$ is the positive real axis and $W^s(p)$ is symmetric under rotation by π and under complex conjugation. The primary manifold $W_0^s(p)$ intersects the critical circle J_1 in the two points $c + 1 - \lambda = c + (1 - \lambda)e^0$ and $c - 1 + \lambda = c + (1 - \lambda)e^{i\pi}$; hence the preimages of $W_0^s(p)$ in $W^s(p)$ connect to J_0 with the slopes e^0, $e^{i\pi/2}$, $e^{i\pi}$

and $e^{3\pi/2}$. Correspondingly, all other points in $\mathcal{J}^-$ each connect four branches of $W^s(p)$.

Figure 2(d) shows $\mathcal{J}$, $W^s(p)$, $W^u(p)$ and the fixed points p, q^+ and q^- together. At this set of parameters, the sets $\mathcal{J}$, $W^s(p)$ and $W^u(p)$ interact with each other only in the intersection of $W_0^s(p)$ and J_1 mentioned above. The intersection points of $\mathcal{J}^+$ and $W_0^s(p)$ accumulate on p and the circles in the forward critical set $\mathcal{J}^+$ accumulate on $W^u(p)$, correspondingly.

Figure 2(d) is shown in normal coordinates; in order to study the global behavior of map (1), some figures in Sections 3, 4 and 5 will show a compactification of $\mathbb{C}$ to the Poincaré disk via the transformation

$$\begin{aligned} T : \mathbb{C} \cup \{\infty\} &\to \overline{\mathbb{D}}_1(0) \\ z &\mapsto \frac{z}{1+|z|}. \end{aligned} \tag{7}$$

This transformation maps the origin to itself and infinity onto the unit circle.

3 Initial tangency bifurcations

In the transition from nonchaotic to wild chaotic dynamics in map (1) the forward critical set $\mathcal{J}^+$, the backward critical set $\mathcal{J}^-$, the stable set $W^s(p)$ and the unstable set $W^u(p)$ interact with each other in four types of local tangency bifurcations; see the list in Section 1. Since $\mathcal{J}^+$ accumulates on $W^u(p)$ and, after the first homoclinic tangency, $W^u(p)$ and $W^s(p)$ accumulate on themselves, we will encounter infinite sequences of all types of tangency bifurcations. Globally, these sequences of bifurcations lead to the appearance of homoclinic orbits, reconnections of the stable set $W^s(p)$, self-intersections of the unstable set $W^u(p)$ and, as a consequence, to a reorganization of the phase space; see sections 3.3 and 4.3.

In this section we explain the local behavior and the global consequences of the first three types of tangency bifurcations, that appear when the parameters $a = 0.8$ and $\lambda = 0.8$ are fixed and c is decreased along the real line from $c = 1.3$. For $c = 1.3$ the map (1) is not chaotic, the stable set $W^s(p)$ and the unstable set $W^u(p)$ do not intersect and $W^u(p)$ does not intersect itself; see Figure 2.

3.1 The homoclinic tangency

At a *homoclinic tangency* the unstable set $W^u(p)$ is tangent to the stable set $W^s(p)$. An intersection point of $W^s(p)$ and $W^u(p)$ is called a *homoclinic point*. It belongs to a *homoclinic orbit*, which converges to the saddle point p under forward and backward time. Since map (1) has two preimage branches, this means that a homoclinic point has a sequence of preimages converging to p. However, the homoclinic tangency does not involve the critical set $\mathcal{J}$, so that it is essentially the same as for diffeomorphisms; see [26] and [49].

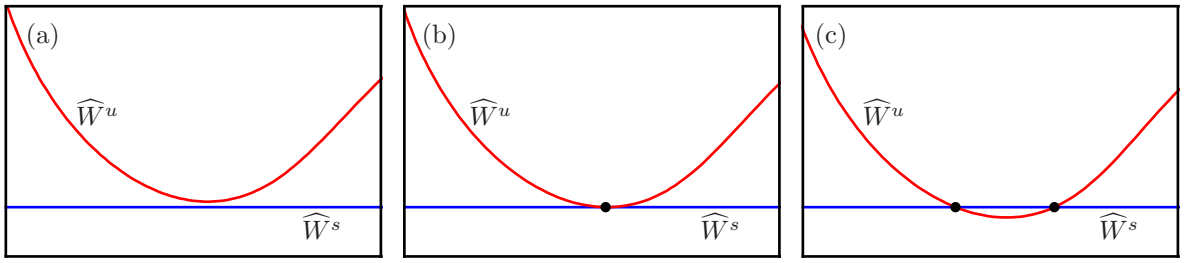

Figure 3: Local pictures of a segment $\widehat{W}^s$ of the stable set $W^s(p)$ (blue curve), a segment $\widehat{W}^u$ of the unstable set $W^u(p)$ (red curve) and their intersection points (black dots) for $a = 0.8$ and $\lambda = 0.8$, at $c = 1.27$ before the first homoclinic tangency in panel (a), at $c \approx 1.266$ at the tangency in panel (b), and at $c = 1.26$ after the tangency in panel (c).

Figure 3 shows the local unfolding of the first homoclinic tangency of a segment $\widehat{W}^s$ of the stable set $W^s(p)$ and a segment $\widehat{W}^u$ of the unstable set $W^u(p)$. Panel (a) shows $\widehat{W}^s$ and $\widehat{W}^u$ before the homoclinic tangency

where they do not intersect. Panel (b) shows the moment of the bifurcation when $\widehat{W}^s$ and $\widehat{W}^u$ are tangent at the homoclinic point indicated by a black dot. This homoclinic point belongs to a nongeneric homoclinic orbit. At $c = 1.26$ after the bifurcation this homoclinic point has split up into two homoclinic points marked by the two black intersection points of $\widehat{W}^s$ and $\widehat{W}^u$ in panel (c), which belong to two generic homoclinic orbits.

All images of a homoclinic tangency and the sequence of its preimages that stays on $W^u(p)$ are homoclinic tangencies as well. Therefore, at a homoclinic tangency, one single homoclinic orbit is born and splits into two homoclinic orbits after the bifurcation.

Since the two sides $W^u_+(p)$ and $W^u_-(p)$ of $W^u(p)$ are separated by the primary manifold $W^s_0(p)$ of the stable set $W^s(p)$, $W^u(p)$ does not intersect itself before the first homoclinic tangency. This means that each point of $W^u(p)$ has one unique sequence of preimages converging to the saddle point p. After or at the first homoclinic tangency $W^u_+(p)$ and $W^u_-(p)$ start interacting with each other in an *unstable tangency*. This type of tangency gives rise to points on $W^u(p)$ that have two distinct sequences of preimages converging to p that lie on the two sides of $W^u(p)$. It can only occur in noninvertible maps, since the unstable sets in diffeomorphisms are immersed manifolds and, therefore, are free of self-intersections.

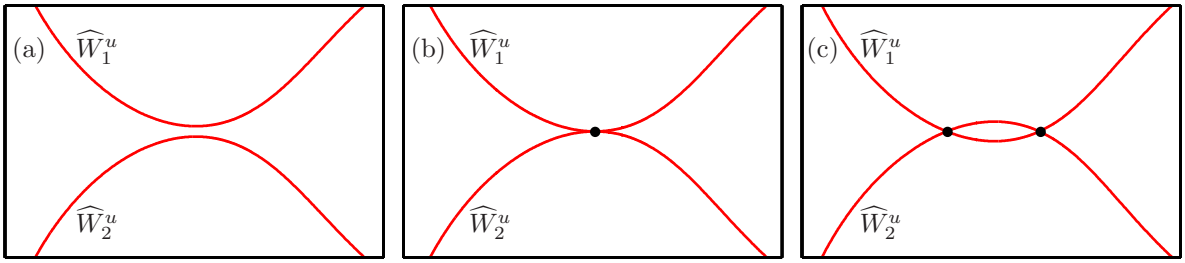

Figure 4: Local pictures of two segments $\widehat{W}^u_1$ and $\widehat{W}^u_2$ of the unstable set $W^u(p)$ (red curve) and their intersection points (black dots) for $a = 0.8$, $\lambda = 0.8$, at $c = 1.27$ before the first unstable tangency in panel (a), at $c \approx 1.266$ at the tangency in panel (b) and at $c = 1.26$ after the tangency in panel (c).

Figure 4 shows the local unfolding of the first unstable tangency of two segments $\widehat{W}^u_1 \subset W^u_+(p)$ and $\widehat{W}^u_2 \subset W^u_-(p)$ for the same parameter values as the unfolding of the first homoclinic tangency shown in Figure 3. Panel (a) shows $\widehat{W}^u_1$ and $\widehat{W}^u_2$ at $c = 1.27$, before the first unstable tangency. Before the bifurcation, $\widehat{W}^u_1$ and $\widehat{W}^u_2$ do not intersect. Panel (b) shows the moment of the bifurcation when $\widehat{W}^u_1$ and $\widehat{W}^u_2$ are tangent at the point indicated by a black dot. After the bifurcation this point has split up into two intersection points shown as black dots in panel (c). Each of these points now has one sequence of preimages converging to p on $W^u_+(p)$ and one sequence of preimages converging to p on $W^u_-(p)$.

All images, but only a finite sequence of preimages of an unstable tangency are unstable tangencies as well; the preimages of an unstable tangency are only unstable tangencies as long as the sequences of preimages coincide. This finite sequence of preimages ends in the point of self-intersection of $W^u(p)$ that has its two preimages on the two sides of $W^u(p)$. Therefore, at an unstable tangency, two orbits are born that converge to p under backward iteration and coincide from some point under forward iteration. After the bifurcation, these orbits split into four orbits that converge to p under backward iteration and each two corresponding orbits coincide from some point under forward iteration.

For real c, the two sides $W^u_+(p)$ and $W^u_-(p)$ are complex conjugated, and, therefore, at each homoclinic tangency of $W^u_+(p)$ and $W^s_0(p)$, we also have a tangency of $W^u_-(p)$ and $W^s_0(p)$; see Figure 4. In particular, for $c \in \mathbb{R}$, the first homoclinic and the first unstable tangency take place at the same time. For $c \in \mathbb{C}\backslash\mathbb{R}$, however, homoclinic tangencies and unstable tangencies generally occur at different parameter values and, in particular, the first unstable tangency occurs *after* the first homoclinic tangency, because $W^s_0(p)$ separates the two sides of $W^u(p)$.

As we will discuss in Section 6.3, the unstable tangency does not correspond to any bifurcation in the underlying n-dimensional vector field, but only occurs due to the reduction to the two-dimensional map (1).

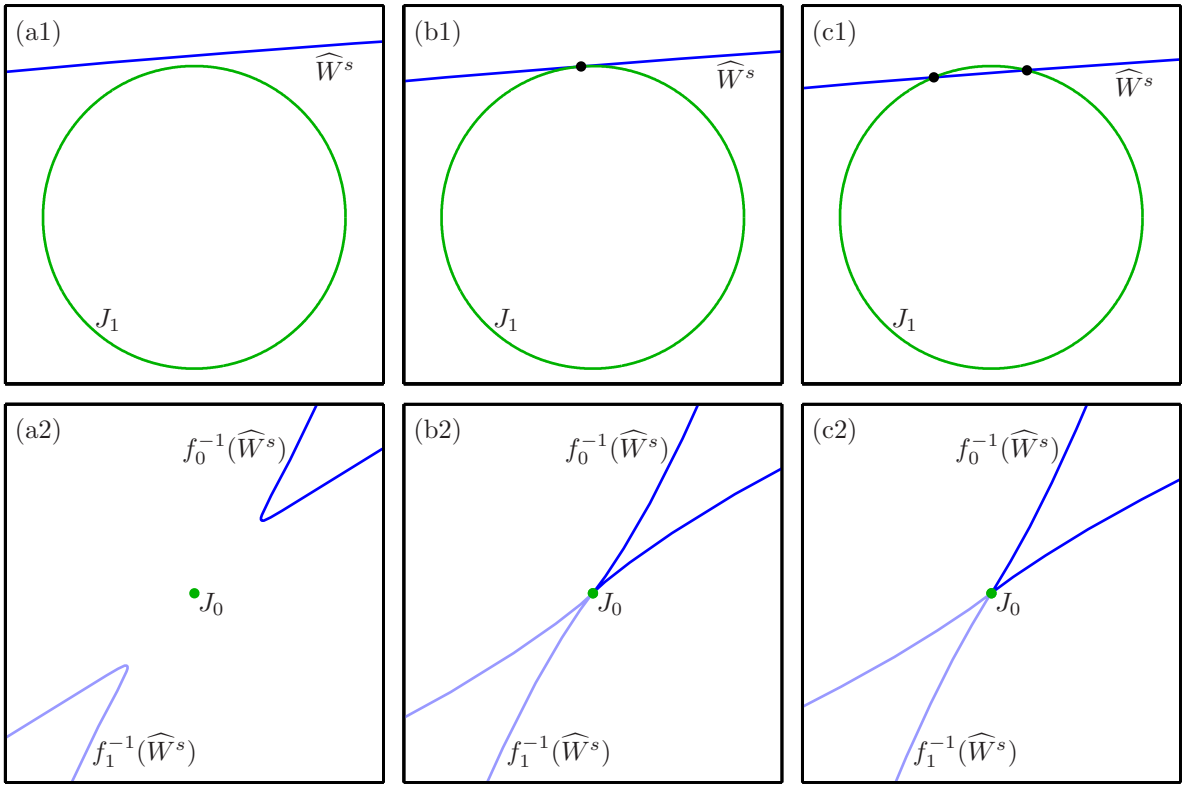

Figure 5: Local pictures of the stable set $W^s(p)$ (blue curve) with the critical circle J_1 (green circle) in the first row and the corresponding preimages with the critical point J_0 (green dot) in the second row before, approximately at and after a forward critical tangency. The parameter values are $a = 0.8$, $\lambda = 0.8$ and $c = 1.25$ in column (a), $c \approx 1.234$ in column (b), and $c = 1.22$ in column (c). The top row shows a segment $\widehat{W}^s \subset W^s(p)$ near J_1 and the bottom row shows its preimages $f_0^{-1}(\widehat{W}^s)$ (blue) and $f_1^{-1}(\widehat{W}^s)$ (light blue) in $W^s(p)$ near J_0.

Therefore, we do not see it as a crucial ingredient in the transition to wild chaos and will focus our analysis on the other four tangency bifurcations.

3.2 The forward critical tangency

We now consider the *forward critical tangency* where a branch of the stable set $W^s(p)$ is tangent to a circle in the forward critical set $\mathcal{J}^+$; as a consequence, certain higher-order preimage branches each split into two disconnected segments at points in the backward critical set $\mathcal{J}^-$.

Figure 5 shows how the forward critical tangency unfolds with images before, at and after a forward critical tangency. The panels in the top row of Figure 5 show a local segment $\widehat{W}^s \subset W^s(p)$ near J_1; the bottom row shows its preimages $f_0^{-1}(\widehat{W}^s)$ (dark blue) and $f_1^{-1}(\widehat{W}^s)$ (light blue) near J_0. Figure 5(a) shows the situation before the forward critical tangency; here, $\widehat{W}^s$ does not intersect J_1 and its two preimages $f_0^{-1}(\widehat{W}^s)$ and $f_1^{-1}(\widehat{W}^s)$ are not connected to J_0. At the moment of bifurcation, $\widehat{W}^s$ is tangent to J_1, shown in panel (b1). Therefore, $f_0^{-1}(\widehat{W}^s)$ and $f_1^{-1}(\widehat{W}^s)$ connect up with J_0; more precisely, the segment $\widehat{W}^s$ intersects J_1 in exactly one point, namely, at $(1-\lambda)e^{i\varphi} + c$ for some $\varphi \in [0, \pi)$; as a consequence, $f_0^{-1}(\widehat{W}^s)$ and $f_1^{-1}(\widehat{W}^s)$ consist of two segments each that form cusps at J_0 at angles $\varphi/2$ and $\varphi/2 + \pi$, respectively; see panel (b2). At $c = 1.22$ after the bifurcation $\widehat{W}^s$ intersects J_1 in two points, shown as black dots in Figure 5(c1). The segment of $\widehat{W}^s$ between these points does not have a preimage. Hence the two segments of $f_0^{-1}(\widehat{W}^s)$ and the two segments of $f_1^{-1}(\widehat{W}^s)$

open up their angle at J_0 according to the location of the two intersection points on J_1; see panel (c2).

All images of a forward critical tangency between $W^s(p)$ and a circle in $\mathcal{J}^+$ are forward critical tangencies, but only a certain finite sequence of preimages form forward critical tangencies. As a consequence of the tangency between $W^s(p)$ and J_1, preimages of the corresponding segment of $W^s(p)$ split up into two segments not only at J_0, but at all points in the backward critical set $\mathcal{J}^-$. This way, a forward critical tangency gives rise to a reconnection of the stable set $W^s(p)$ at all points in the backward critical set $\mathcal{J}^-$.

3.3 Global consequences of the initial tangency bifurcations

Recall that, if the primary manifold $W^s(p)$ intersects the critical circle J_1, the forward critical set $\mathcal{J}^+$ accumulates on the unstable set $W^u(p)$. In addition, after the first homoclinic tangency, $W^u(p)$ accumulates on itself: The points on the homoclinic orbits accumulate on the saddle fixed point p on $W^u(p)$ and the segments of $W^u(p)$ between these points accumulate on $W^u(p)$, accordingly. For the same reason, the stable set $W^s(p)$ accumulates on itself after the first homoclinic tangency.

This complicated accumulation of $\mathcal{J}^+$ and $W^u(p)$ on $W^u(p)$ and $W^s(p)$ on itself leads to complicated accumulating sequences of bifurcations: Immediately after the first homoclinic tangency, an infinite sequence of homoclinic tangencies accumulates on each homoclinic tangency, an infinite sequence of unstable tangencies accumulates on each unstable tangency and an infinite sequence of forward critical tangencies accumulates on each homoclinic tangency. Globally these infinitely many bifurcations reorganize the dynamics of map (1) on the entire complex plane. We illustrate this for a series of decreasing values of c.

Figure 6 shows the three fixed points p, q^+ and q^- the stable set $W^s(p)$, the unstable set $W^u(p)$ and the critical set $\mathcal{J}$ on the Poincaré disk for $a = 0.8$ and $\lambda = 0.8$ and $c = 1.3,\ 1.27,\ 1.26$ and 1.23 in panels (a)–(d), respectively. We show $W^s(p)$ up to the 13th preimage of the primary manifold $W^s_0(p)$. Panel (a) shows the situation at the same parameter values as in Figure 2; this is well before the first homoclinic tangency. Here, $W^s(p)$ and $W^u(p)$ do not intersect, the only intersection points of $W^s(p)$ with $\mathcal{J}^+$ are the two intersection points of each $J_k \subset \mathcal{J}^+$ with $W^s_0(p)$, and four branches of $W^s(p)$ connect up accordingly with $J_{-k} \in \mathcal{J}^-$. Panel (b) shows the situation at $c = 1.27$ immediately before the first homoclinic tangency. We note that $W^u(p)$ lies closer to $W^s(p)$. Panel (c) shows the situation at $c = 1.26$ shortly after the first homoclinic and the first unstable tangency. In between the first homoclinic tangency at $c \approx 1.266$ and $c = 1.26$ an infinite sequence of homoclinic tangencies, an infinite sequence of unstable tangencies and an infinite sequence of forward critical tangencies occurred leading to all branches in $W^s(p)$ connecting up with each point in $\mathcal{J}^-$ in the way shown in Figure 5. Panel (d) shows the sets at $c = 1.23$, well after the first homoclinic tangency. Between $c = 1.26$ and $c = 1.23$, infinitely many additional homoclinic, unstable and forward critical tangencies occurred, where each of the latter ones led to two additional intersection points of $W^s(p)$ with each curve in $\mathcal{J}^+$ and four additional branches of $W^s(p)$ connecting up at each point in $\mathcal{J}^-$.

4 Subsequent tangency bifurcations

In this section we introduce two types of subsequent bifurcations that occur when c is decreased further along the real line. The first is the backward critical tangency, which is caused by the interaction of the unstable set $W^u(p)$ with the backward critical set $\mathcal{J}^-$. The other is the forward-backward tangency that is generated by the interaction of the forward critical set $\mathcal{J}^+$ with the backward critical set $\mathcal{J}^-$.

4.1 The backward critical tangency

At a *backward critical tangency* a segment of the unstable set $W^u(p)$ moves over a point in the backward critical set $\mathcal{J}^-$. After the bifurcation, there are two distinct points on this segment that map to the same point under an iterate of (1). As a consequence, the higher-order images of this segment have self-intersections and form loops around the circles in the forward critical set $\mathcal{J}^+$.

Figure 7 shows how the backward critical tangency unfolds with images before, at and after a backward critical tangency. The panels in the top row of Figure 7 show the critical point J_0, a segment $\widehat{W}^u \subset W^u(p)$ and

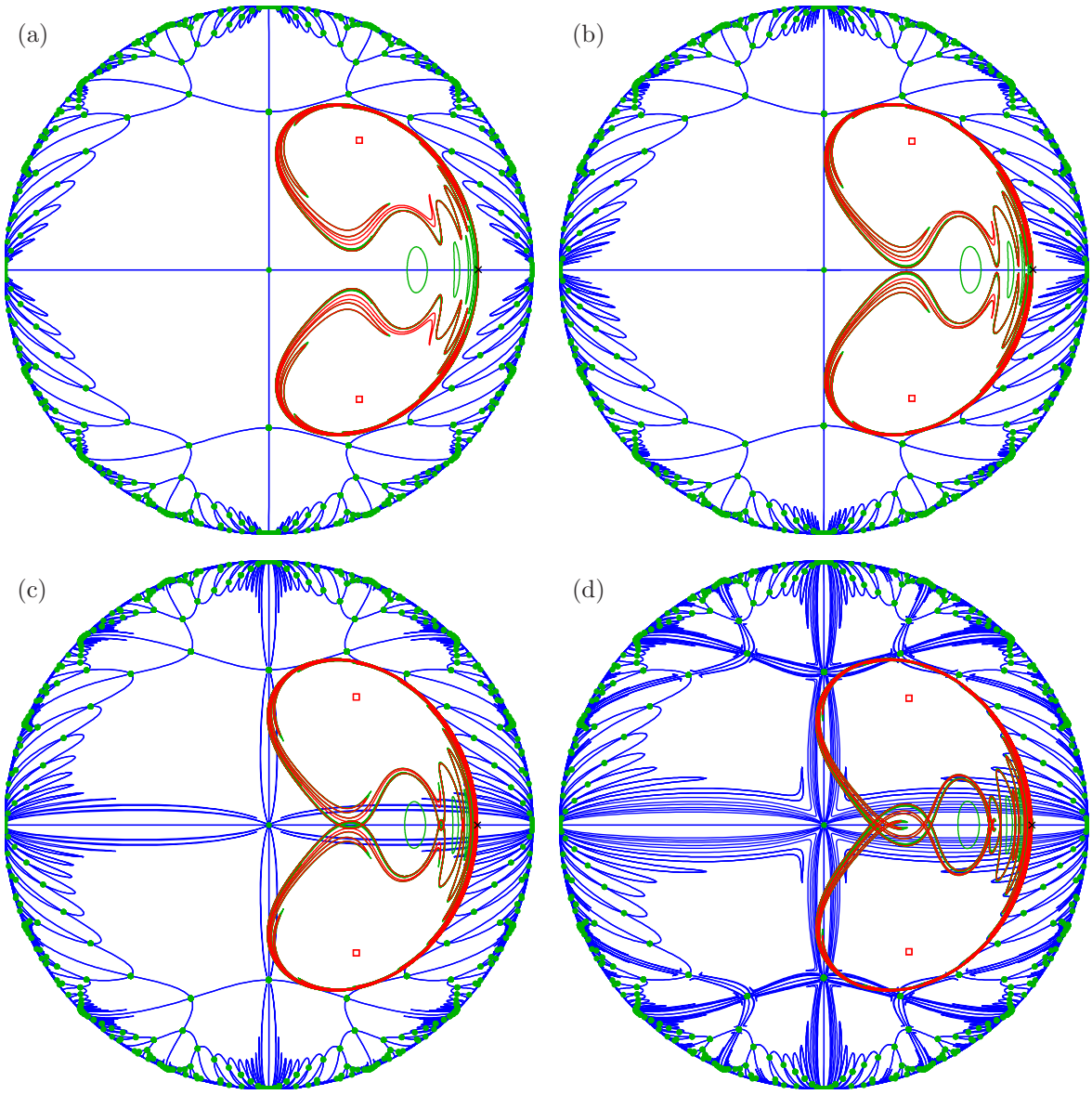

Figure 6: The stable set $W^s(p)$ (blue curves), unstable set $W^u(p)$ (red curve) and critical set $\mathcal{J}$ (green) on the Poincaré disk for $a = 0.8$, $\lambda = 0.8$, at $c = 1.3$ (a), at $c = 1.27$ (b), at $c = 1.26$ (c) and at $c = 1.23$ (d).

its rotationally symmetric partner $-\widehat{W}^u$, which is defined by

$$-\widehat{W}^u := \{z : -z \in \widehat{W}^u\} = f_1^{-1}(f(\widehat{W}^u)).$$

Note that $-\widehat{W}^u$ is not contained in $W^u(p)$. The bottom row shows the critical circle J_1 and the image $f(\widehat{W}^u) = f(-\widehat{W}^u) \subset W^u(p)$. We associate a direction with $\widehat{W}^u$, indicated by the arrows, which imposes a direction for $f(\widehat{W}^u)$. The first column shows the position of J_0, J_1, $\widehat{W}^u$ and $-\widehat{W}^u$ before the bifurcation. In Figure 7(a1), $\widehat{W}^u$ and $-\widehat{W}^u$ do not intersect, so in panel (a2) $f(\widehat{W}^u)$ does not intersect itself. Notice that $f(\widehat{W}^u)$ goes around J_1 clockwise as indicated by the arrows. The second column shows the bifurcation at the moment of tangency for $c \approx 1.143$. The critical point J_0 now lies on $\widehat{W}^u$ and is the only point in the intersection of $\widehat{W}^u$ and $-\widehat{W}^u$;

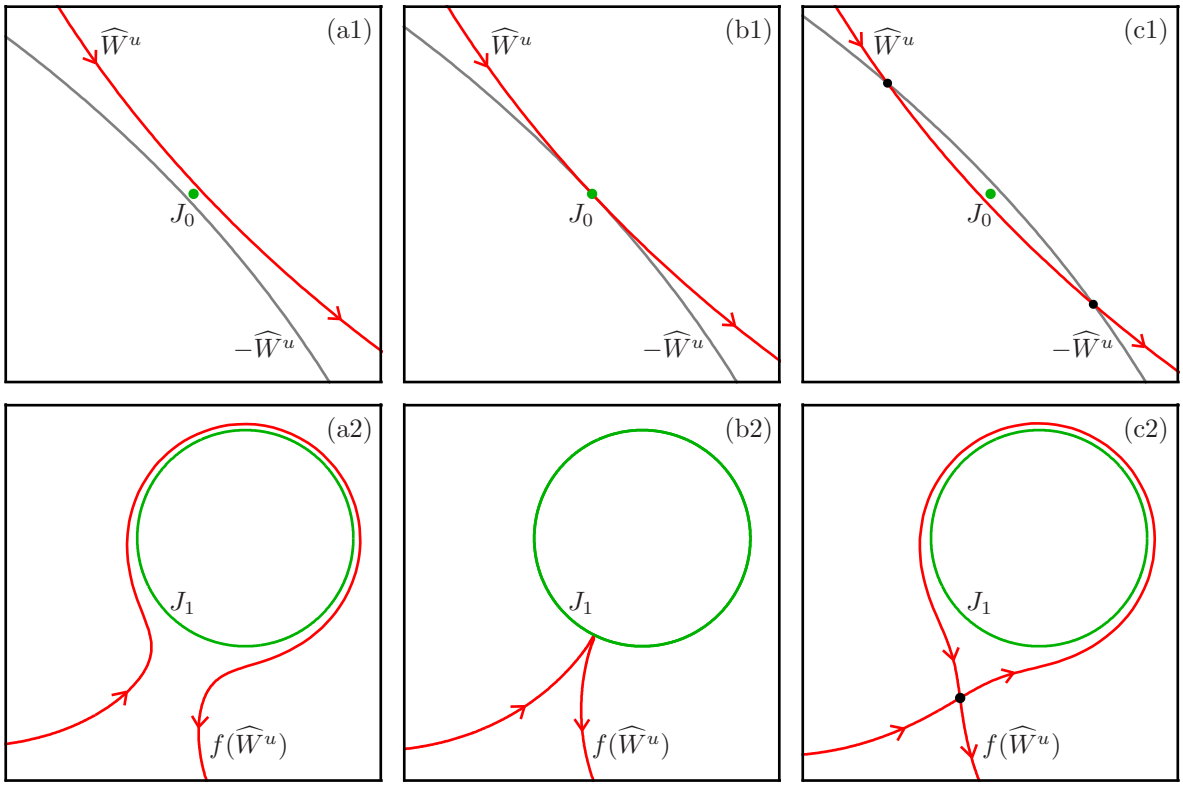

Figure 7: Local pictures of the unstable set $W^u(p)$ (red curve), its negative $-W^u(p)$ (gray curve) and the critical point J_0 (green dot) in the first row and $W^u(p)$ and the critical circle J_1 (green circle) in the second row before, approximately at and after the backward critical tangency. The parameter values are $a = 0.8$, $\lambda = 0.8$ and $c = 1.144$ in column (a), $c = 1.143$ in column (b) and $c = 1.142$ in column (c). The top row shows a segment $\widehat{W}^u \subset W^u(p)$ near J_0, its negative $-\widehat{W}^u$ and their intersection points (black dots); the bottom row shows their image $f(\widehat{W}^u) \subset W^u(p)$ near J_1 and the image of the intersection points (black dot).

see panel (b1). As a consequence, the image $f(\widehat{W}^u \backslash J_0)$ consists of two branches that form a cusp at J_1. If $e^{i\varphi}$ is the tangent vector of $\widehat{W}^u$ at J_0 for some $\varphi \in [0, \pi)$, then the cusp of $f(\widehat{W}^u)$ at J_1 is at the point $e^{i2\varphi} + c$. The direction on $f(\widehat{W}^u \backslash J_0)$ is the same as before the bifurcation. The third column shows the position of J_0, J_1, $\widehat{W}^u$ and $-\widehat{W}^u$ at $c = 1.142$, after the bifurcation. The segments $\widehat{W}^u$ and $-\widehat{W}^u$ now intersect in two points (black dots) in panel (c1). These two points map to the same point (denoted by the black dot) under the map (1) in panel (c2). The image $f(\widehat{W}^u)$ now intersects itself at this point and forms a loop around J_1. The directions of $f(\widehat{W}^u)$ below the point of self-intersection are locally the same as before the bifurcation, but $f(\widehat{W}^u)$ now goes around J_1 anti-clockwise, as indicated by the arrows.

If a point in the backward critical set $\mathcal{J}^-$ lies on $W^u(p)$ in a backward critical tangency, its images up to J_0 lie on $W^u(p)$ as well and it has a unique infinite sequence of preimages in $\mathcal{J}^-$ lying on $W^u(p)$. As a consequence, $W^u(p)$ forms cusps at all the circles in the forward critical set $\mathcal{J}^+$ and, after the bifurcation, $W^u(p)$ forms loops around all circles in $\mathcal{J}^+$.

Before the first backward critical tangency, $W^u_+(p)$ and $W^u_-(p)$ are immersed manifolds. Immediately afterwards, at least one of them exhibits loops around all the curves in $\mathcal{J}^+$ and is no longer an immersed manifold. The self-intersections of $W^u(p)$ generated in a backward critical tangency are of a different nature than the ones generated in an unstable tangency: in an unstable tangency, two intersections of $W^u_+(p)$ and $W^u_-(p)$ are born, which each corresponds to two sequences of preimages converging to p on $W^u_+(p)$ and $W^u_-(p)$, respectively.

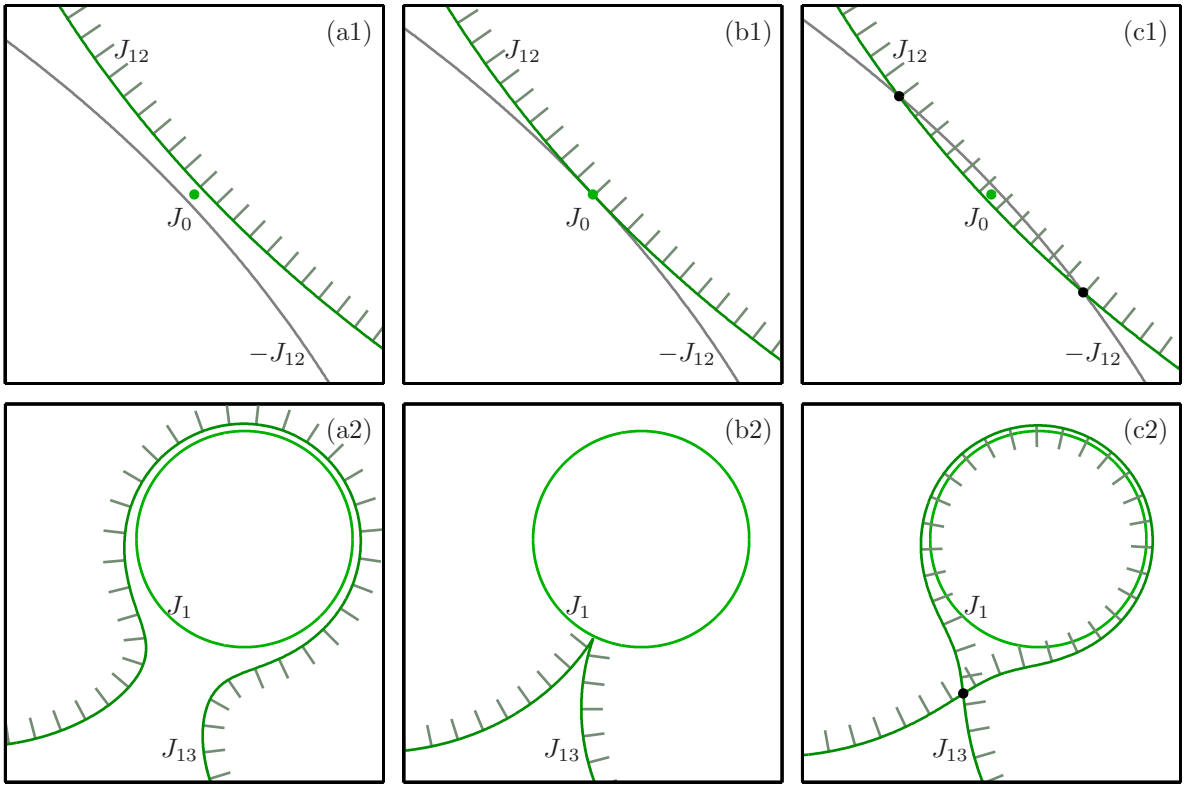

Figure 8: Local pictures of the forward critical set $\mathcal{J}^+$ (green curves), its negative $-\mathcal{J}^+$ (gray curves) and the critical point J_0 (green dot) in the first row and $\mathcal{J}^+$ and the critical circle J_1 (green circle) in the second row before, approximately at and after the forward-backward critical tangency. The parameter values are $a = 0.8$, $\lambda = 0.8$ and $c = 1.143$ in column (a), $c = 1.13953$ in column (b) and $c = 1.137$ in column (c). The top row shows a segment of the circle $J_{12} \subset \mathcal{J}^+$ near J_0, a segment of its negative $-J_{12}$ and their intersection points (black dots), the bottom row shows their image segment on the circle $J_{13} \subset \mathcal{J}^+$ near J_1 and the image of the intersection points (black dot).

In a backward critical tangency, one self-intersection of either $W^u_+(p)$ or $W^u_-(p)$ is born, which corresponds to two sequences of preimages converging to p on the same side $W^u_+(p)$ or $W^u_-(p)$. Furthermore, as we will discuss in Section 6.3, the backward critical tangency corresponds to a heteroclinic bifurcation in the underlying n-dimensional vector field, whereas the unstable tangency only occurs due to the reduction to the two-dimensional map (1).

4.2 The forward-backward critical tangency

At a *forward-backward critical tangency* a circle in $\mathcal{J}^+$ passes over a point in $\mathcal{J}^-$, which results in the images of this circle to form loops around all circles in $\mathcal{J}^+$. The forward-backward critical tangency is similar to the backward critical tangency, except that $\mathcal{J}^-$ interacts with $\mathcal{J}^+$ instead of $W^u(p)$.

Figure 8 shows the unfolding of a forward-backward critical tangency with images before, at and after the bifurcation. The panels in the top row of Figure 8 show the critical point J_0, segments of the circle J_{12} in $\mathcal{J}^+$ and its rotational symmetric partner $-J_{12}$, which is defined by

$$-J_{12} := \{z : -z \in J_{12}\}.$$

The bottom row shows the critical circle J_1 and segments of the image $J_{13} = f(J_{12}) = f(-J_{12})$. Note that

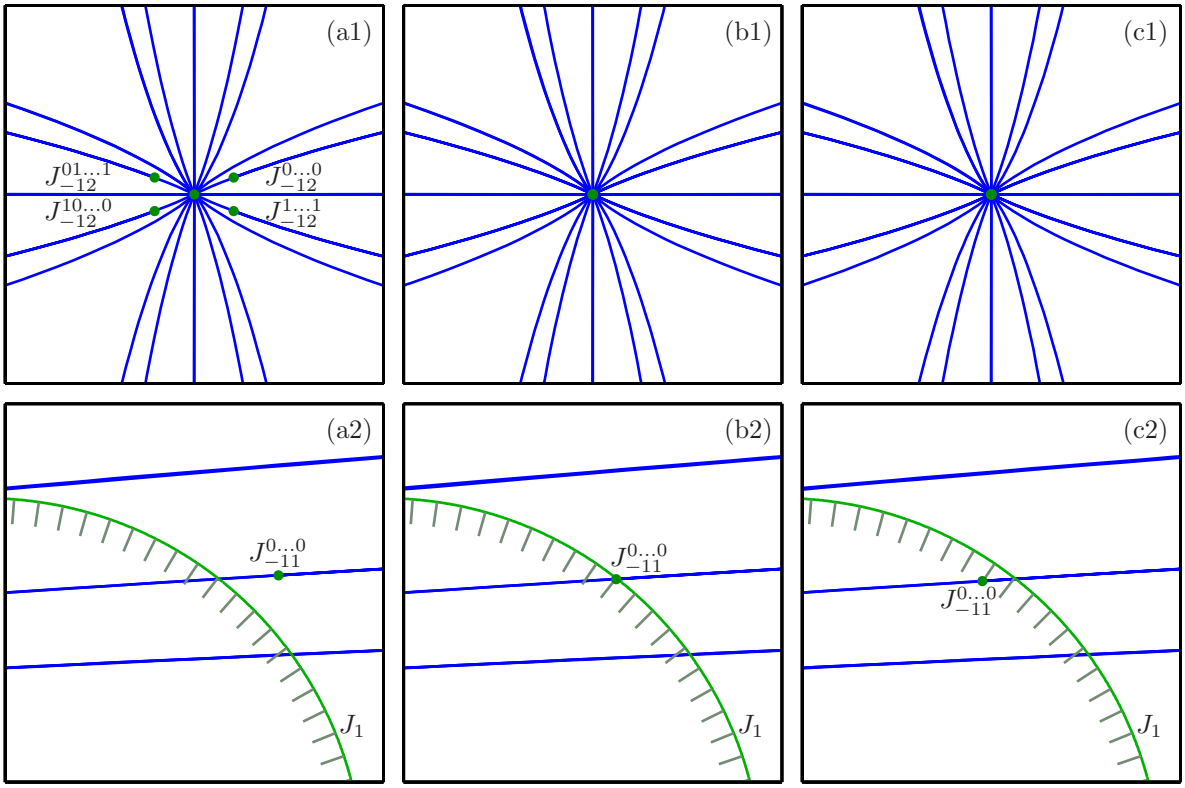

Figure 9: Local pictures of the stable set $W^s(p)$ (blue), the backward critical set $\mathcal{J}^-$ (green dots) and the critical circle J_1 (green circle) before, approximately at and after the forward-backward critical tangency. The parameter values are $a = 0.8$, $\lambda = 0.8$ and $c = 1.1396$ in column (a), $c = 1.13953$ in column (b) and $c = 1.1395$ in column (c). The top row shows four points $J_{-12}^{0\cdots0}$, $J_{-12}^{10\cdots0}$, $J_{-12}^{1\cdots1}$, $J_{-12}^{01\cdots1} \in \mathcal{J}^-$ near J_0, the bottom row shows the point $J_{-11}^{0\cdots0} \in \mathcal{J}^-$ near J_1.

$-J_{12} \not\subset \mathcal{J}^+$. The green direction markers indicate which sides correspond to the region bounded by the circles J_{12} or J_{13}. The first column shows the situation at $c = 1.143$ before the bifurcation. In panel (a1) we see that J_{12} and $-J_{12}$ do not intersect and J_0 lies outside J_{12}. Thus, in panel (a2), there is no self-intersection of J_{13} and J_1 lies outside J_{13}, as indicated by the direction markers. Panels (b1) and (b2) show the corresponding curves and J_0 at the bifurcation at $c \approx 1.13953$. The critical point J_0 now lies in the intersection of J_{12} and $-J_{12}$ as shown in panel (b1). Hence, the image $J_{13} = f(J_{12}\backslash J_0) = f(-J_{12}\backslash J_0)$ forms a cusp on J_1. If $e^{i\varphi}$ is the tangent vector of J_{12} at J_0 for some $\varphi \in [0, \pi)$, then the cusp of J_{13} at J_1 is at the point $e^{i2\varphi} + c$. Column (c) shows the positions of the curves with respect to J_0 and J_1 at $c = 1.137$, after the bifurcation. The circles J_{12} and $-J_{12}$ intersect in two points, shown as black dots in panel (c1), both of which map to the point of self-intersection of J_{13}, denoted by a black dot in panel (c2). The image J_{13} is no longer a topological circle, because the point of self-intersection leads to an additional closed loop around the critical circle J_1. Note that J_0 now lies inside the circle J_{12} and J_1 lies inside the additional loop of J_{13}.

The forward-backward critical tangency illustrated in Figure 8 also has consequences for the 12-th preimages J_{-12} and J_{-11} of J_0 and J_1, respectively. The illustration in Figure 9 before, at and after the forward-backward critical tangency shows that certain points in J_{-11} move inside J_1. The panels in the bottom row show the point $J_{-11}^{0\cdots0} \in J_{-11}$ near J_1 whereas the top row shows its two preimages $J_{-12}^{0\cdots0}$, $J_{-12}^{10\cdots0} \in J_{-12}$ together with $J_{-12}^{1\cdots1}$, $J_{-12}^{01\cdots1} \in J_{-12}$ near J_0. We also plot $W^s(p)$, because all points in J_{-11} and J_{-12} are branch points of $W^s(p)$. Figure 9(a) shows the situation at $c = 1.1396$, before the bifurcation. The point $J_{-11}^{0\cdots0}$ lies outside

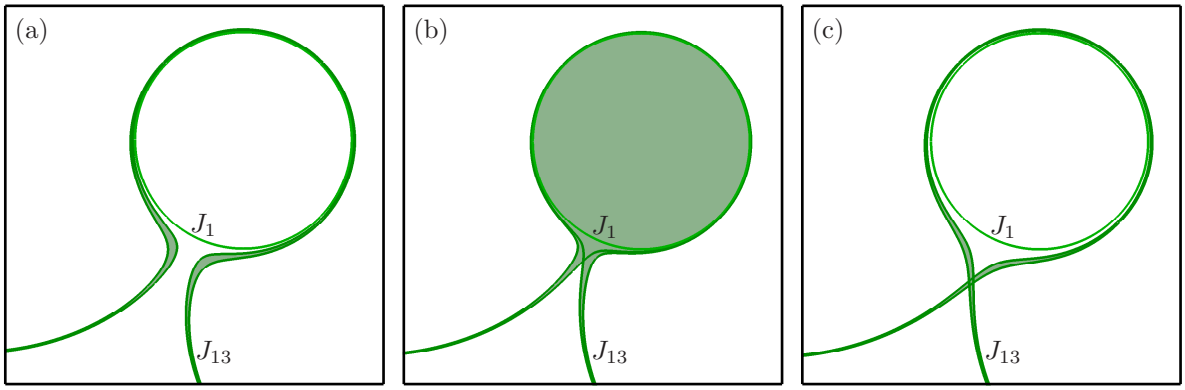

Figure 10: Local pictures of the circle J_{13} (dark green curve) and the critical circle J_1 (green circle) for $a = 0.8$, $\lambda = 0.8$, at $c = 1.14$ before a pair of forward-backward critical tangencies in column (a), at $c = 1.1393$ between the tangencies in column (b) and at $c = 1.138$ after both tangencies in column (c). The interior of J_{13} is shaded green.

the area bounded by J_1 and its preimages are at a certain distance from J_0. At the moment of bifurcation, at $c \approx 1.13953$, the point $J_{-11}^{0\cdots0}$ lies on J_1 and its preimages have disappeared into J_0; see column (b). At $c = 1.1395$, after the bifurcation, $J_{-11}^{0\cdots0}$ lies inside J_1. Hence, all possible sequences of preimages of J_0 that pass through $J_{-11}^{0\cdots0}$ end in $J_{-11}^{0\cdots0}$ and are finite orbits in forward time. At the same time, the branches of $W^s(p)$ that connected the points in the sequences of preimages of $J_{-11}^{0\cdots0}$ have disappeared.

Since the circles in $\mathcal{J}^+$ are elongated closed curves with very sharp corners, we expect forward-backward critical tangencies to occur in pairs. For example, when J_0 enters J_{12} as above, we expect J_0 to exit J_{12} on the other side for a nearby parameter value. When J_0 exits J_{12} on the other side, $J_{-11}^{0\cdots0}$ exits J_1 on the other side and the sequences of preimages going through $J_{-11}^{0\cdots0}$ become infinite again in forward time.

Figure 10 shows J_1 and J_{12} before, between and after a pair of forward-backward critical tangencies when J_0 enters and then again leaves the circle J_{11}. The interior of J_{12} is shaded green. Panel (a) shows the situation at $c = 1.14$ before both tangencies, when J_{12} does not intersect itself and J_1 lies outside J_{12}. At $c = 1.11393$ between the two bifurcations, J_0 is inside J_{11}, there is one point of self-intersection of J_{12} and J_1 lies inside the additional loop of J_{12}; see panel (b). Panel (c) shows the situation at $c = 1.138$, after the two bifurcations. The critical circle J_1 lies outside J_{12} again and J_{12} now has four points of self-intersection.

There is a first backward critical tangency but no first forward-backward critical tangency. However, for $\mathrm{Im}(c)$ sufficiently small, there is a "last" forward-backward critical tangency: At $|c| = 1 - \lambda$, the critical point J_0 enters the critical circle J_1. After this bifurcation the backward critical set $\mathcal{J}^-$ consists only of the critical point J_0 and the circles in the forward critical set $\mathcal{J}^+$ are nested, i.e., J_k lies inside J_{k+1} for all $k \geq 1$.

4.3 Global consequences of the subsequent tangency bifurcations

Similar to the sequence of initial bifurcations, the sequence of subsequent bifurcations has a complicated accumulating structure: Due to the accumulation of $\mathcal{J}^+$ and $W^u(p)$ on $W^u(p)$ and $W^s(p)$ on itself, immediately after the first backward critical tangency, an infinite sequence of backward critical tangencies accumulates on each backward critical tangency and an infinite sequence of forward-backward critical tangencies accumulates on each backward critical tangency.

Globally, the backward and forward-backward critical tangencies change the asymptotic behavior of sequences of points in $\mathcal{J}^-$. Since the points in $\mathcal{J}^-$ act as branch points of the stable set $W^s(p)$, the dynamics on the entire plane changes. In addition, the backward critical tangencies change the "direction" of the dynamics on the unstable set $W^u(p)$ near $\mathcal{J}^+$ in the way indicated by the direction markers in Figure 7. We now illustrate the consequences for the global dynamics of the map (1).

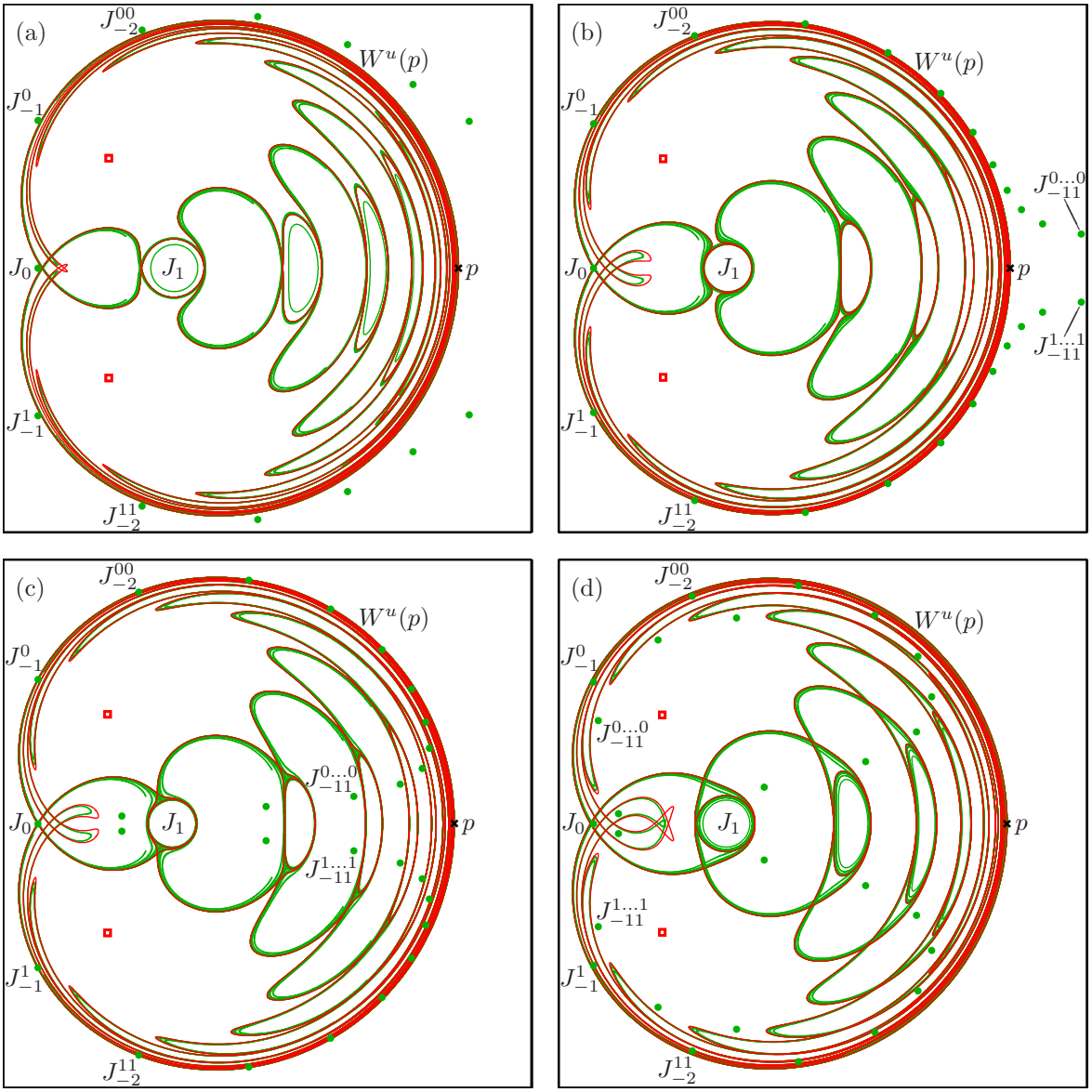

Figure 11: The critical set $\mathcal{J}$ (green) and the unstable set $W^u(p)$ (red curve) for $a = 0.8$, $\lambda = 0.8$, with $c = 1.16$ in panel (a), $c = 1.144$ in panel (b), $c = 1.142$ in panel (c) and $c = 1.13$ in panel (d); compare Figure 12.

Let us first discuss the consequences of backward and forward-backward critical tangencies for the critical set $\mathcal{J}$ and the unstable set $W^u(p)$. Figure 11 shows the transitions of these sets for $a = 0.8$ and $\lambda = 0.8$ and four different values of c, namely, $c = 1.16$, $c = 1.144$, $c = 1.142$ and $c = 1.13$ in panels (a)–(d), respectively. Panel (a) shows $\mathcal{J}$ and $W^u(p)$ for $c = 1.16$, well before the first backward critical tangency. In this parameter regime, the critical point J_0, the sequence of its first preimages $\{J_{-k}^{0\cdots0}\}_{k\geq0}$ and the sequence of its second preimages $\{J_{-k}^{1\cdots1}\}_{k\geq0}$ lie outside the region bounded by $W^u(p)$. The two sides $W_+^u(p)$ and $W_-^u(p)$ intersect each other (due to unstable tangencies), but not themselves. Panel (b) shows the situation at $c = 1.144$, just before the first backward critical tangency. The two sequences $\{J_{-k}^{0\cdots0}\}_{k\geq0}$ and $\{J_{-k}^{1\cdots1}\}_{k\geq0}$ have come closer to $W^u(p)$; e.g. the eleventh first preimage $J_{-11}^{0\cdots0}$ and the eleventh second preimage $J_{-11}^{1\cdots1}$ of J_0 have emerged on the

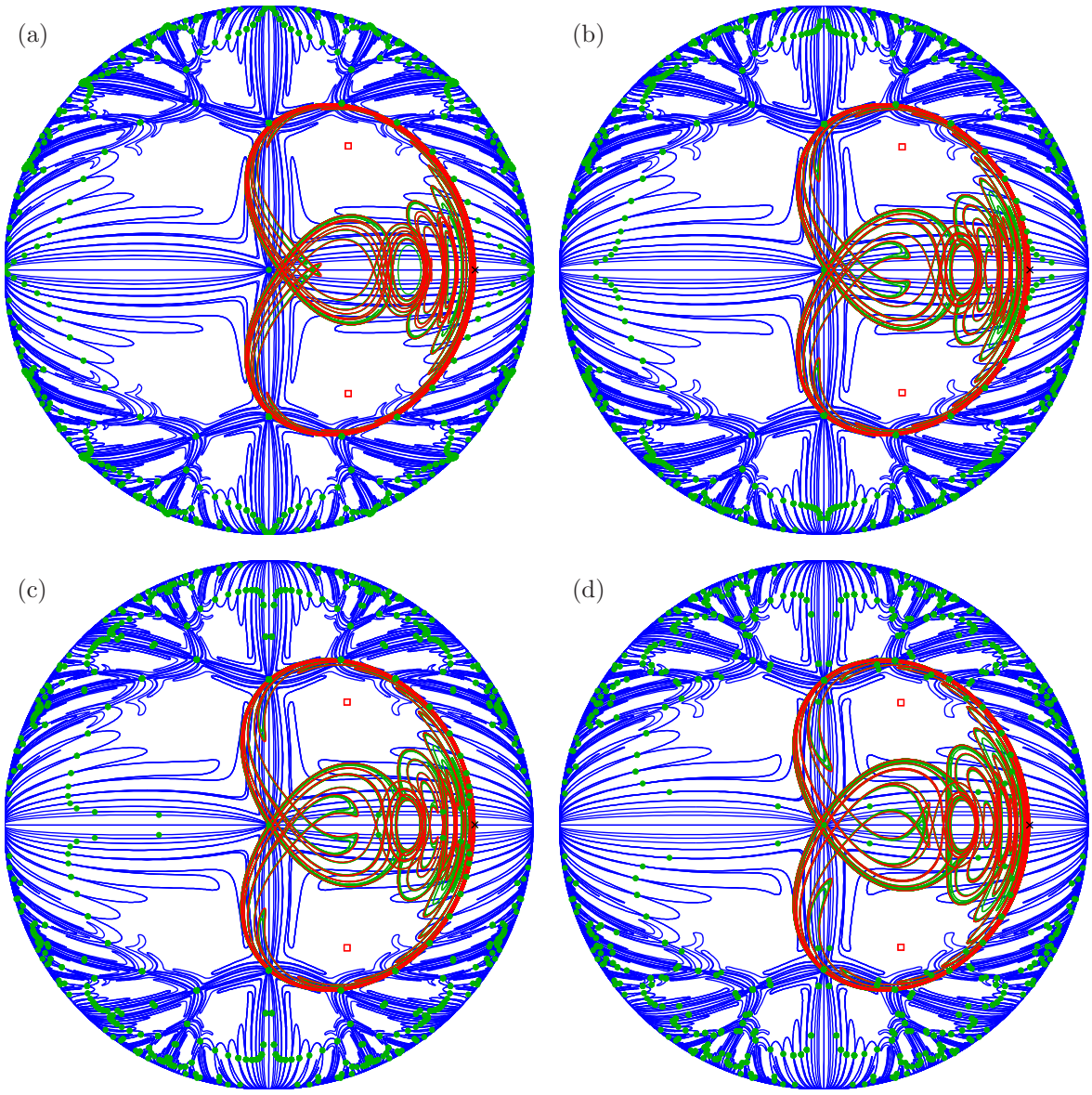

Figure 12: The stable set $W^s(p)$ (blue curves), unstable set $W^u(p)$ (red curve) and critical set $\mathcal{J}$ (green) on the Poincaré disk for $a = 0.8$, $\lambda = 0.8$, at $c = 1.16$ (a), at $c = 1.144$ (b), at $c = 1.142$ (c) and at $c = 1.13$ (d); compare with Figures 6 and 11.

right-hand side of panel (b). The situation at $c = 1.142$, just after the first backward critical tangency, is shown in panel (c). In between the first backward critical tangency at $c \approx 1.143$ and $c = 1.142$ an infinite sequence of backward critical tangencies and an infinite sequence of forward-backward critical tangencies occurred. As a consequence, $\{J_{-k}^{0\cdots0}\}_{k\geq0}$, $\{J_{-k}^{1\cdots1}\}_{k\geq0}$ and infinitely many other sequences of preimages of J_0 have moved inside the area bounded by $W^u(p)$ and have passed through the interior of infinitely many circles in $\mathcal{J}^+$; compare Figures 7 (c1) and 8 (c1). For example, the eleventh preimages $J_{-11}^{0\cdots0}$ and $J_{-11}^{1\cdots1}$ of J_0 are now located between the circles J_2 and J_3; this means that they each have had a pair of forward-backward critical tangencies with each circle in the forward critical set $\mathcal{J}^+$. At the same time, $W^u(p)$ and the circles in $\mathcal{J}^+$ have formed infinitely

many loops around the circles in $\mathcal{J}^+$; see, for example, just above and below the critical circle J_1 and compare Figures 7 (c2) and 8 (c2). As a consequence, there exist infinitely many self-intersections of $\mathcal{J}^+$, $W^u_+(p)$ and $W^u_-(p)$. In each of the backward critical tangencies, the direction of the dynamics on $W^u(p)$ near the curves in $\mathcal{J}^+$ has changed (compare with Figure 7). Panel (d) shows the sets at $c = 1.13$, well after the first backward critical tangency. Infinitely many more backward and forward-backward critical tangencies have occurred. The critical point J_0 has moved well inside the region bounded by $W^u(p)$ and, thus, the loops of $W^u(p)$ created in the first backward critical tangency are now well separated from the circles in $\mathcal{J}^+$ they revolve around. Also, the eleventh preimages $J^{0\cdots0}_{-11}$ and $J^{1\cdots1}_{-11}$ of J_0 are now located between J_0 and J^0_{-1} or J^1_{-1}, respectively.

Figure 12 shows the fixed points p, q^+ and q^- and the sets $\mathcal{J}$, $W^s(p)$ and $W^u(p)$ on the Poincaré disk for the same parameter values as Figure 11; compare with Figure 6. In panel (a), well before the first backward critical tangency, all sequences of points in $\mathcal{J}^-$ go to infinity. As an example, the sequence of first preimages $\{J^{0\cdots0}_{-k}\}_{k\geq0}$ of J_0 go to infinity. Due to earlier forward critical tangencies, eventually the points in this sequence are connected to J_0 by branches of the stable set $W^s(p)$. Therefore, these branches of $W^s(p)$ go to infinity as well. Immediately before the first backward critical tangency, in panel (b), $W^u(p)$ and the points in $\mathcal{J}^-$, which are the branch points of $W^s(p)$, have come closer together. Figure 12(c) shows the sets at $c = 1.142$, immediately after the first backward critical tangency. There has been an infinite sequence of backward and forward-backward critical tangencies leading to infinitely many sequences of points in $\mathcal{J}^-$ entering the region bounded by $W^u(p)$ and becoming finite and infinite again in forward time while moving through the circles in $\mathcal{J}^+$. At the same time the other sequences of points in $\mathcal{J}^-$ do not converge to infinity any longer but stay in the compact regions that are the corresponding preimages of the region bounded by $W^u(p)$. Panel (d) shows the situation at $c = 1.13$ well after the first backward critical tangency; there have been infinitely many more backward and forward-backward critical tangencies.

Figure 13 shows the fixed point p and the sets $\mathcal{J}$, $W^s(p)$ and $W^u(p)$ for $a = 0.8$, $\lambda = 0.8$ and $c = 0.8$ to illustrate the geometry of wild chaos for $c \in \mathbb{R}$. As we will discuss in Section 5, our numerical calculations suggest that these parameter values lie in the wild chaotic parameter regime, i.e., where all four types of tangency bifurcations have occurred infinitely many times. For Figure 13, we computed $W^s(p)$ with higher-order preimages of $W^s_0(p)$ and $W^u(p)$ up to a longer arclength than in Figures 6 and 12 to emphasize the complicated and self-accumulating nature of $W^s(p)$ and $W^u(p)$ on the plane in the wild chaotic regime for $c \in \mathbb{R}$.

5 Bifurcation diagrams

We now discuss the organization of two-parameter bifurcation diagrams that we obtain by following the tangency bifurcations introduced in sections 3 and 4 in two parameters.

5.1 The symmetric case of $c \in \mathbb{R}$

Recall that for $c \in \mathbb{R}$ map (1) is symmetric under complex conjugation: the saddle fixed point p is real, its primary manifold $W^s_0(p)$ is the positive real line and the fixed points $q^\pm$ and the sets $W^s(p)$, $W^u(p)$ and $\mathcal{J}$ are symmetric under complex conjugation. Therefore, all bifurcations of their parts above $W^s_0(p)$ occur at the same parameter values as the bifurcations of their parts below $W^s_0(p)$.

Figure 14 shows the bifurcation diagram of map (1) in the (a, λ)-plane for $c = 1$, which is the parameter region considered in [9]. Panel (a) shows only the local bifurcations (black) of the fixed points. The curve NS is the curve of Neimarck-Sacker bifurcations of q^+ and q^-; these points are sinks for parameter values (a, λ) to the left of NS and sources to the right. At $a = 1$, another source appears at infinity on the positive real line, which only exists for $a > 1$. Since one can think of this bifurcation as a branch point at infinity, we denote it by BP. This source disappears with the saddle point p in a fold bifurcation on the limit point curve LP. The curves LP and BP both end in the bifurcation point LPBP at $(a, \lambda) = (1, 1)$, at which p disappears with the source at infinity.

Figure 14(b) shows a global view of the (a, λ)-plane of the local bifurcations from panel (a) together with the global bifurcations of the sets $W^s(p)$, $W^u(p)$ and $\mathcal{J}$. The magenta curve H^0 is the first homoclinic tangency

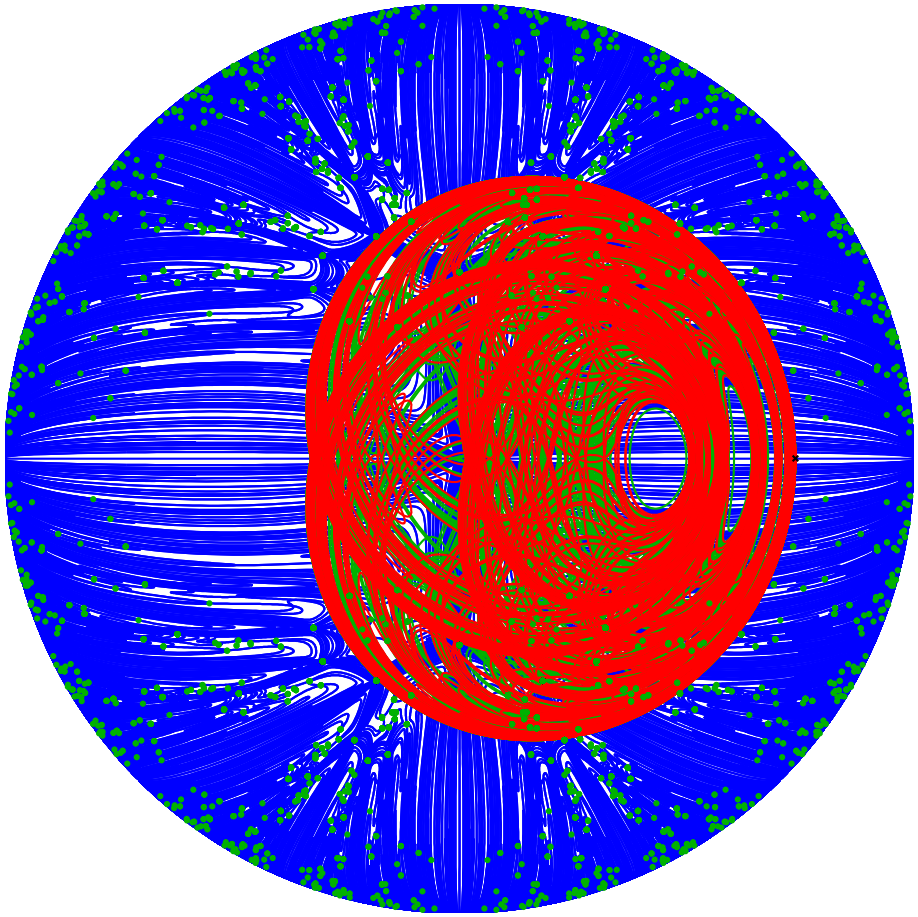

Figure 13: The fixed point p (black cross), its stable set $W^s(p)$ (blue curves), its unstable set $W^u(p)$ (red curve) and the critical set $\mathcal{J}$ (green) on the Poincaré disk for $a = 0.8$, $\lambda = 0.8$ and $c = 0.8$; compare with Figures 6 and 12.

of $W^s(p)$ and $W^u(p)$. To the right of H^0 lie the dark magenta and purple curves H^1 and H^2 as labeled in the enlargements in panels (c) and (d); they are curves of homoclinic tangencies that belong to the sequence of homoclinic tangencies accumulating on H^0 (see Section 3.1). The red curve labeled B^0 is the first backward critical tangency of $W^u(p)$ and $\mathcal{J}^-$. The two orange curves B^1 and B^2 to its right are backward critical tangencies that belong to the sequence of backward critical tangencies accumulating on B^0 (see Section 4.1). The five blue curves F^k, $k \in \{8, 10, 12, 14, 16\}$, are forward critical tangencies of the circles J_k with the part of $W^s_0(p)$ between J_0 and J_1. They belong to the sequence of forward critical tangencies accumulating on H^0 (see Section 3.2). The curve FB^{10} denotes a forward backward critical tangency of J_{10} with J_1. It belongs to the sequence of forward-backward critical tangencies accumulating on B^0 (see Section 4.2). FB^{10} is a topological circle that corresponds to a pair of forward-backward critical tangencies as was shown in Figure 10. The curves H^0, H^1, H^2, B^0, B^1, B^2 and F^k, $k \in \{8, 10, 12, 14, 16\}$, when followed in the direction of decreasing λ, all end at different points on LP, because on LP the sets $W^s(p)$ and $W^u(p)$ disappear together with p. The closed curve FB^{10} continues to the right of LP, because it only involves the critical set $\mathcal{J}$. The other end points of F^k, $k \in \{8, 10, 12, 14, 16\}$ also lie on LP and they accumulate on the point LPBP. The other end points of H^0, H^1, H^2, B^0, B^1 and B^2 extend beyond $\lambda > 1$. At $\lambda = 0$ and $\lambda = 1$, map (1) changes from folding the plane in a 2-to-1-fashion to folding it in a 4-to-1-fashion, and the analysis of the bifurcations in these parameter regimes lies beyond the scope of this paper.

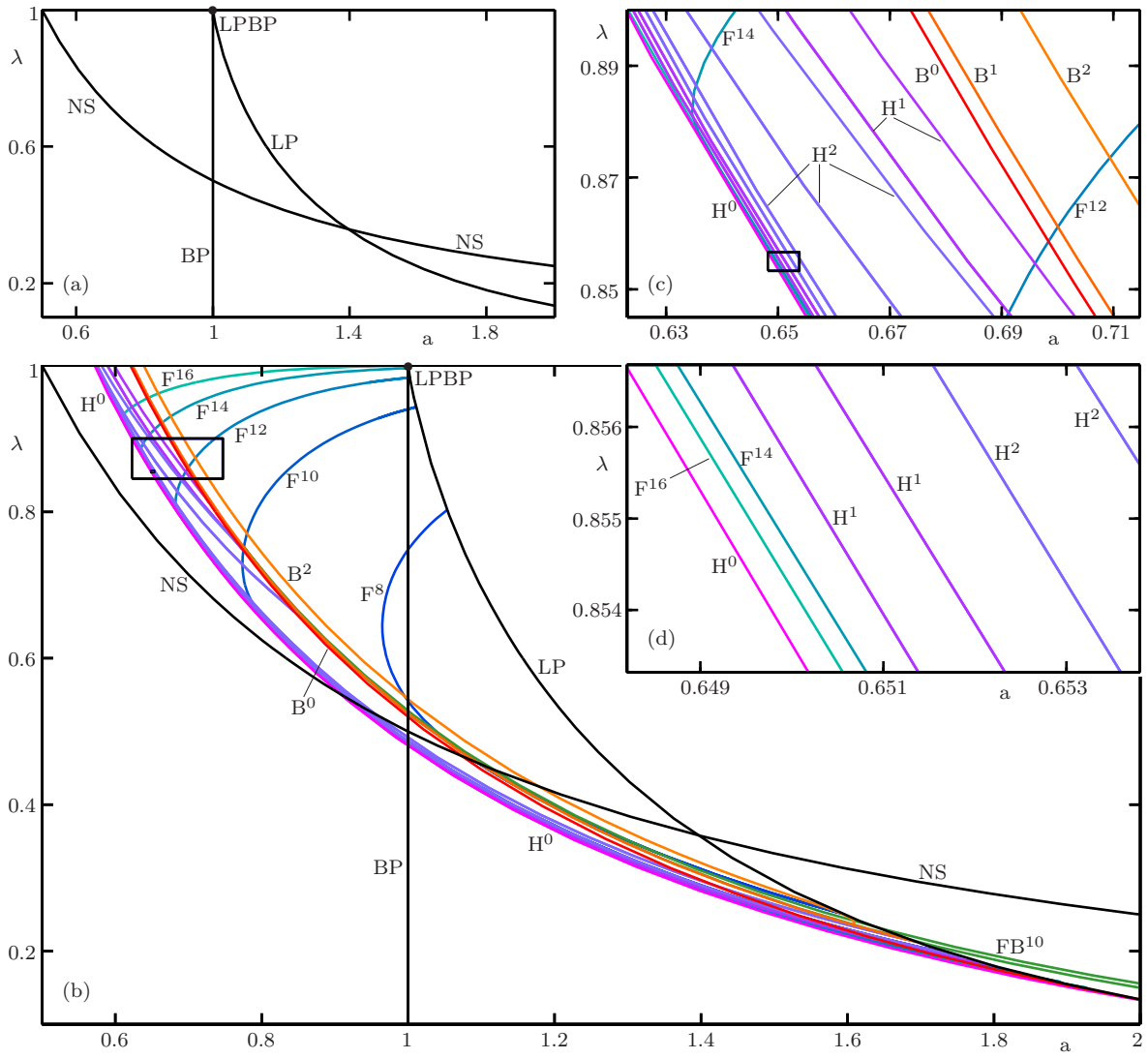

Figure 14: The bifurcation diagram in the (a, λ)-plane for $c = 1$. Panel (a) shows the local bifurcations of the fixed points in black; these are the Neimarck-Sacker bifurcation NS of $q^{\pm}$, the bifurcation BP in which a source appears at infinity on the positive real line, the fold bifurcation LP of this source with p and the bifurcation point LPBP at $(a, \lambda) = (1, 1)$, at which p disappears with the source at infinity. Panel (b) shows, in addition, the global bifurcations of $W^s(p)$, $W^u(p)$ and $\mathcal{J}$. These are the first homoclinic tangency H^0 (magenta), two further homoclinic tangencies (dark magenta and purple), five forward critical tangencies F^k (blue), $k \in \{8, 10, 12, 14, 16\}$, the first backward critical tangency B^0 (red), two further backward critical tangencies (orange) and the forward-backward critical tangency FB^{10}. Panels (c) and (d) show enlargements of the bifurcation diagram in panel (b) inside the black boxes $(a, \lambda) \in [0.567, 0.9] \times [0.8, 1]$ and $(a, \lambda) \in [0.6482, 0.6538] \times [0.8533, 0.8567]$.

Figures 14(c) and (d) show enlargements of the bifurcation diagram in panel (b) inside the black boxes $(a, \lambda) \in [0.567, 0.9] \times [0.8, 1]$ and $(a, \lambda) \in [0.6482, 0.6538] \times [0.8533, 0.8567]$, respectively, showing the arrangement of curves in more detail. The first homoclinic bifurcation curve H^0 is the left most curve in these enlargements, and to its right follow the forward critical tangency curves F^{16} and F^{14}, the homoclinic tangency curves H^1 (twice), H^2 (four times) and H^1 (twice), and the backward critical tangency curves B^0, B^1 and B^2. The

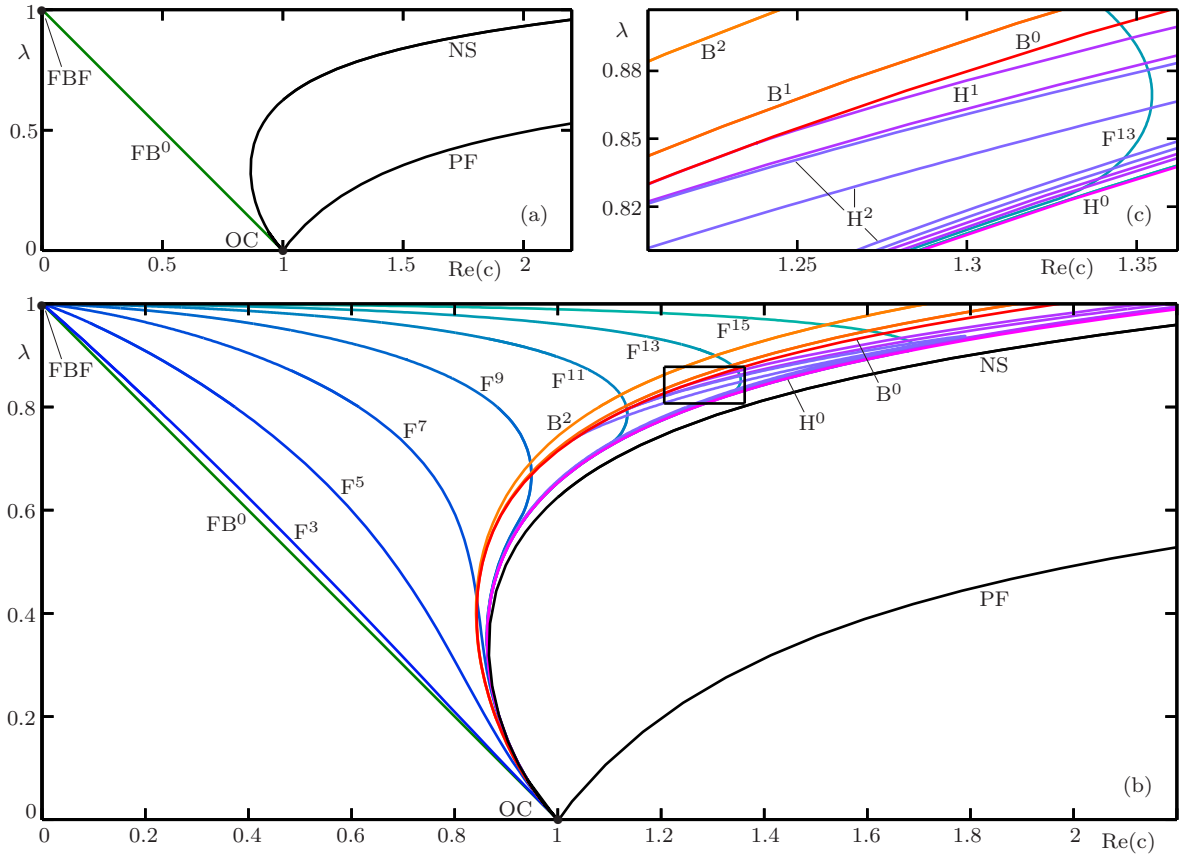

Figure 15: The bifurcation diagram in the $(\mathrm{Re}(c), \lambda)$-plane for $a = 0.8$ and $\mathrm{Im}(c) = 0$. Panel (a) shows the local bifurcations of the fixed points p, $q^{\pm}$, the critical point J_0 and the critical circle J_1. These are the pitchfork bifurcation PF (black) of p and $q^{\pm}$, the Neimarck-Sacker bifurcation NS (black) of $q^{\pm}$, the "last" forward-backward critical tangency FB^0 (green) of J_0 and J_1 and the bifurcation points FBF at $(\mathrm{Re}(c), \lambda) = (0, 1)$ and OC at $(\mathrm{Re}(c), \lambda) = (1, 0)$. Panel (b) shows, in addition, the global bifurcations of $W^s(p)$, $W^u(p)$ and $\mathcal{J}$. These are the first homoclinic tangency H^0 (magenta), two further homoclinic tangencies (dark magenta and purple), seven forward critical tangencies F^k (blue), the first backward critical tangency B^0 (red) and three further backward critical tangencies (orange). Panel (c) shows an enlargement of the bifurcation diagram in panel (b) inside the black box $(\mathrm{Re}(c), \lambda) \in [1.206, 1.362] \times [0.807, 0.878]$. Compare with Figures 6 and 12 for the corresponding transitions in phase space for fixed $\lambda = 0.8$ and decreasing $\mathrm{Re}(c)$.

homoclinic tangency curves H^1 and H^2 are crossed several times when a or λ are increased because they make sharp turns (not visible in the figures), which correspond to the sharp turns of $W^u(p)$ due to its self-accumulating nature.

The transitions discussed in Sections 3 and 4 were for decreasing $c \in \mathbb{R}$ with $(a, \lambda) = (0.8, 0.8)$ fixed. Let us now consider what the bifurcation diagram looks like if we vary $c \in \mathbb{R}$. Figure 15 shows the bifurcation diagram in the $(\mathrm{Re}(c), \lambda)$-plane for $a = 0.8$ and $\mathrm{Im}(c) = 0$, i.e. map (1) is still symmetric under rotation by π. The line $\mathrm{Re}(c) = 1$ corresponds to the line $a = 0.8$ in Figure 14. Panel (a) shows the local bifurcations of the fixed points p, q^+ and q^-, the critical point J_0 and the critical circle J_1. The black curve NS is the curve of Neimarck-Sacker bifurcations of q^+ and q^- that also occurs in (a, λ)-plane for $c = 1$ (see Figure 14(a)). These points are sinks for parameter values $(\mathrm{Re}(c), \lambda)$ to the right of NS and sources to the left. The black curve PF is a pitchfork bifurcation of p, q^+ and q^- that occurs due to the conjugational symmetry of the map (1) for

$\mathrm{Im}(c) = 0$. For $(\mathrm{Re}(c), \lambda)$ above PF, p is a saddle and $q^{\pm}$ are sinks and below PF, p is a sink and $q^{\pm}$ have disappeared. The green curve FB^0 is the curve of "last" forward-backward critical tangencies, at which J_0 lies on J_1, and it is given analytically by $c = 1 - \lambda$. When J_0 enters J_1 at FB^0, all preimages of J_0 in $\mathcal{J}^-$ disappear and all images of J_1 in $\mathcal{J}^+$ lie nested in each other. At the same time, the fixed points q^+ and q^- disappear into the critical point J_0. The curves FB^0, NS and PF all intersect at the point OC at $(\mathrm{Re}(c), \lambda) = (1, 0)$. Here, map (1) is given as $f(z) = (z/|z|)^2 + 1$ and the entire punctured plane $\mathbb{C}^*$ is mapped to $\partial\overline{\mathbb{D}}_1(1)$, which coincides with J_1. Therefore, p, q^+, q^- and J_0 all lie on J_1. Since PF and FB^0 only exist for $c \neq 1$, these bifurcations do not appear in the (a, λ)-plane for $c = 1$ in Figure 14(a). Similarly, the curves BP and LP in Figure 14(a) lie at $a \geq 1$ and are therefore absent in the $(\mathrm{Re}(c), \lambda)$-plane for $a = 0.8$ in Figure 15(a).

Figure 15(b) shows a global view of the $(\mathrm{Re}(c), \lambda)$-plane of the local bifurcations from panel (a) together with the global bifurcations of the sets $W^s(p)$, $W^u(p)$ and $\mathcal{J}$. As in Figure 14(b), H^0 (magenta), H^1 (dark magenta) and H^2 (purple) are the first and two further homoclinic tangencies, and B^0 (red), B^1 (dark orange) and B^2 (orange) are the first and two further backward critical tangencies. Furthermore, F^k, $k \in \{3, 5, 7, 9, 11, 13, 15\}$, are forward critical tangencies of the circles J_k with the part of $W_0^s(p)$ between J_0 and J_1. Instead of starting at different points on the curve LP as in Figure 14(b), here, the curves H^0, H^1, H^2, B^0, B^1, B^2 and F^k, $k \in \{3, 5, 7, 9, 11, 13, 15\}$, all emanate from the point OC, which appears to be an organizing center of the bifurcations in the $(\mathrm{Re}(c), \lambda)$-plane. At OC, the image of map (1) is $\partial\overline{\mathbb{D}}_1(1)$, and increasing λ from OC to $\lambda > 0$ "unfolds" the image of map to $\mathbb{C}\backslash\overline{\mathbb{D}}_{1-\lambda}(c)$. Finally, we note that the other end point of each curve F^k, $k \in \{3, 5, 7, 9, 11, 13, 15\}$, is the point FBF at $(\mathrm{Re}(c), \lambda) = (0, 1)$: Here, J_1 is a point and coincides with J_0 so that all images of J_1 in $\mathcal{J}^+$ have disappeared.

Figure 15(c) shows an enlargement of the bifurcation diagram in panel (b) inside the black box $(\mathrm{Re}(c), \lambda) \in [1.206, 1.362] \times [0.807, 0.878]$ showing the arrangement of curves in more detail. The curve of first homoclinic tangencies H^0 can be seen at the bottom right, followed to its left by the forward critical tangency curves F^{15} (close to H^0, hardly visible) and F^{13}, the homoclinic tangency curves H^1 (twice), H^2 (four times) and H^1 (twice), and the backward critical tangency curves B^0, B^1 and B^2. As in Figure 14, the homoclinic tangency curves H^1 and H^2 are crossed several times when λ is increased or $\mathrm{Re}(c)$ is decreased, because they form very sharp turns (not visible in the figure) due to the self-accumulating nature of $W^u(p)$.

5.2 The general case of $c \in \mathbb{C}$

We now investigate how the bifurcation structure observed in Figures 14 and 15 for $c \in \mathbb{R}$ changes if we allow general $c \in \mathbb{C}$, so that the conjugational symmetry of map (1) is broken. In general, we will find the same tangency bifurcations for the upper and lower parts of $W^s(p)$, $W^u(p)$ and $\mathcal{J}$, but they occur at different parameter values.

Figure 16 shows the bifurcation diagram in the $(\mathrm{Re}(c), \mathrm{Im}(c))$-plane for $a = 0.8$ and $\lambda = 0.8$. The locus $\mathrm{Im}(c) = 0$ corresponds to the locus $\lambda = 0.8$ in Figure 15. Figure 16(a) shows the local bifurcations of p, $q^{\pm}$, J_0 and J_1: at the fold bifurcations LP_+ and LP_- (black), q^+ and q^- disappear with p, respectively. LP_+ and LP_- form a single curve that intersects the real line at $(\mathrm{Re}(c), \mathrm{Im}(c)) \approx (-0.23, 0)$. At these parameter values, both q^+ and q^- are on the negative real line and switch roles. The black curves NS^+ and NS^- are the Neimarck-Sacker bifurcations of q^+ and q^-, respectively, and their intersection at $(\mathrm{Re}(c), \mathrm{Im}(c)) \approx (1.35, 0)$ corresponds to the curve NS in $(\mathrm{Re}(c), \lambda)$-plane shown in Figure 15(a). To the right of $\mathrm{NS}_{\pm}$, the points $q^{\pm}$ are sinks, and to the left they are sources. The curves $\mathrm{NS}_{\pm}$ end on $\mathrm{LP}_{\pm}$, because $q^{\pm}$ disappear with p. The "last" forward-backward critical tangency FB^0 (green) corresponds to the curve FB^0 in Figure 15(a).

Figure 16(b) shows a global view in the $(\mathrm{Re}(c), \mathrm{Im}(c))$-plane of the local bifurcations from panel (a) together with the global bifurcations of the upper and lower parts of $W^s(p)$, $W^u(p)$ and $\mathcal{J}$. Here we show fewer curves than in Figures 14(b) and 15(b) to make the diagram clearer. The complex conjugated curves $\mathrm{H}^0_{\pm}$ (magenta) and $\mathrm{B}^0_{\pm}$ (red) are the first homoclinic and backward critical tangencies of $W^u_{\pm}(p)$, respectively, and they correspond to H^0 and B^0 in Figures 14(b) and 15(b) for $\mathrm{Im}(c) = 0$. The blue curves $\mathrm{F}^k_{\pm}$, $k \in \{3, 7, 13\}$ are curves of forward critical tangencies of the upper or lower parts of the circles J_k with $W_0^s(p)$ near J_0, respectively. The upper and lower part of J_k, $k \geq 1$, are the $(k-1)$-th image of the upper and lower half circle of J_1, respectively. The blue curves F^*_+ and F^*_- are the curves of "first" forward critical tangencies in the following sense: thus far, we have only looked at parameter values, where one side of the primary manifold $W_0^s(p)$ of the stable set $W^s(p)$ goes

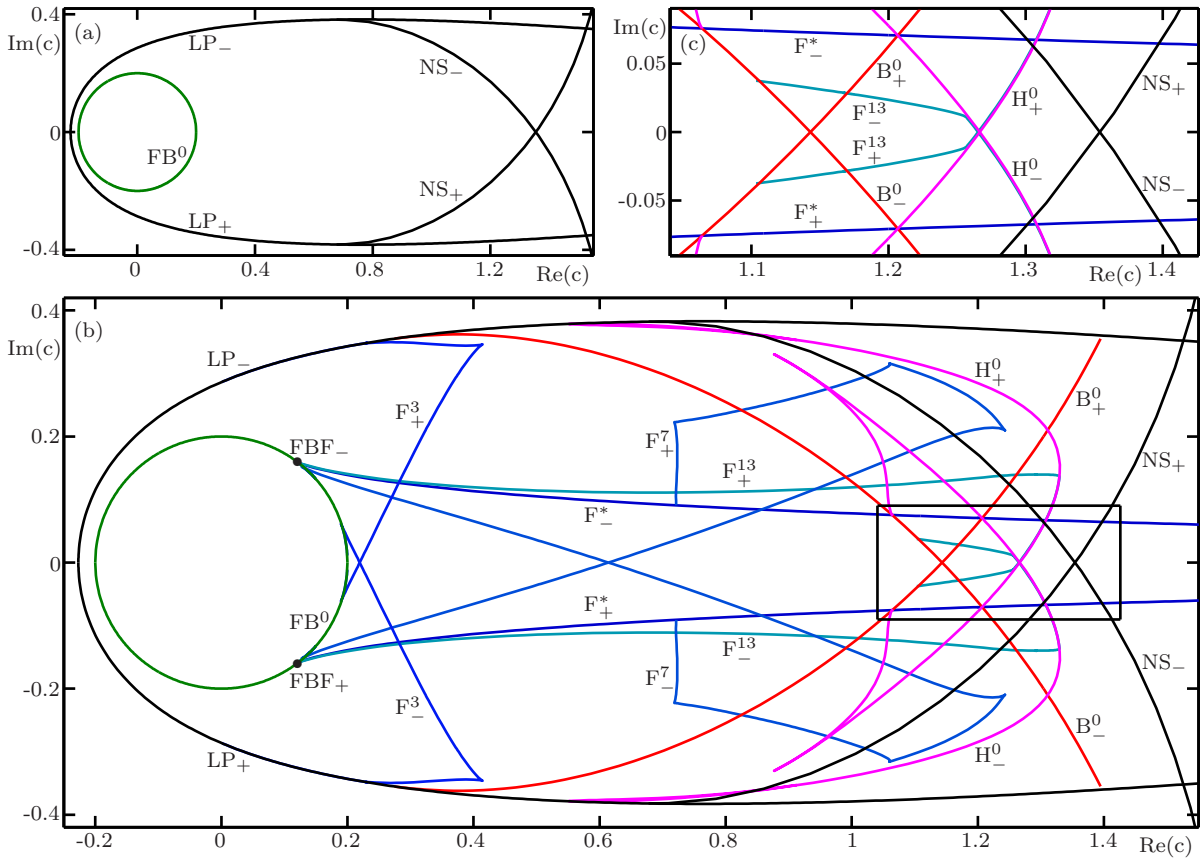

Figure 16: The bifurcation diagram in the $(\mathrm{Re}(c), \mathrm{Im}(c))$-plane for $a = 0.8$ and $\lambda = 0.8$. Panel (a) shows the local bifurcations of p, $q^{\pm}$, J_0 and J_1. These are the "last" forward-backward critical tangency FB^0 (green), the fold bifurcations LP_+ and LP_- (black) of p with q^+ and q^- and the Neimarck-Sacker bifurcations NS_+ and NS_- (black) of q^+ and q^-. Panel (b) shows, in addition, the main global bifurcation curves of the upper/lower parts of $W^s(p)$, $W^u(p)$ and $\mathcal{J}$. These are the first homoclinic tangencies $\mathrm{H}^0_{\pm}$ (magenta), the first backward critical tangencies $\mathrm{B}^0_{\pm}$ (red) of $W^u_{\pm}(p)$ and the forward critical tangencies $\mathrm{F}^*_{\pm}$, $\mathrm{F}^3_{\pm}$, $\mathrm{F}^7_{\pm}$ and $\mathrm{F}^{13}_{\pm}$ of the upper/lower parts of curves in $\mathcal{J}^+$, respectively. The black dots $\mathrm{FBF}_{\pm}$ are bifurcation points on FB^0. Panel (c) shows an enlargement of the black box $(\mathrm{Re}(c), \mathrm{Im}(c)) \in [1.0407, 1.426] \times [-0.0902, 0.0902]$ in panel (b).

to infinity and the other side intersects the critical circle J_1 and ends in the critical point J_0. However, this is only the case for parameters $(\mathrm{Re}(c), \mathrm{Im}(c))$ inside the region bounded by FB^0, F^+_+ and F^*_-. On the curves $\mathrm{F}^*_{\pm}$, the stable set $W^s_0(p)$ is tangent to the upper or lower half circle of J_1, respectively, and for parameters $(\mathrm{Re}(c), \mathrm{Im}(c))$ above the curve F^*_- or below the curve F^*_+, $W^s_0(p)$ does not intersect J_1 and, therefore, does not end in J_0. The curves $\mathrm{F}^*_{\pm}$ and $\mathrm{F}^k_{\pm}$, $k \in \{3, 7, 13\}$, all start in the points $\mathrm{FBF}_{\pm}$ on FB^0 and end on other bifurcation curves. The points FBF_+ and FBF_- play similar roles as the bifurcation point FBF in Figure 15: J_0 lies on each circle in $\mathcal{J}^+$ and they are all tangent to $W^s(p)$ in J_1. The curves $\mathrm{B}^0_{\pm}$ start on $\mathrm{LP}_{\pm}$ and end on $\mathrm{LP}_{\mp}$. The curves $\mathrm{H}^0_{\pm}$ start on $\mathrm{LP}_{\mp}$ and end at the intersection of $\mathrm{B}^0_{\pm}$ and $\mathrm{F}^*_{\pm}$: parameters $(\mathrm{Re}(c), \mathrm{Im}(c))$ on H^0_+ approaching $\mathrm{B}^0_{\pm} \cap \mathrm{F}^*_{\pm}$ correspond to the tangency between $W^s_0(p)$ and $W^u_{\pm}$ approaching the upper/lower side of J_1. In the limit, it becomes a tangency between $W^s_0(p)$ and the upper/lower side of J_1 and then disappears.

Figure 16(c) shows an enlargement of the bifurcation diagram in panel (b) inside the black box $(\mathrm{Re}(c), \mathrm{Im}(c)) \in [1.0407, 1.426] \times [-0.0902, 0.0902]$ to emphasize that the bifurcations are crossed in the same order for decreasing $\mathrm{Re}(c)$ as in the previous bifurcation diagrams, if we choose paths in between the curves F^*_+ and F^*_-: We first

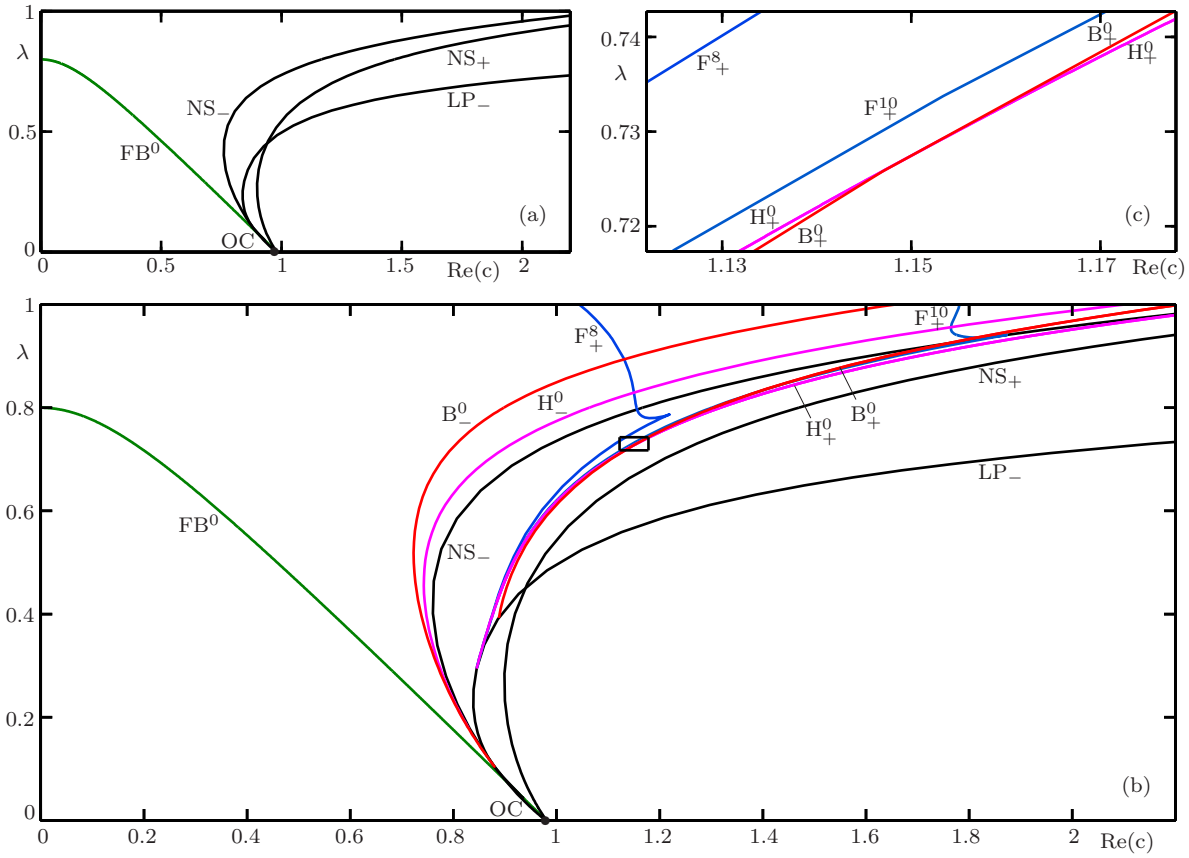

Figure 17: The bifurcation diagram in the $(\mathrm{Re}(c), \lambda)$-plane for $a = 0.8$, $\mathrm{Im}(c) = 0.2$. Panel (a) shows the local bifurcations of p, $q^{\pm}$, J_0 and J_1. These are the "last" forward-backward critical tangency FB^0 (green), the fold bifurcation LP_- (black) of p with q^- and the Neimarck-Sacker bifurcations NS_+ and NS_- (black) of q^+ and q^-. Panel (b) shows, in addition, the main global bifurcation curves of the upper/lower parts of $W^s(p)$, $W^u(p)$ and $\mathcal{J}$. These are the first homoclinic tangencies $\mathrm{H}^0_{\pm}$ (magenta), the first backward critical tangencies $\mathrm{B}^0_{\pm}$ (red) of $W^u_{\pm}(p)$, respectively, and the forward critical tangencies F^8_+ and F^{10}_+ of the upper parts of curves in $\mathcal{J}^+$. The black dot OC at $(\mathrm{Re}(c), \lambda) = (\sqrt{0.96}, 0)$ is a bifurcation point on FB^0. Panel (c) shows an enlargement of the black box $(\mathrm{Re}(c), \lambda) \in [1.122, 1.178] \times [0.717, 0.743]$ in panel (b); compare Figure 15 for $\mathrm{Im}(c) = 0$.

encounter NS_+ and NS_-, then H^0_+ and H^0_-, and then B^0_+ and B^0_-. Immediately above F^*_- or below F^*_+, these six curves are crossed in a different order, but still the two sequences of curves $\mathrm{NS}_{\pm}$, $\mathrm{H}^0_{\pm}$ and $\mathrm{B}^0_{\pm}$ corresponding to the upper/lower part $W^u_{\pm}(p)$ are crossed in the same order, respectively. We observe in panel (b) that this order persists until the curves H^0_+ and B^0_+ and the curves H^0_- and B^0_- intersect at $(\mathrm{Re}(c), \mathrm{Im}(c)) \approx (1.31, \pm 0.21)$. Above/below this intersection, $\mathrm{B}^0_{\pm}$ is crossed before $\mathrm{H}^0_{\pm}$.

Figure 17 shows the bifurcation diagram in the $(\mathrm{Re}(c), \lambda)$-plane for $a = 0.8$ and $\mathrm{Im}(c) = 0.2$. The line $\lambda = 0.8$ corresponds to the line $\mathrm{Im}(c) = 0.2$ in Figure 16. We show fewer curves than in Figure 15 for $\mathrm{Im}(c) = 0$ to make the diagram easier to understand. Figure 17(a) shows the local bifurcations of p, $q^{\pm}$, J_0 and J_1. The curve FB^0 corresponds to the "last" forward-backward critical tangency FB^0 also occurring for $\mathrm{Im}(c) = 0$ in Figure 15(a) and $\lambda = 0.8$ in Figure 16(a). It is defined by the condition $(1 - \lambda)^2 = \mathrm{Re}(c)^2 + \mathrm{Im}(c)^2$. The curve LP_- (black) is the curve of fold bifurcations in Figure 17(a), at which p and q^- disappear. For parameter values $(\mathrm{Re}(c), \lambda)$ to the right of LP_-, the fixed point q^+ is the only fixed point of map (1). The curve LP_- corresponds to the curve PF of pitchfork bifurcations in Figure 15(a), which one could think of as fold bifurcations of q^+

and q^- that occur at the same parameter values for $\mathrm{Im}(c) = 0$ due to the additional symmetry. The two curves NS_+ and NS_- (black) are the curves of Neimarck-Sacker bifurcations of q^+ and q^-, respectively. To the right of $\mathrm{NS}_\pm$, the points $q^\pm$ are sinks and to the left, they are sources. The curves $\mathrm{NS}_\pm$ correspond to the curve NS in Figure 17(a), where the Neimarck-Sacker bifurcations of q^+ and q^- occur at the same parameter values due to the symmetry. Similar to Figure 15(a), the curves FB^0, LP_- and NS_+ end in the point OC at $(\sqrt{0.96}, 0)$, which is where $\lambda = 0$ on FB^0. However, the curve NS_- ends on LP$-$, at which q^- disappears with p.

Figure 17(b) shows a global view of the $(\mathrm{Re}(c), \lambda)$-plane of the local bifurcations from panel (a) together with the global bifurcations of the sets $W^s(p)$, $W^u_\pm(p)$ and $\mathcal{J}$. The curves $\mathrm{H}^0_\pm$ (magenta) and $\mathrm{B}^0_\pm$ (red) in Figure 17(b) are the first homoclinic and backward critical tangencies of the upper and lower sides $W^u_\pm(p)$, respectively, for $\mathrm{Im}(c) = 0.2$. They correspond to the curves H^0 and B^0 in Figure 15(b) for $\mathrm{Im}(c) = 0$. Our computations indicate that these curves in Figure 17(b) end at different points on LP_-, where q^- and p disappear, rather than at OC as in Figure 15(b). Therefore, for $\mathrm{Im}(c) = 0.2$, the point OC is no longer an organizing center for the global bifurcations in the $(\mathrm{Re}(c), \lambda)$-plane.

Figure 17(c) shows an enlargement of the black box $(\mathrm{Re}(c), \lambda) \in [1.122, 1.178] \times [0.717, 0.743]$ shown in panel (b) to emphasize the change in order in which the bifurcations are crossed for decreasing $\mathrm{Re}(c)$ or increasing λ. The curves H^0_+ and B^0_+ intersect at $(\mathrm{Re}(c), \lambda) \approx (1.15, 0.73)$. This intersection plays the same role as the intersection of H^0_+ and B^0_+ in Figure 16: for $\mathrm{Im}(c) = 0.2$, decreasing $\mathrm{Re}(c)$ and fixed λ above this intersection, H^0_+ is crossed before B^0_+ (as for $\mathrm{Im}(c) = 0$ in Figure 15(c)), but below this intersection, one encounters B^0_+ before H^0_+ (as for $(\mathrm{Re}(c), \mathrm{Im}(c))$ above or below F^*_- and F^*_+ in Figure 16(c)).

Overall, we see that, for decreasing $\mathrm{Re}(c)$ in $(\mathrm{Re}(c), \lambda)$-plane for $\mathrm{Im}(c) = 0.2$, the upper and lower sides $W^u_\pm(p)$ and corresponding upper and lower parts of $\mathcal{J}^+$ each undergo essentially the same sequences of bifurcations as for $\mathrm{Im}(c) = 0$, but the sequence involving $W^u_+(p)$ and the upper part of $\mathcal{J}^+$ starts before the sequence involving $W^u_-(p)$ and the lower part of $\mathcal{J}^+$.

5.3 Regions of wild chaos

Recall, that Bamón, Kiwi and Rivera-Letelier proved the existence of a wild Lorenz-like attractor in map (1) for $c = 1$ and $a, \lambda \in (0, 1)$ both sufficiently close to 1. In the bifurcation diagram in the (a, λ)-plane shown in Figure 14(b), this corresponds to parameter values (a, λ) to the left of BP that are sufficiently close to the bifurcation point LPBP at $(a, \lambda) = (1, 1)$. In the proof, the authors make assumptions that restrict this parameter regime to a very small neighborhood of LPBP. However, our numerical computations suggest that the area of existence of this attractor extends to a much larger set of parameters, namely, to the open region bounded by LP, B^0 and $\lambda = 1$. For parameter values (a, λ) below the curve H^0, the system is nonchaotic. Starting with H^0, the system undergoes an infinite sequence of homoclinic tangencies (including H^1 and H^2), accumulating on each other as the parameter values (a, λ) are moved towards LPBP. Due to the homoclinic tangle caused by these tangencies, the system becomes chaotic; this happens via the same mechanisms as in planar diffeomorphisms, which are free of wild chaos. However, the map (1) also undergoes an infinite sequences of forward critical tangencies (including F^k, $k \in \{8, 10, 12, 14, 16\}$). In fact, each of the infinitely many homoclinic tangencies is accumulated by an infinite sequence of forward critical tangencies. These bifurcations lead to infinitely many branches of $W^s(p)$ connecting up at each point in $\mathcal{J}^-$. This corresponds to a local change of $W^s(p)$ near each point in $\mathcal{J}^-$. Therefore, forward critical tangencies do not affect the occurrence of homoclinic tangencies until $\mathcal{J}^-$ interacts with $W^u(p)$ in the first backward critical tangency B^0. For (a, λ) above B^0, the system undergoes infinite sequences of backward critical tangencies (including B^1 and B^2) and forward-backward critical tangencies (including FB^{10}) accumulating on each backward critical tangency. Therefore, immediately above B^0, all four types of tangency bifurcations occur. Since these tangency bifurcations are pairwise interactions of the four sets $W^s(p)$, $W^u(p)$, $\mathcal{J}^+$ and $\mathcal{J}^-$, their occurrences influence one another. For example, forward critical tangencies and backward critical tangencies influence the occurrence of homoclinic tangencies as described above. Overall, we view the complicated accumulating structure of the four tangency bifurcations as the creating mechanism of wild chaos. Therefore, we suggest that the regime of existence of the wild Lorenz-like attractor is the open region bounded by the curves B^0, LP, and $\lambda = 1$. The transition shown in Figures 6 and 12 is an example of this sequence of bifurcations.

The same sequences of bifurcations occur in the $(\mathrm{Re}(c), \lambda)$-plane shown in Figure 15(b) for $a = 0.8$ and

$\mathrm{Im}(c) = 0$ by moving $(\mathrm{Re}(c), \lambda)$ towards the bifurcation point FBF at $(\mathrm{Re}(c), \lambda) = (0, 1)$. Therefore, we suggest that the regime of existence of the wild Lorenz-like attractor extends to parameters $(\mathrm{Re}(c), \lambda)$ inside the open region bounded by B^0, FB^0 and $\lambda = 1$ in Figure 15.

As we have seen in Figures 16 and 17, for $|\mathrm{Im}(c)|$ sufficiently large and decreasing $\mathrm{Re}(c)$, one encounters the first backward critical tangency $\mathrm{B}^{\pm}$ of the upper/lower side $W^u_{\pm}(p)$ of $W^u(p)$ before the first homoclinic tangency $\mathrm{H}^0_{\pm}$. Past $\mathrm{H}^0_{\pm}$, all four types of tangencies still occur in infinite sequences, which we see as evidence that the regime of existence of the wild Lorenz-like attractor even extends to those values of $\mathrm{Im}(c)$. In the case of the bifurcation diagram in the $(\mathrm{Re}(c), \mathrm{Im}(c))$-plane for $a = 0.8$ and $\lambda = 0.8$, shown in Figure 16(c), this refers to the open annulus bounded by FB^0 on the inside and the following curve segments on the outside: the segment of LP_- between the negative real line and the starting point of H^0_+, the segment of H^0_+ until its intersection with B^0_+, the segment of B^0_+ until its intersection with B^0_- on the real line, and the corresponding complex conjugates of these curve segments. In the case of the bifurcation diagram in the $(\mathrm{Re}(c), \lambda)$-plane for $a = 0.8$ and $\mathrm{Im}(c) = 0.2$, shown in Figure 17(b), this refers to the open region bounded by FB^0, the line segment $\{(0, \lambda) \mid 0.8 \le \lambda \le 1\}$, the line segment $\lambda = 1$ until its intersection with B^0, the segment of B^0 until its intersection with H^0, and H^0 until the point $\mathrm{OC} = (\sqrt{0.96}, 0)$.

The curves FB^0, B^0, H^0 and $\lambda = 1$ in Figures 14 and 15 correspond to two-dimensional surfaces in the $(\mathrm{Re}(c), a, \lambda)$-space with $\mathrm{Im}(c) = 0$. Here, we expect the wild chaos to exist in the region bounded by FB^0, B^0 and $\lambda = 1$.

In the full $(\mathrm{Re}(c), \mathrm{Im}(c), a, \lambda)$-space, the bifurcations FB^0, $\mathrm{B}^0_{\pm}$, $\mathrm{H}^0_{\pm}$, $\mathrm{LP}_{\pm}$ and $\lambda = 1$ form three-dimensional hypersurfaces with the following properties: B^0_+ and H^0_+ intersect B^0_- and H^0_- in the two-dimensional surfaces B^0 and H^0 at $\mathrm{Im}(c) = 0$. The hypersurfaces LP_- and LP_+ only exist for $\mathrm{Im}(c) > 0$ or $\mathrm{Im}(c) < 0$, respectively, and meet at the two-dimensional surface PF at $\mathrm{Im}(c) = 0$. $\mathrm{H}^0_{\pm}$ ends on $\mathrm{LP}_{\mp}$ on one side. Also, B^0_+ and B^0_- intersect H^0_+ and H^0_- in two-dimensional surfaces for $\mathrm{Im}(c) > 0$ or $\mathrm{Im}(c) < 0$, respectively. Therefore, we expect the region of existence of wild chaos in $(\mathrm{Re}(c), \mathrm{Im}(c), a, \lambda)$-space to be bounded by the corresponding parts of FB^0, $\lambda = 1$, $\mathrm{LP}^{\pm}$, $\mathrm{H}^0_{\pm}$ and $\mathrm{B}^0_{\pm}$.

5.4 Transition for $\mathrm{Im}(c) = 0.2$

We discussed the transitions on the plane that occur when $\mathrm{Re}(c)$ is decreased in the $(\mathrm{Re}(c), \mathrm{Im}(c))$-plane in Figure 16 and the $(\mathrm{Re}(c), \lambda)$-plane in Figure 17 to illustrate the different transitions in the upper and lower parts of $W^u(p)$ and $W^s(p)$ when the conjugational symmetry is broken. Figure 18 shows p, $q^{\pm}$, $W^s(p)$, $W^u(p)$ and $\mathcal{J}$ on the Poincaré disk for $a = 0.8$, $\lambda = 0.8$ and $c = 1.32 + 0.2i$, $1.315 + 0.2i$, $1.311 + 0.2i$ and $1.3 + 0.2i$ in panels (a)–(d), respectively; compare with Figures 11 and 12, which illustrate the sequences of bifurcations for the case $\mathrm{Im}(c) = 0$. Note that the primary manifold $W^s_0(p)$ through p does not intersect the critical circle J_1, because the parameter values lie above the curve F^*_- in Figure 16. In this parameter range of $\mathrm{Re}(c)$, the lower fixed point q^- is still a sink, whereas the upper fixed point q^+ has already turned into a source in the Neimarck-Sacker bifurcation NS_+. Panel (a) shows the situation at $c = 1.32 + 0.2i$ just before the first homoclinic tangency H^0_+ of the upper side $W^u_+(p)$ with $W^s(p)$. Panel (b) shows the situation at $c = 1.315 + 0.2i$ just after H^0_+, but before the first backward critical tangency B^0_+. Now, $W^u_+(p)$ accumulates on itself and $W^s(p)$ accumulates on itself from one side. Recall, that for $\mathrm{Im}(c) = 0$, each homoclinic tangency implies an unstable tangency; see Section 3.1. For $\mathrm{Im}(c) \neq 0$, however, the two sides $W^u_+(p)$ and $W^u_-(p)$ are not symmetric and, therefore, are in general not tangent to $W^s_0(p)$ at the same parameter values. Panel (c) shows the situation at $c = 1.311 + 0.2i$, just before B^0_+. The unstable set $W^u(p)$ does not have any self-intersections yet. Panel (d) shows the sets at $c = 1.3 + 0.2i$, that is, just after B^0. Now, the upper side $W^u_+(p)$ intersects itself in infinitely many loops around circles in $\mathcal{J}^+$. The two sides $W^u_+(p)$ and $W^u_-(p)$ still do not intersect each other because there has not been an unstable tangency.

We continue the series of global pictures on the Poincaré disk in Figure 19 where $\mathrm{Re}(c)$ is decreased further. In this parameter range of $\mathrm{Re}(c)$, both fixed points q^+ and q^- have turned into sources; i.e. $\mathrm{Re}(c)$ lies to the left of NS_+ and NS_-. Panel (a) shows the situation at $c = 1.07 + 0.2i$, just before the first homoclinic tangency H^0_- of the lower side $W^u_-(p)$ with $W^s(p)$. This parameter value is after the first unstable tangency, at which $W^u_+(p)$ and $W^u_-(p)$ are tangent for the first time. Panel (b) shows the situation at $c = 1.05 + 0.2i$, just after H^0_-, but before the first backward critical tangency B^0_-. Now, $W^u_-(p)$ accumulates on itself as well, so that

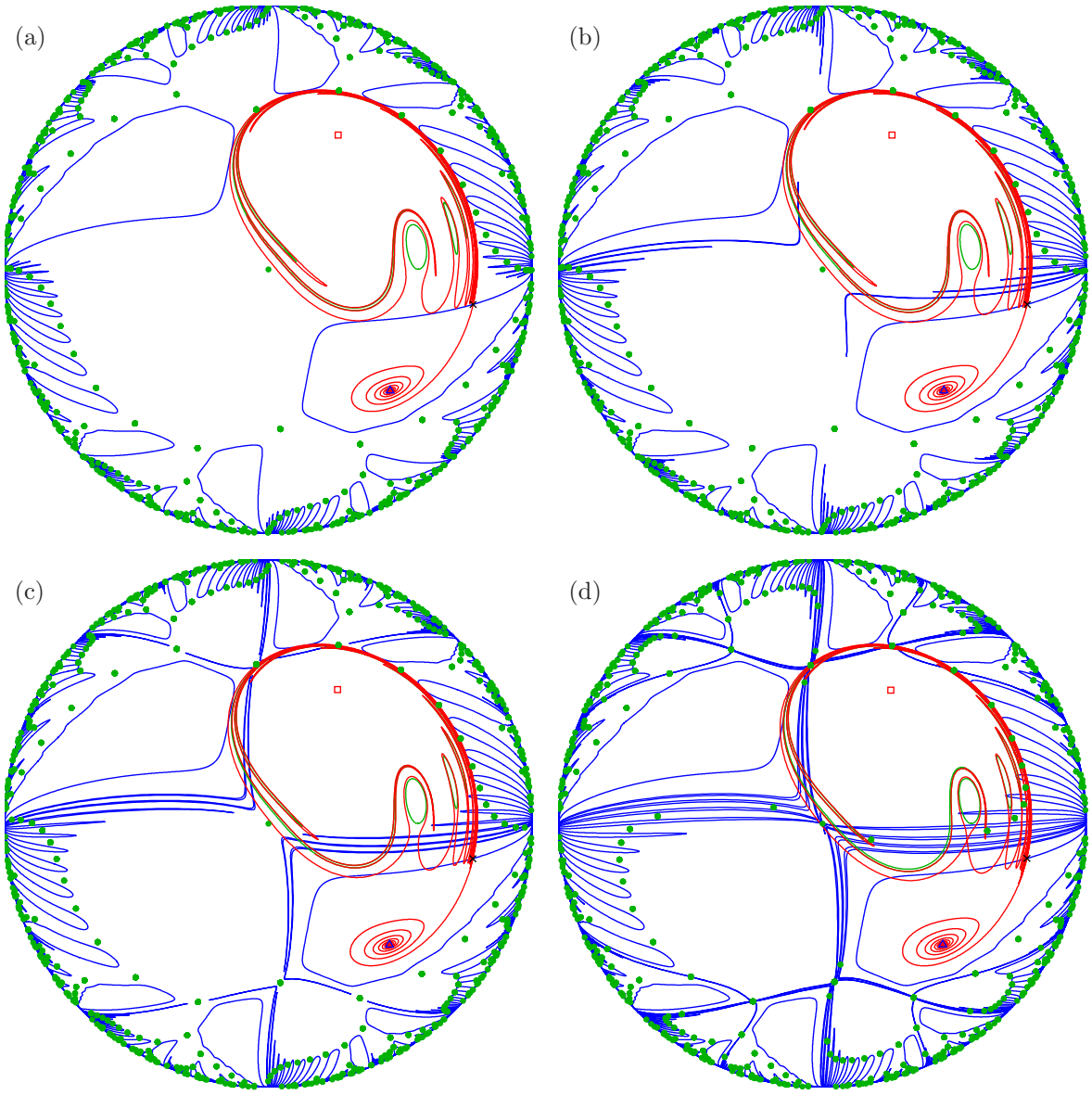

Figure 18: The stable set $W^s(p)$ (blue curves), unstable set $W^u(p)$ (red curve) and critical set $\mathcal{J}$ (green) on the Poincaré disk for $a = 0.8$, $\lambda = 0.8$, at $c = 1.32 + 0.2i$ (a), at $c = 1.315 + 0.2i$ (b), at $c = 1.311 + 0.2i$ (c) and at $c = 1.3 + 0.2i$ (d); compare with Figures 6, 12 and 17.

the entire unstable set $W^u(p)$ accumulates on itself. Also, $W^s(p)$ now accumulates on itself from both sides. Panel (c) shows the situation at $c = 0.97 + 0.2i$, just before B^0_-. Note that the lower side $W^u_-(p)$ does not have any self-intersections yet. Panel (d) shows the sets at $c = 0.89 + 0.2i$, that is, just after B^0_-. As expected, $W^u_-(p)$ forms loops around all circles in $\mathcal{J}^+$ and intersects itself in infinitely many points, correspondingly.

Figure 20 shows the fixed point p and the sets $W^s(p)$, $W^u(p)$ and $\mathcal{J}$ for $a = 0.8$, $\lambda = 0.8$ and $c = 0.7 + 0.2i$. Comparing with Figure 13 for $c \in \mathbb{R}$, we see that $W^s(p)$ and $W^u(p)$ also accumulate on themselves and $W^u(p)$ and $\mathcal{J}^+$ also form infinitely many loops around all circles in $\mathcal{J}^+$, but in Figure 20 the holes in the closure of $W^u(p)$ induced by the circles in $\mathcal{J}^+$ are not symmetric, and have moved up along the upper side $W^u_+(p)$.

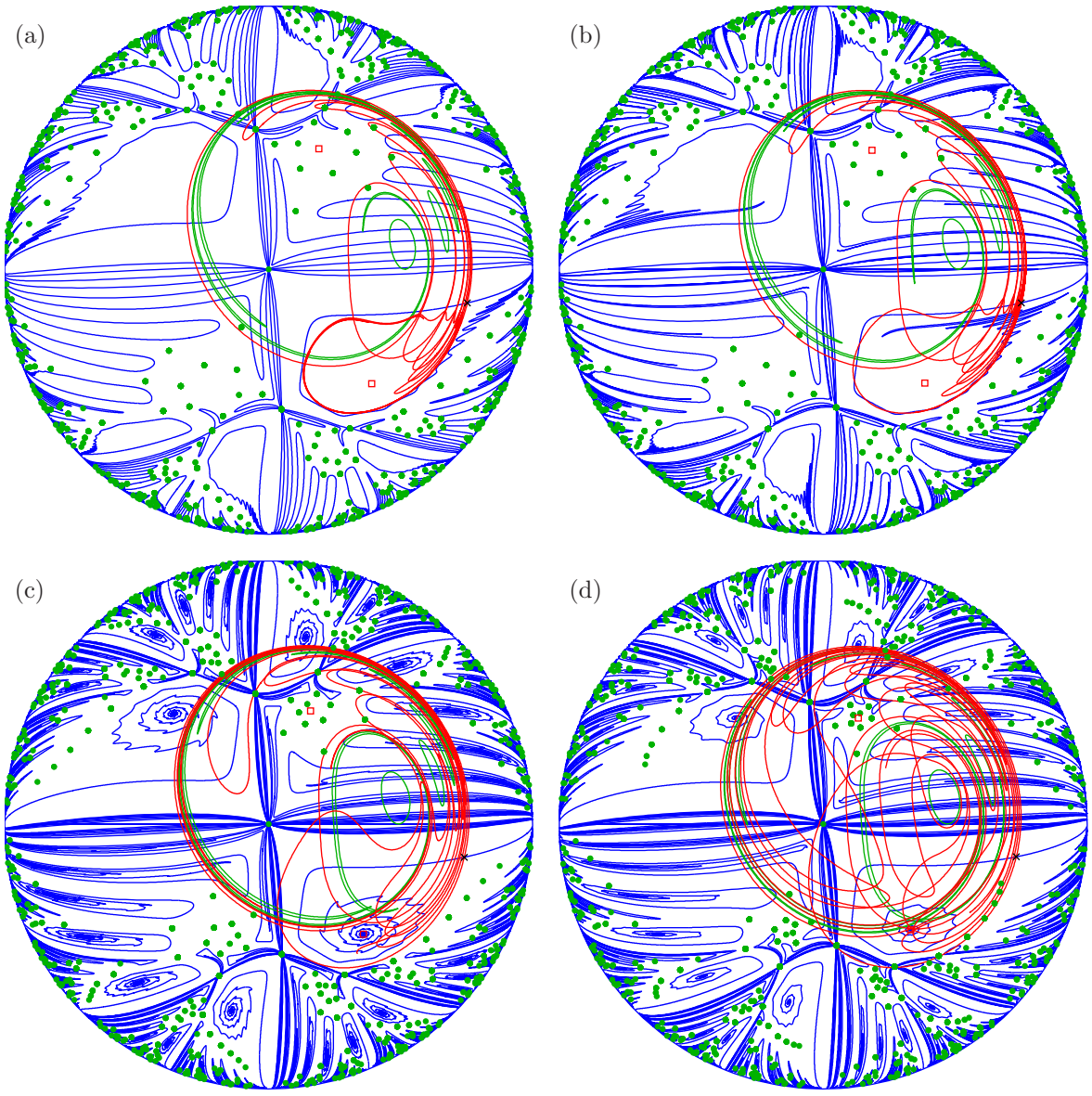

Figure 19: The stable set $W^s(p)$ (blue curves), unstable set $W^u(p)$ (red curve) and critical set $\mathcal{J}$ (green) on the Poincaré disk for $a = 0.8$, $\lambda = 0.8$, at $c = 1.07 + 0.2i$ (a), at $c = 1.05 + 0.2i$ (b), at $c = 0.97 + 0.2i$ (c) and at $c = 0.89 + 0.2i$ (d); compare with Figures 6, 12, 17 and 18.

Furthermore, we note that the parameter values in Figure 20 lie above the curve F^*_- in the bifurcation diagram in Figure 16, so that the primary manifold $W^s_0(p)$ spirals towards q^- without being connected to J_0 (which is obscured by $\mathcal{J}^+$ and $W^u(p)$ in Figure 20). Therefore, the preimages of $W^s_0(p)$ spiral towards the preimages of q^- without being connected to points in $\mathcal{J}^-$; see, e.g., the spiraling branch of $W^s(p)$ underneath the first intersection of $W^u_+(p)$ and $W^u_-(p)$ near the negative imaginary axis. As argued in Section 5.3, we believe that the parameters values for Figure 20 lie in the wild chaotic parameter regime and, therefore, this figure illustrates the geometry of wild chaos for $c \in \mathbb{C}\backslash\mathbb{R}$ in a similar fashion as Figure 13 shows the geometry of wild chaos for $c \in \mathbb{R}$.

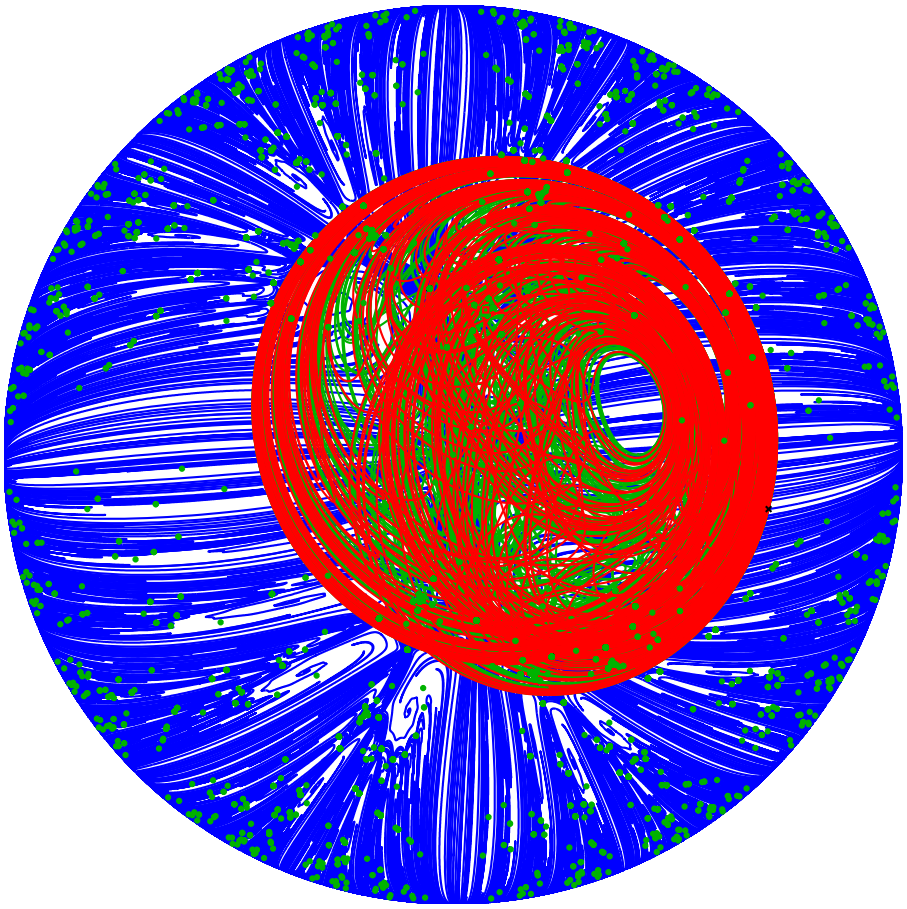

Figure 20: The fixed point p (black cross), its stable set $W^s(p)$ (blue curves), its unstable set $W^u(p)$ (red curve) and the critical set $\mathcal{J}$ (green) on the Poincaré disk for $a = 0.8$, $\lambda = 0.8$ and $c = 0.7 + 0.2i$; compare with Figures 13, 18 and 19.

6 Role of the bifurcations in the formation of the wild Lorenz-like attractor

In this section, we explain the construction of the Lorenz-like attractor in the n-dimensional vector field in [9], for $n \geq 5$. We then discuss how the tangency bifurcations in map (1) relate to bifurcations in this vector field.

6.1 Geometric Lorenz-attractor in $\mathbb{R}^3$

Let us first recall the classical construction of a Lorenz-like attractor in $\mathbb{R}^3$. An attractor of a three-dimensional vector-field is called a *geometric Lorenz-attractor* if it has the following properties [3, 27]:

1. The attractor contains an equilibrium x that has two stable eigenvalues $\lambda_1 < \lambda_2 < 0$ and one unstable eigenvalue $\lambda_3 > 0$ such that $\lambda_3 > -\lambda_2$.

2. There is a two-dimensional Poincaré cross-section Σ, such that the two-dimensional Poincaré return map $\hat{f}$ defined on $\Sigma \backslash \hat{J}_0$ is smooth. The curve $\hat{J}_0$ is the last intersection (in forward time) of the stable manifold of x with Σ: Points on $\hat{J}_0$ go to x and do not return to Σ under the flow of the vector field.

3. The Poincaré cross-section Σ admits a smooth stable invariant foliation that is uniformly contracted by $\hat{f}$. The leaves of this foliation are curves, including $\hat{J}_0$, and the associated quotient space of Σ is a compact interval I.

4. The two-dimensional invertible Poincaré return map $\hat{f}$ can be reduced to a one-dimensional noninvertible map f by taking the quotient map of $\hat{f}$ acting on the quotient space I. The map f is smooth and uniformly expanding on $I\backslash\{J_0\}$ and it is discontinuous and has unbounded derivative at J_0, where $J_0 := \hat{J}_0 \cap I$ is the critical point of f.

The Lorenz attractor itself is a geometric Lorenz attractor [54] and, as mentioned in the introduction, geometric Lorenz attractors are typical attractors in three-dimensional vector fields [43].

6.2 Lorenz-like Construction of the Map

There is a trivial way to construct Lorenz-like attractors in any dimension by embedding a three-dimensional geometric Lorenz-attractor into a transversally contracting three-dimensional submanifold of a higher-dimensional manifold. However, this construction leads to the same dynamical behavior as in the three-dimensional case. Therefore, in order to obtain richer dynamical behavior, the unstable dimension of the singularity should be at least two.

In [9], Bamón, Kiwi and Rivera-Letelier construct an attractor in an n-dimensional vector field, for $n \geq 5$, that has an equilibrium with unstable dimension two. Here, the idea is to create a higher-dimensional analogue of the geometric Lorenz-attractor in dimension $n \geq 5$: As in the three-dimensional construction, the equilibrium x contained in the attractor has two stable eigenvalues $\lambda_1 < \lambda_2 < 0$ and one unstable eigenvalue $\lambda_3 > 0$. But here, the multiplicity of the unstable eigenvalue is two and the multiplicity of the strong stable eigenvalue is $n-3$. Further, in addition to $\lambda_3 > -\lambda_2$, they require $-\lambda_1 > \lambda_3$. Correspondingly, the Poincaré cross-section Σ and the Poincaré return map $\hat{f}$ are $(n-1)$-dimensional and the first intersection $\hat{J}_0$ of the stable manifold of x with Σ is $(n-3)$-dimensional. The uniformly contracting foliation on $\Sigma\backslash\hat{J}_0$ now consists of $(n-3)$-dimensional leaves. The quotient space of Σ by the foliation in the n-dimensional construction in [9] is a compact two-dimensional set B. As a consequence, the quotient map f of $\hat{f}$ by this foliation is a two-dimensional noninvertible map acting on B. This map is discontinuous and has unbounded derivative at the critical point $J_0 = \hat{J}_0 \cap B$ and it is smooth and uniformly expanding on $B\backslash J_0$.

In [9] the authors construct a Lorenz-like attractor with these properties starting from the two-dimensional noninvertible map f given by (1) for $c = 1$ and then extend it to an $(n-1)$-dimensional diffeomorphism that is contracting on the other $n-3$ variables. In particular, for $n > 5$, this n-dimensional vector field is an embedding of the five-dimensional vector field into a transversally contracting five-dimensional submanifold of the n-dimensional space. Therefore, it is sufficient to study the properties of the Lorenz-like attractor for the case $n = 5$, which we will do from now on.

The construction of the five-dimensional vector field from the map (1) is made as follows. The Poincaré section Σ is defined as

$$\Sigma := B \times \overline{\mathbb{D}}_1(0),$$

where $B := \overline{\mathbb{D}}_{2/(1-\lambda)}(0)$, and $\hat{J}_0$ is given as

$$\hat{J}_0 := J_0 \times \overline{\mathbb{D}}_1(0),$$

where $J_0 = \{0\}$ is the critical point of map (1). Then, the four-dimensional local diffeomorphism $\hat{f}$ is defined as

$$\begin{aligned} \hat{f} : B\backslash J_0 \times \overline{\mathbb{D}}_1(0) &\to B \times \overline{\mathbb{D}}_1(0) \\ (z, w) &\mapsto \left(f(z), \frac{z}{2|z|} + \beta |z|^b \frac{|z|}{z} w \right), \end{aligned} \tag{8}$$

where $f : B\backslash J_0 \to B$ is given by map (1) for $c = 1$, $a := -\lambda_2/\lambda_3 < 1$, $b := -\lambda_1/\lambda_3 > 1$ and $\beta > 0$ is arbitrarily small such that $\hat{f}$ is well defined and injective. This definition of $\hat{f}$ is a lift of the two-dimensional noninvertible map f to a four-dimensional invertible map $\hat{f}$.

The Poincaré section $\Sigma = B \times \overline{\mathbb{D}}_1(0)$ is foliated by the foliation

$$\{\{z\} \times \overline{\mathbb{D}}_1(0)\}_{z \in B}.$$

This foliation consists of two-dimensional leaves, including $\hat{J}_0$. By construction, the map $\hat{f}$ is uniformly contracting on this foliation. Furthermore, the quotient space of Σ by this foliation is the compact two-dimensional set B and the map $f : B \backslash J_0 \to B$ defined by (1) is the quotient map of $\hat{f}$ acting on the quotient space B.

To suspend the map $\hat{f}$ to a vector field X, the authors of [9] first construct a vector field $\tilde{X}$ defined on $[-2, 3] \times B \times \overline{\mathbb{D}}_1(0)$ that has an equilibrium $\tilde{x}$ with the eigenvalues λ_1, λ_2 and λ_3 with multiplicities two, one and two, respectively, as required above and that has $\hat{f}$ as a Poincaré map. They then map $\tilde{X}$ to a vector field X defined on the five-dimensional torus $\mathbb{T}^5 := \mathbb{R}/\mathbb{Z} \times D^4$, that has an equilibrium x with the same eigenvalues and multiplicities as $\tilde{x}$; here, D^4 is the four-dimensional closed unit ball in $\mathbb{R}^4$. Note that the fixed point p of the map f does not correspond to the equilibrium x of the vector field X, but to a periodic orbit Γ of X; the equilibrium x of X does not lie in the Poincaré section Σ.

6.3 Consequences of the tangency bifurcations for the vector field

We now explain the consequences of the bifurcations of the planar map (1) for the five-dimensional vector field X. Let us first take a closer look at the meaning of the invariant sets of map (1) for the vector field X.

We denote the stable and unstable sets of the saddle fixed point p by $W^s_f(p)$ and $W^u_f(p)$ to emphasize that they belong to the two-dimensional noninvertible map f defined on $B \backslash J_0$.

The four-dimensional Poincaré return map $\hat{f}$ has a corresponding saddle fixed point

$$\hat{p} := \left(p, \frac{1}{2(1 - \beta|p|^b)} \right) \in (B \backslash J_0) \times \overline{\mathbb{D}}_1(0).$$

This fixed point $\hat{p}$ has two eigenvalues given by the stable and unstable eigenvalues of p, and one additional strong stable eigenvalue with multiplicity two. Therefore, it has a three-dimensional stable manifold $W^s_{\hat{f}}(\hat{p})$ and a one-dimensional unstable manifold $W^u_{\hat{f}}(\hat{p})$ in Σ. Note that these sets are immersed manifolds, because $\hat{f}$ is a diffeomorphism. The saddle $\hat{p}$ of the four-dimensional map $\hat{f}$ gives rise to a saddle periodic orbit Γ of the vector field X, which has stable and unstable manifolds $W^s_X(\Gamma)$ and $W^u_X(\Gamma)$ of dimensions four and two, respectively. Therefore, for some smooth $h : B \to \mathbb{D}$, we get

$$W^s_X(\Gamma) \cap \Sigma = W^s_{\hat{f}}(\hat{p}) = W^s_f(p) \times \overline{\mathbb{D}}_1(0) \tag{9}$$

$$\text{and} \qquad W^u_X(\Gamma) \cap \Sigma = W^u_{\hat{f}}(\hat{p}) = \{(z, h(z)) | z \in W^u_f(p)\}. \tag{10}$$

The existence of the equilibrium x of X manifests itself through the forward and backward critical sets $\mathcal{J}^+$ and $\mathcal{J}^-$ in the map f. Hence, for the five-dimensional vector field X, these sets also correspond to invariant manifolds, namely, the stable and unstable manifolds of the equilibrium x of X, denoted $W^s_X(x)$ and $W^u_X(x)$, respectively. In particular, by construction, $\hat{J}_0 = J_0 \times \overline{\mathbb{D}}_1(0)$ is the last intersection of $W^s_X(x)$ with Σ before $W^s_X(x)$ does not return to Σ under the flow of X. Consequently, the entire set of intersections of $W^s_X(x)$ with Σ is given by the set of points on Σ that *eventually* do not return to Σ, i.e., all preimages of $\hat{J}_0$ under $\hat{f}$. Analogously to the construction for f, we define this set as the *backward critical set*

$$\widehat{\mathcal{J}}^- := \cup_{k \geq 0} \hat{f}^{-k}(\hat{J}_0)$$

of the map $\hat{f}$. It can also be written as the product of the backward critical set $\mathcal{J}^-$ of map (1) with the disk $\overline{\mathbb{D}}_1(0)$, and so we get

$$W^s_X(x) \cap \Sigma = \widehat{\mathcal{J}}^- = \mathcal{J}^- \times \overline{\mathbb{D}}_1(0). \tag{11}$$

The critical circle J_1 of the two-dimensional map f given by (1) can be constructed as the multi-valued image of the critical point J_0, defined as the limit

$$J_1 = \left\{ \lim_{r \to 0} f(re^{i\varphi}) \mid \varphi \in [0, 2\pi) \right\} = \left\{ (1 - \lambda)e^{i2\varphi} + 1 \mid \varphi \in [0, 2\pi) \right\}.$$

2D noninvertible map	4D invertible Poincaré map	5D vector field
$f : B\backslash J_0 \to B$ $z \mapsto (1-\lambda+\lambda\lvert z\rvert^a)\left(\frac{z}{\lvert z\rvert}\right)^2+1$	$\hat{f} : B\backslash J_0 \times \overline{\mathbb{D}}_1(0) \to B \times \overline{\mathbb{D}}_1(0)$ $(z,w) \mapsto \left(f(z), \frac{z}{2\lvert z\rvert}+\beta\lvert z\rvert^b\frac{\lvert z\rvert}{z}w\right)$	$X : \mathbb{T}^5 \to \mathbb{T}^5$ constructed s.t. $\hat{f}$ Poincaré map, x equilibrium
p saddle fixed point $W^s_f(p)$, of dimension one $W^u_f(p)$, of dimension one	$\hat{p}$ saddle fixed point $W^s_{\hat{f}}(\hat{p})$, of dimension three $W^u_{\hat{f}}(\hat{p})$, of dimension one	Γ saddle periodic orbit $W^s_X(\Gamma)$, of dimension four $W^u_X(\Gamma)$, of dimension two
 $\mathcal{J}^-$, isolated points $\mathcal{J}^+$, of dimension one	 $\widehat{\mathcal{J}}^-$, of dimension two $\widehat{\mathcal{J}}^+$, of dimension one	x equilibrium $W^s_X(x)$, of dimension three $W^u_X(x)$, of dimension two
homoclinic tangency of p $W^s_f(p) \cap W^u_f(p)$	homoclinic tangency of $\hat{p}$ $W^s_{\hat{f}}(\hat{p}) \cap W^u_{\hat{f}}(\hat{p})$	homoclinic bifurcation of Γ $W^s_X(\Gamma) \cap W^u_X(\Gamma)$
forward critical tangency $W^s_f(p) \cap \mathcal{J}^+$	 $W^s_{\hat{f}}(\hat{p}) \cap \widehat{\mathcal{J}}^+$	heteroclinic bifurcation of x to Γ $W^s_X(\Gamma) \cap W^u_X(x)$
backward critical tangency $W^u_f(p) \cap \mathcal{J}^-$	 $W^u_{\hat{f}}(\hat{p}) \cap \widehat{\mathcal{J}}^-$	heteroclinic bifurcation of Γ to x $W^u_X(\Gamma) \cap W^s_X(x)$
forw. backw. critical tangency $\mathcal{J}^- \cap \mathcal{J}^+$	 $\widehat{\mathcal{J}}^- \cap \widehat{\mathcal{J}}^+$	homoclinic bifurcation of x $W^s_X(x) \cap W^u_X(x)$

Table 1: Correspondences between the invariant sets of f, the invariant sets of $\hat{f}$ and invariant manifolds of Γ and x of X and the resulting correspondences between the tangency bifurcations of these sets.

In the same fashion, we can construct a set $\hat{J}_1$ as the limit

$$\hat{J}_1 := \left\{ \lim_{r\to 0} \hat{f}(re^{i\varphi}, w) \mid \varphi \in [0, 2\pi), w \in \overline{\mathbb{D}}_1(0) \right\} = \left\{ \left((1-\lambda)e^{i2\varphi} + 1, \frac{1}{2}e^{i\varphi} \right) \;\middle|\; \varphi \in [0, 2\pi) \right\},$$

and think of it as the multi-valued image of the set $\hat{J}_0$. Just as $\hat{J}_0$ consists of all points that do not come back to Σ, but end up at $x \in X$, we can think of $\hat{J}_1$ as the set of points that come from x and do not come back to Σ under the inverse flow of the vector field X. Hence, the set $\hat{J}_1$ is the first intersection of the two-dimensional unstable manifold $W^u_X(x)$ of x with Σ. As before, the entire set of intersections of $W^u_X(x)$ with Σ is given by the set of points on Σ that *eventually* do not come back to Σ under the inverse flow; i.e., all images of $\hat{J}_1$ under $\hat{f}$. Again, analogously to the construction for f, we define this set as the *forward critical set*

$$\widehat{\mathcal{J}}^+ := \cup_{k\geq 0} \hat{f}^k(\hat{J}_1)$$

of the map $\hat{f}$. Hence, we get

$$W^u_X(x) \cap \Sigma = \widehat{\mathcal{J}}^+ \subset \mathcal{J}^+ \times \overline{\mathbb{D}}_1(0). \tag{12}$$

Note that $\widehat{\mathcal{J}}^-$ is equal to $\mathcal{J}^- \times \overline{\mathbb{D}}_1(0)$ in (11), but $\widehat{\mathcal{J}}^+$ is a proper subset of $\mathcal{J}^+ \times \overline{\mathbb{D}}_1(0)$ in (12) by construction of $\hat{f}$.

Table 1 summarizes the invariant manifolds and sets, along with their bifurcations that correspond to the stable, unstable and critical sets of the fixed point p of the two-dimensional map f. As shown in the table, the tangency bifurcations of these sets for the map f have the following consequences for the vector field X: A homoclinic tangency between $W^s_f(p)$ and $W^u_f(p)$ corresponds to a tangency of the manifolds $W^s_{\hat{f}}(\hat{p})$ and $W^u_{\hat{f}}(\hat{p})$ on the Poincaré section Σ. Hence, it corresponds to a homoclinic bifurcation of the stable manifold $W^s_X(\Gamma)$ and the unstable manifold $W^u_X(\Gamma)$ of the periodic orbit Γ in the five-dimensional vector field X; see equalities (9) and (10). Similarly, a forward-backward critical tangency between a point in $\mathcal{J}^-$ and a circle in $\mathcal{J}^+$ corresponds to a homoclinic tangency between the stable and unstable manifolds $W^s_X(x)$ and $W^u_X(x)$ of the equilibrium x; see equalities (11) and (12). In the same manner, a forward critical tangency of a circle in $\mathcal{J}^+$ and $W^s_f(p)$ on

the plane leads to the birth of a heteroclinic orbit that connects from x to Γ in the five-dimensional vector field X; see equalities (12) and (9); and, a backward critical tangency of a point in $\mathcal{J}^-$ and $W^u_f(p)$ corresponds to the birth of an heteroclinic orbit that connects from Γ to x; see equalities (11) and (10).

Note that the unstable tangency, that is, a tangency of $W^u_f(p)$ with itself, does not correspond to a tangency of $W^u_{\hat{f}}(\hat{p})$ with itself in Σ. The unstable sets $W^u_f(p) \subset B$ and $W^u_{\hat{f}}(\hat{p}) \subset \Sigma$ are both one-dimensional, but $W^u_{\hat{f}}(\hat{p})$ is an immersed manifold and, therefore, cannot have self-intersections. Hence, the self-tangency of $W^u_f(p)$ only occurs in the projection of Σ onto B along the uniformly contracted foliation, and has no meaning for the four-dimensional diffeomorphism $\hat{f}$ or the five-dimensional vector field X.

In Section 5.3, we identified infinite accumulating sequences of homoclinic, forward critical, backward critical and forward-backward critical tangencies as the creating mechanism of wild chaos in map (1). For the vector field X, they correspond to the birth of infinitely many coexisting homoclinic and heteroclinic orbits connecting x and Γ with each other and themselves.

7 Conclusions

In this paper, we investigated the transition to wild chaos in the dynamics of the two-dimensional noninvertible map (1). The authors of [9] proved the existence of wild chaos in the noninvertible map f given by (1) for parameters $c = 1$ and $a, \lambda \in (0, 1)$ sufficiently close to $(a, \lambda) = (1, 1)$. The saddle point p lies in the hyperbolic set that becomes wild when the parameters are moved into this regime. Therefore, the homoclinic tangencies of the stable and unstable sets of p indicate how the wild chaos appears geometrically. We have discovered, that these homoclinic tangencies are deeply intertwined with three other types of tangency bifurcations of the map, namely, the forward critical, backward critical and forward-backward critical bifurcations (Sections 3 and 4). All four types of tangency bifurcations appear in infinite sequences that accumulate on each other. First, there is an initial sequence of bifurcations that starts with a first homoclinic tangency and consists of an infinite sequence of homoclinic and an infinite sequence of forward critical tangencies accumulating on each homoclinic tangency. Then, in addition, there is a subsequent sequence of bifurcations that starts with a backward critical tangency and consists of an infinite sequence of backward critical and an infinite sequence of forward-backward critical tangencies accumulating on each backward critical tangency.

By following the bifurcations in two parameters, we find essentially the same bifurcation structure for $a, \lambda \in (0, 1)$ and $c \in \mathbb{C}$ when the parameters are moved towards $a = 1$, $\lambda = 1$ and $c = 0$ and, therefore, we see it as the generating mechanism of wild chaos in this map. Our numerical calculations suggest that the parameter region of wild chaos in the four-dimensional $(\mathrm{Re}(c), \mathrm{Im}(c), a, \lambda)$-space is bounded by parts of the hypersurfaces of "last" forward backward critical tangencies, first backward critical tangencies, first homoclinic tangencies, fold bifurcations and $\lambda = 1$. In [9], the authors impose strong assumptions on the parameter regime to prove the existence of wild chaos in map (1), which means that their proof only guarantees wild chaos in a very small parameter region near the point $(a, \lambda, c) = (1, 1, 1)$. Our results indicate that the geometric ingredients, which we believe are sufficient for existence of wild chaos, are present in a much larger parameter region.

The stable and unstable sets of the fixed point p of the map correspond to stable and unstable manifolds of the periodic orbit Γ of the underlying five-dimensional vector field X. The forward and backward critical sets correspond to stable and unstable manifolds of the equilibrium x of X. Therefore, the homoclinic, forward critical, backward critical and forward-backward critical tangencies of the map correspond to homoclinic and heteroclinic bifurcations of x and Γ in the vector field X, respectively. In particular, in the wild chaotic parameter regime, infinitely many homoclinic orbits of x and Γ and infinitely many heteroclinic cycles between x and Γ are born that accumulate on each other. Since x and Γ lie in the wild hyperbolic set, these bifurcations are characteristic for the bifurcations of the stable and unstable manifolds of the entire hyperbolic set. Therefore, we believe that these infinitely many homoclinic tangencies of the hyperbolic set accumulate on each other in such a dense way, that they are robust.

In future work, we plan to investigate if the regime of existence of the wild Lorenz-like attractor extends to other parameter regimes of the map; e.g., near $a = 2$ and $\lambda = 1$, where (1) is the quadratic map $z \mapsto z^2 + c$. Furthermore, we want to find out if map (1) admits (robust) heterodimensional cycles, e.g. between the fixed points $q^{\pm}$ and the saddle point p, and how they relate to the robust homoclinic tangencies in this map.

Acknowledgments

We thank Jan Kiwi for drawing our attention to the map (1) and Juan Rivera-Letelier for stimulating discussions concerning details of the proof in [9] and for his comments on an earlier draft of this manuscript. Furthermore, we thank Enrique Pujals for helpful discussions about robust nonhyperbolicity. The research of S. H. was funded by doctoral scholarships from the University of Bristol and the University of Auckland and a six-month scholarship from the German Academic Exchange Service (DAAD).

A Numerical Methods

In this section we explain the numerical methods we use for computing the stable and unstable sets $W^s(p)$ and $W^u(p)$ and how we adapt the methods for finding and continuing homoclinic tangencies in two parameters to find and continue the forward critical, backward critical and forward-backward critical tangencies.

A.1 Computation of the Stable and the Unstable Set

The stable and unstable sets of the map (1) do not admit an analytical expression. Hence, we compute them numerically. For the computation of the unstable set $W^u(p)$ we use the method proposed in [34] for calculating one-dimensional (un)stable manifolds. This method has been implemented in the DsTool environment [8, 18, 35]. Each side of $W^u(p)$ is approximated by a piecewise-linear approximation $\mathrm{Lin}(p, z_1, \ldots, z_N)$ given by line segments between consecutive points of $(p, z_1, \ldots, z_N)$, which are obtained in the following way. The first two points are the saddle fixed point p and a point z_1 in its unstable eigenspace at some small distance δ_0 from p. If the points $(p, z_1, \ldots, z_k)$, $k \geq 1$, in the approximation of $W^u(p)$ have already been calculated, the next point z_{k+1} is taken at distance δ_k from z_k such that $z_{k+1} = f(z)$ for some $z \in \mathrm{Lin}(p, z_1, \ldots, z_k)$. If the angle between the points z_{k-1}, z_k and z_{k+1} satisfies a certain angle condition, the point z_{k+1} is accepted. Otherwise, this step is repeated for a smaller value of δ_k, to ensure an appropriate representation of the manifold where $W^u(p)$ has large curvature.

For diffeomorphisms the stable manifold can be computed with the same algorithm by computing the unstable manifold of the inverse map. Unfortunately, this does not work for the stable set $W^s(p)$ of map (1), because the map has no unique inverse and $W^s(p)$ consists of infinitely many branches. However, we can define a local inverse f_{loc}^{-1} near the saddle point p of (1), such that $f_{loc}^{-1}(p) = p$. This will be one of the two preimages f_0^{-1} or f_1^{-1} defined in (6). We then use DsTool to calculate the primary manifold $W_0^s(p)$ of f as the unstable manifold of f_{loc}^{-1}.

In order to compute the remainder of the stable set $W^s(p)$ from the primary manifold $W_0^s(p)$, we make use of the fact that we know the two inverse maps f_0^{-1} and f_1^{-1} explicitly; see equation (6). The preimages of $W_0^s(p)$ build up the entire stable set $W^s(p)$. If $\mathrm{Im}(c)$ is such that $W_0^s(p)$ does not intersect the critical circle J_1, we approximate the stable set directly by taking all preimages of $W_0^s(p)$ up to a certain order. However, if we used this method for the case that $W_0^s(p)$ intersects J_1, we would recalculate parts of the primary manifold in each step. Therefore, we take the preimages of $-W_0^s(p) \cup W_{J_0J_1}$ instead, where $-W_0^s(p)$ is the symmetric counterpart of the primary manifold in the left-half plane and $W_{J_0J_1}$ is the segment of $W_0^s(p)$ that connects the critical point J_0 to the critical circle J_1. The union of these preimages (together with $W_0^s(p)$) also make up the entire stable set $W^s(p)$, and each part is calculated only once.

Let W_0 be an approximation of $W_0^s(p)$ or $-W_0^s(p) \cup W_{J_0J_1}$ depending on $\mathrm{Im}(c)$, as calculated with the method in [34]. Furthermore, assume that $W_0, W_{-1}, \ldots, W_{-k}$, where W_{-j} is an approximation of $f^{-1}(W_{-(j-1)})$ for $1 \leq j \leq k$, have already been calculated. Note that W_{-j} consists of the approximations of 2^j curve segments. The next preimage approximation $W_{-(k+1)}$ is taken as the two preimages $f_0^{-1}(W_{-k}) \cup f_1^{-1}(W_{-k})$ of W_{-k}. We accept $W_{-(k+1)}$ if the angles between three consecutive points satisfy certain conditions. Otherwise, we add points to W_{-k} using interpolation and recalculate $W_{-(k+1)}$. This step is repeated a couple of times, if necessary.

A.2 Numerical continuation of the critical tangency bifurcations

In order to detect and continue the tangency bifurcations, we start by transforming the map (1) to a map $f:\ \mathbb{R}^2\backslash(0,0)\times A\to\mathbb{R}^2$ with real coordinates, that is, for $z=(x,y)$ and $\alpha=(\lambda,a,\mathrm{Re}(c),\mathrm{Im}(c))$,

$$f(z,\alpha):=\left((1-\lambda+\lambda\sqrt{x^2+y^2}^a)\frac{x^2-y^2}{x^2+y^2}+\mathrm{Re}(c),(1-\lambda+\lambda\sqrt{x^2+y^2}^a)\frac{2xy}{x^2+y^2}+\mathrm{Im}(c)\right).$$

The homoclinic tangency: Let $p=p(\alpha)$ be the corresponding saddle fixed point of f with $f(p(\alpha),\alpha)=p(\alpha)$. Recall that $\hat{z}$ is a homoclinic point for p if it converges to p under forward iteration of f and has a sequence of preimages converging to p; i.e, $\lim_{n\to\infty}f^n(\hat{z})=p$ and there is a sequence $\{\hat{z}_k\}_{k\geq 0}$ with $\hat{z}_0=\hat{z}$, $\hat{z}_n=f(\hat{z}_{n+1})$ for $n\geq 0$ and $\lim_{n\to\infty}\hat{z}_n=p$. The corresponding homoclinic orbit is then given as $\{\hat{z}_k\}_{k\geq 0}\cup\{f^k(\hat{z})\}_{k\geq 1}$. Following the method suggested by Beyn and Kleinkauf in [10], this homoclinic orbit can be approximated by a finite orbit segment $\{z_1,\ldots,z_N\}$ that, together with the saddle fixed point $z_0:=p$, satisfies the boundary value problem:

$$f(z_0,\alpha)-z_0=0 \qquad \text{(fixed point condition)}, \tag{13}$$
$$f(z_k,\alpha)-z_{k+1}=0, k=1,\ldots,N-1 \qquad \text{(orbit condition)}, \tag{14}$$
$$(z_1-z_0)q_u^T=0 \qquad \text{(left boundary condition)}, \tag{15}$$
$$(z_N-z_0)q_s^T=0 \qquad \text{(right boundary condition)}. \tag{16}$$

Here, q_s and q_u are the stable and the unstable eigenvector of the saddle point z_0, respectively. For $Z=(z_0,z_1,\ldots,z_N,\alpha)$, let $F^H(Z,\alpha)$ be the left-hand side of the boundary value problem (13)–(16) such that the problem is equivalent to solving $F^H(Z,\alpha)=0$. A regular solution of this equation corresponds to a transversal homoclinic orbit and, therefore, can be continued in one parameter. At a homoclinic tangency, however, the solution additionally satisfies the rank 1 deficiency condition

$$\det(D_Z F^H(Z,\alpha))=0 \text{ (tangency condition)}. \tag{17}$$

The boundary value problem (13)–(17) consists of $2N+3$ equations with $2(N+1)$ unknowns, namely, $z_0,z_1,\ldots,z_N$. Therefore, continuation in two parameters gives us a one-dimensional branch of solutions. The detection and continuation of homoclinic tangencies with this method is implemented in the Matlab software package Cl_MatContM [15, 22, 25]. Here, the initial segments of manifold to detect a transversal homoclinic points as their intersection points are computed with the method from [34]. These homoclinic points are then used as seeds in Newtons method to get an initial solution of (13)–(16). This solution can be followed in one parameter until (17) is satisfied to get an initial solution of (13)–(17).

We adapt the boundary value problem (13)–(17) and the corresponding Cl_MatContM code to continue in two parameters also the forward critical, backward critical, forward-backward critical and unstable tangencies that we found in map (1). To this end, we keep the fixed point condition (13) and the orbit condition (14), but change the boundary and tangency conditions (15), (16) and (17).

The forward critical tangency: In the forward critical tangency, the stable set $W^s(p)$ is tangent to the critical circle $J_1=\partial\overline{\mathbb{D}}_{1-\lambda}(c)$, so the boundary value problem to follow it in two parameters becomes

$$f(z_0,\alpha)-z_0=0 \qquad \text{(fixed point condition)}, \tag{18}$$
$$f(z_k,\alpha)-z_{k+1}=0, k=1,\ldots,N-1 \qquad \text{(orbit condition)}, \tag{19}$$
$$||z_1-c||-1+\lambda=0 \qquad \text{(left boundary condition)}, \tag{20}$$
$$(z_N-z_0)q_s^T=0 \qquad \text{(right boundary condition)}, \tag{21}$$
$$\det(D_Z F^F(Z,\alpha))=0 \qquad \text{(tangency condition)}.. \tag{22}$$

Here, $F^F(Z,\alpha)$ is the left-hand side of (18)–(21). An initial solution of (18)–(22) can be found by using an intersection point of J_1 and $W^s(p)$ as an initial solution of (18)–(21) and following it in one parameter until (22) is satisfied.

The backward critical tangency: In the backward critical tangency, the critical point $J_0 = \{0\}$ lies on the unstable set $W^u(p)$, so there are two boundary conditions, but no tangency condition. The boundary value problem is

$$f(z_0, \alpha) - z_0 = 0 \qquad \text{(fixed point condition)}, \tag{23}$$
$$f(z_k, \alpha) - z_{k+1} = 0, k = 1, \ldots, N-1 \qquad \text{(orbit condition)}, \tag{24}$$
$$(z_1 - z_0) q_u^T = 0 \qquad \text{(left boundary condition)}, \tag{25}$$
$$z_N = 0 \qquad \text{(right boundary condition)}. \tag{26}$$

Recall that $z_N \in \mathbb{R}^2$, so that the right boundary condition (26) is a two-dimensional equation. Therefore, this boundary value problem (23)–(26) consists of $2N + 3$ equations with $2(N + 1)$ unknowns as before. An initial solution can be found by using the point on $W^u(p)$ closest to J_0 and a sequence of its preimages on $W^u(p)$ as a seed for Newtons method.

The forward-backward critical tangency: In the forward-backward critical tangency, an iterate of the critical point $J_0 = \{0\}$ lies on the critical circle J_1. Again, there is no tangency condition, but two boundary conditions of which the right boundary condition is a two-dimensional equation. The boundary value problem becomes:

$$f(z_0, \alpha) - z_0 = 0 \qquad \text{(fixed point condition)} \tag{27}$$
$$f(z_k, \alpha) - z_{k+1} = 0, k = 1, \ldots, N-1 \qquad \text{(orbit condition)} \tag{28}$$
$$||z_1 - c|| - 1 + \lambda = 0 \qquad \text{(left boundary condition)} \tag{29}$$
$$z_N = 0 \qquad \text{(right boundary condition)}. \tag{30}$$

An initial solution can be found in the same manner as for the case of a backward critical tangency, by starting on a circle $J_k \in \mathcal{J}^+$ instead of on $W^u(p)$.

References

[1] R. H. Abraham, L. Gardini, and C. Mira, *Chaos in Discrete Dynamical Systems*, Springer-Verlag, New York, 1997. A visual introduction in 2 dimensions.

[2] V. S. Afrajmovich, V. V. Bykov, and L. P. Sil′nikov, *The origin and structure of the Lorenz attractor*, Dokl. Akad. Nauk SSSR, 234 (1977), pp. 336–339. In Russian.

[3] ——, *On structurally unstable attracting limit sets of Lorenz attractor type*, Trudy Moskov. Mat. Obshch., 44 (1982), pp. 150–212. In Russian.

[4] A. Agliari, L. Gardini, and C. Mira, *On the fractal structure of basin boundaries in two-dimensional noninvertible maps*, Internat. J. Bifur. Chaos Appl. Sci. Engrg., 13 (2003), pp. 1767–1785. Dynamical systems and functional equations (Murcia, 2000).

[5] K. T. Alligood, E. Sander, and J. A. Yorke, *Crossing bifurcations and unstable dimension variability*, Phys. Rev. Lett., 96 (2006), p. 244103.

[6] M. Asaoka, *Hyperbolic sets exhibiting C^1-persistent homoclinic tangency for higher dimensions*, Proc. Amer. Math. Soc., 136 (2008), pp. 677–686.

[7] ——, *Erratum to "Hyperbolic sets exhibiting C^1-persistent homoclinic tangency for higher dimensions"*, Proc. Amer. Math. Soc., 138 (2010), p. 1533.

[8] A. Back, J. Guckenheimer, M. Myers, F. Wicklin, and P. Worfolk, *DsTool: Computer assisted exploration of dynamical systems*, Notices Amer. Math. Soc, 39 (1992), pp. 303–309.

[9] R. Bamón, J. Kiwi, and J. Rivera-Letelier, *Wild Lorenz like attractors.* Preprint available at `http://arxiv.org/abs/math/0508045`, 2006.

[10] W.-J. Beyn and J.-M. Kleinkauf, *The numerical computation of homoclinic orbits for maps*, SIAM J. Numer. Anal., 34 (1997), pp. 1207–1236.

[11] C. Bonatti and L. Díaz, *Robust heterodimensional cycles and C^1-generic dynamics*, J. Inst. Math. Jussieu, 7 (2008), pp. 469–525.

[12] C. Bonatti, L. J. Díaz, and M. Viana, *Dynamics beyond Uniform Hyperbolicity*, vol. 102 of Encyclopaedia of Mathematical Sciences, Springer-Verlag, Berlin, 2005. A global geometric and probabilistic perspective, Mathematical Physics, III.

[13] Y. Cao, S. Luzzatto, and I. Rios, *The boundary of hyperbolicity for Hénon-like families*, Ergodic Theory Dynam. Systems, 28 (2008), pp. 1049–1080.

[14] J. C. Cathala, *Basin properties in two-dimensional noninvertible maps*, Internat. J. Bifur. Chaos Appl. Sci. Engrg., 8 (1998), pp. 2147–2189.

[15] A. Dhooge, W. Govaerts, and Y. A. Kuznetsov, *MatCont: a Matlab package for numerical bifurcation analysis of ODEs*, ACM Trans. Math. Software, 29 (2003), pp. 141–164.

[16] E. J. Doedel, B. Krauskopf, and H. M. Osinga, *Global bifurcations of the Lorenz manifold*, Nonlinearity, 19 (2006), pp. 2947–2972.

[17] ——, *Global invariant manifolds in the transition to preturbulence in the Lorenz system*, Indag. Math. (N.S.), 22 (2011), pp. 222–240.

[18] J. P. England, B. Krauskopf, and H. M. Osinga, *Computing one-dimensional stable manifolds and stable sets of planar maps without the inverse*, SIAM J. Appl. Dyn. Syst., 3 (2004), pp. 161–190.

[19] ——, *Bifurcations of stable sets in noninvertible planar maps*, Internat. J. Bifur. Chaos Appl. Sci. Engrg., 15 (2005), pp. 891–904.

[20] G. B. Ermentrout and D. H. Terman, *Mathematical Foundations of Neuroscience*, vol. 35 of Interdisciplinary Applied Mathematics, Springer, New York, 2010.

[21] R. J. Field and L. Györgyi, *Chaos in Chemistry and Biochemistry*, World Scientific, 1993.

[22] R. K. Ghaziani, W. Govaerts, Y. A. Kuznetsov, and H. G. E. Meijer, *Numerical continuation of connecting orbits of maps in Matlab*, J. Difference Equ. Appl., 15 (2009), pp. 849–875.

[23] S. V. Gonchenko, I. I. Ovsyannikov, C. Simó, and D. Turaev, *Three-dimensional Hénon-like maps and wild Lorenz-like attractors*, Internat. J. Bifur. Chaos Appl. Sci. Engrg., 15 (2005), pp. 3493–3508.

[24] S. V. Gonchenko, L. P. Shilnikov, and D. V. Turaev, *On global bifurcations in three-dimensional diffeomorphisms leading to wild Lorenz-like attractors*, Regul. Chaotic Dyn., 14 (2009), pp. 137–147.

[25] W. Govaerts, Y. A. Kuznetsov, R. Khoshsiar Ghaziani, and H. G. E. Meijer, *Cl_MatContM: a toolbox for continuation and bifurcation of cycles of maps*, 2008. Available at `http://sourceforge.net/projects/matcont`.

[26] J. Guckenheimer and P. Holmes, *Nonlinear Oscillations, Dynamical systems, and Bifurcations of Vector Fields*, Springer, New York, 1986.

[27] J. Guckenheimer and R. F. Williams, *Structural stability of Lorenz attractors*, Inst. Hautes Études Sci. Publ. Math., (1979), pp. 59–72.

[28] I. Gumowski and C. Mira, *Recurrence and Discrete Dynamic Systems*, vol. 809 of Lecture Notes in Mathematics, Springer, Berlin, 1980.

[29] M. Hénon, *A two-dimensional mapping with a strange attractor*, Comm. Math. Phys., 50 (1976), pp. 69–77.

[30] C. A. Hobbs and H. M. Osinga, *Bifurcations of the global stable set of a planar endomorphism near a cusp singularity*, Internat. J. Bifur. Chaos Appl. Sci. Engrg., 18 (2008), pp. 2207–2222.

[31] A. Katok and B. Hasselblatt, *Introduction to the Modern Theory of Dynamical Systems*, Encyclopedia of Mathematics and Its Applications, Cambridge University Press, 1996.

[32] H. Kitajima, H. Kawakami, and C. Mira, *A method to calculate basin bifurcation sets for a two-dimensional noninvertible map*, Internat. J. Bifur. Chaos Appl. Sci. Engrg., 10 (2000), pp. 2001–2014.

[33] E. J. Kostelich, I. Kan, C. Grebogi, E. Ott, and J. A. Yorke, *Unstable dimension variability: a source of nonhyperbolicity in chaotic systems*, Phys. D, 109 (1997), pp. 81–90.

[34] B. Krauskopf and H. Osinga, *Growing* $1D$ *and quasi-*$2D$ *unstable manifolds of maps*, J. Comput. Phys., 146 (1998), pp. 404–419.

[35] B. Krauskopf and H. Osinga, *Investigating torus bifurcations in the forced van der Pol oscillator*, in Numerical Methods for Bifurcation Problems and Large-Scale Dynamical Systems (Minneapolis, MN, 1997), vol. 119 of IMA Vol. Math. Appl., Springer, New York, 2000, pp. 199–208.

[36] B. Krauskopf, H. M. Osinga, and B. B. Peckham, *Unfolding the cusp-cusp bifurcation of planar endomorphisms*, SIAM J. Appl. Dyn. Syst., 6 (2007), pp. 403–440 (electronic).

[37] R. López-Ruiz and D. Fournier-Prunaret, *Complex patterns on the plane: different types of basin fractalization in a two-dimensional mapping*, Internat. J. Bifur. Chaos Appl. Sci. Engrg., 13 (2003), pp. 287–310.

[38] E. Lorenz, *Deterministic nonperiodic flow*, Journal of the Atmospheric Sciences, 20 (1963), pp. 130–141.

[39] K. Lüdge and H. Schuster, *Nonlinear Laser Dynamics: From Quantum Dots to Cryptography*, Annual Reviews of Nonlinear Dynamics and Complexity, John Wiley & Sons, 2012.

[40] C. Mira, J.-P. Carcasses, G. Millérioux, and L. Gardini, *Plane foliation of two-dimensional noninvertible maps*, Internat. J. Bifur. Chaos Appl. Sci. Engrg., 6 (1996), pp. 1439–1462.

[41] C. Mira, D. Fournier-Prunaret, L. Gardini, H. Kawakami, and J.-C. Cathala, *Basin bifurcations of two-dimensional noninvertible maps: fractalization of basins*, Internat. J. Bifur. Chaos Appl. Sci. Engrg., 4 (1994), pp. 343–381.

[42] C. Mira, L. Gardini, A. Barugola, and J.-C. Cathala, *Chaotic Dynamics in Two-Dimensional Noninvertible Maps*, vol. 20 of World Scientific Series on Nonlinear Science. Series A: Monographs and Treatises, World Scientific Publishing Co. Inc., River Edge, NJ, 1996.

[43] C. A. Morales, M. J. Pacífico, and E. R. Pujals, *On* C^1 *robust singular transitive sets for three-dimensional flows*, C. R. Acad. Sci. Paris Sér. I Math., 326 (1998), pp. 81–86.

[44] C. G. Moreira, *There are no* C^1*-stable intersections of regular Cantor sets*, Acta Math., 206 (2011), pp. 311–323.

[45] S. Newhouse, J. Palis, and F. Takens, *Bifurcations and stability of families of diffeomorphisms*, Inst. Hautes Études Sci. Publ. Math., (1983), pp. 5–71.

[46] S. E. Newhouse, *Nondensity of axiom* A(a) *on* S^2, in Global Analysis (Proc. Sympos. Pure Math., Vol. XIV, Berkeley, Calif., 1968), Amer. Math. Soc., Providence, R.I., 1970, pp. 191–202.

[47] ———, *The abundance of wild hyperbolic sets and nonsmooth stable sets for diffeomorphisms*, Inst. Hautes Études Sci. Publ. Math., (1979), pp. 101–151.

[48] C.-H. Nien and F. J. Wicklin, *An algorithm for the computation of preimages in noninvertible mappings*, Internat. J. Bifur. Chaos Appl. Sci. Engrg., 8 (1998), pp. 415–422.

[49] J. Palis and W. de Melo, *Geometric Theory of Dynamical Systems*, Springer-Verlag, New York, 1982.

[50] J. Palis and F. Takens, *Hyperbolicity and Sensitive Chaotic Dynamics at Homoclinic Bifurcations*, vol. 35 of Cambridge Studies in Advanced Mathematics, Cambridge University Press, Cambridge, 1993.

[51] M. Shub, *Global Stability of Dynamical Systems*, Springer-Verlag, New York, 1987. With the collaboration of Albert Fathi and Rémi Langevin, Translated from the French by Joseph Christy.

[52] S. Smale, *Differentiable dynamical systems*, Bull. Amer. Math. Soc., 73 (1967), pp. 747–817.

[53] C. Sparrow, *The Lorenz Equations: Bifurcations, Chaos, and Strange Attractors*, vol. 41 of Applied Mathematical Sciences, Springer-Verlag, New York, 1982.

[54] W. Tucker, *The Lorenz attractor exists*, C. R. Acad. Sci. Paris Sér. I Math., 328 (1999), pp. 1197–1202.

[55] R. Ures, *The abundance of hyperbolicity in the C^1 topology*, Ann. Sci. École Norm. Sup. (4), 28 (1995), pp. 747–760.

[56] W. Zhang, B. Krauskopf, and V. Kirk, *How to find a codimension-one heteroclinic cycle between two periodic orbits*, Discrete Contin. Dyn. Syst. Ser. A, 32 (2012), pp. 2825–2851.